THE RELATIONSHIP BETWEEN THE PAIR POLARIZABILITY AND THE SPECTRAL PROFILE OF COLLISION INDUCED LIGHT SCATTERING FOR COMPRESSED CF_4 AND SF_6

A Thesis

Submitted to

the Faculty of Graduate Studies

University of Manitoba

In Partial Fulfillment

of the Requirements for the Degree

Master of Science

by

David Peter Shelton

August 1975

"THE RELATIONSHIP BETWEEN THE PAIR POLARIZABILITY AND THE SPECTRAL PROFILE OF COLLISION INDUCED LIGHT SCATTERING FOR COMPRESSED CF_4 AND SF_6"

by

DAVID P. SHELTON

A dissertation submitted to the Faculty of Graduate Studies of the University of Manitoba in partial fulfillment of the requirements of the degree of

MASTER OF SCIENCE

ACKNOWLEDGEMENT

The author wishes to express gratitude to his research supervisor, Dr. G. C. Tabisz for his friendly guidance throughout the whole period of this study.

ABSTRACT

The collision induced Rayleigh wing in the depolarized light scattering spectrum of two molecular gases has been studied in order to determine the functional form of the pair polarizability anisotropy, $\beta(r)$. Models used to describe the induced polarizability are briefly discussed and then experimental techniques are described. The analysis involves consideration of (i) the low frequency profile alone, (ii) the entire profile, and (iii) the method of moments. Results of the analysis for CF_4 and SF_6 cast doubt on the existence of short range contributions to $\beta(r)$ and indicate the breakdown of the point dipole, Dipole Induced Dipole model.

CONTENTS

LIST OF FIGURES

LIST OF TABLES

CHAPTER 1

INTRODUCTION

1.1 History

The spectrum of light scattered from a gas of non-interacting optically isotropic molecules, with linearly polarized incident light, is composed of lines and bands, shifted in frequency from that of the incident light - the Raman spectrum - and a completely polarized line at zero frequency shift - the Rayleigh line (Figure 1).

In a liquid or dense gas, an additional depolarized component at small frequency shifts is observed, which appears as a broad wing on the sharp Rayleigh line (Figure 2). Initially, observations of the deoplarization ratio of the scattered light were made,[1-3] and later the spectral profile was studied as well.[4-14] The frequency shifted scattering has been ascribed to the anisotropy induced in the molecular polarizability during intermolecular collisions. Hence, the effect is called Collision Induced Light Scattering.

Since the scattering is due entirely to intermolecular collisions, in principle, the study of this scattering is a powerful method for obtaining information on molecular interactions and dynamics in a liquid or dense gas.

The spectral distribution of this depolarized light is given by the Fourier transform of the anisotropic part of the time varying polarizability $\beta(t)$:

$$I(\omega) \propto \left| \int \beta(t) \exp(i\omega t)\, dt \right|^2$$

The polarizability of a group of molecules depends on their relative positions and orientations, since each molecule is distorted by

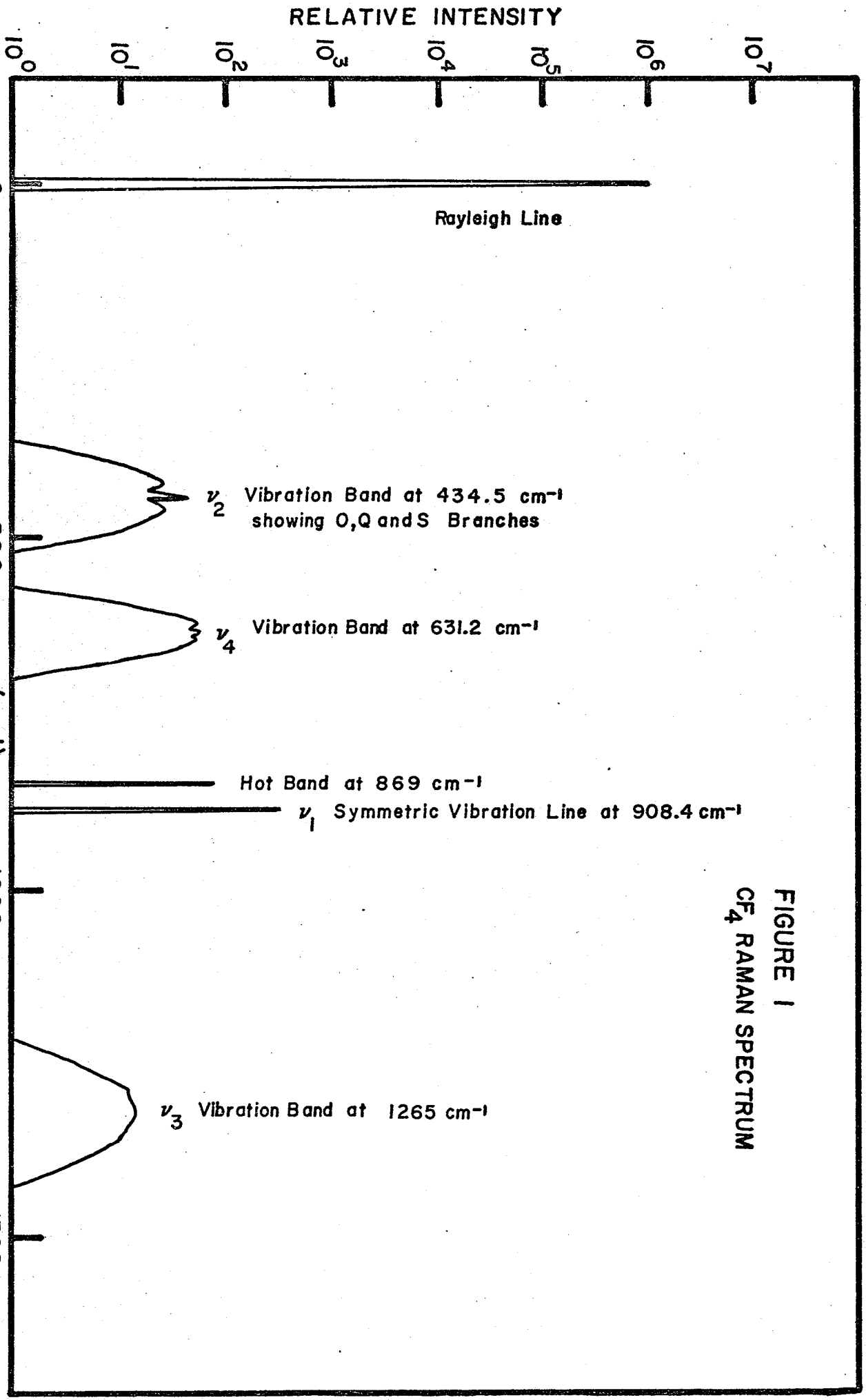

FIGURE 1
CF_4 RAMAN SPECTRUM

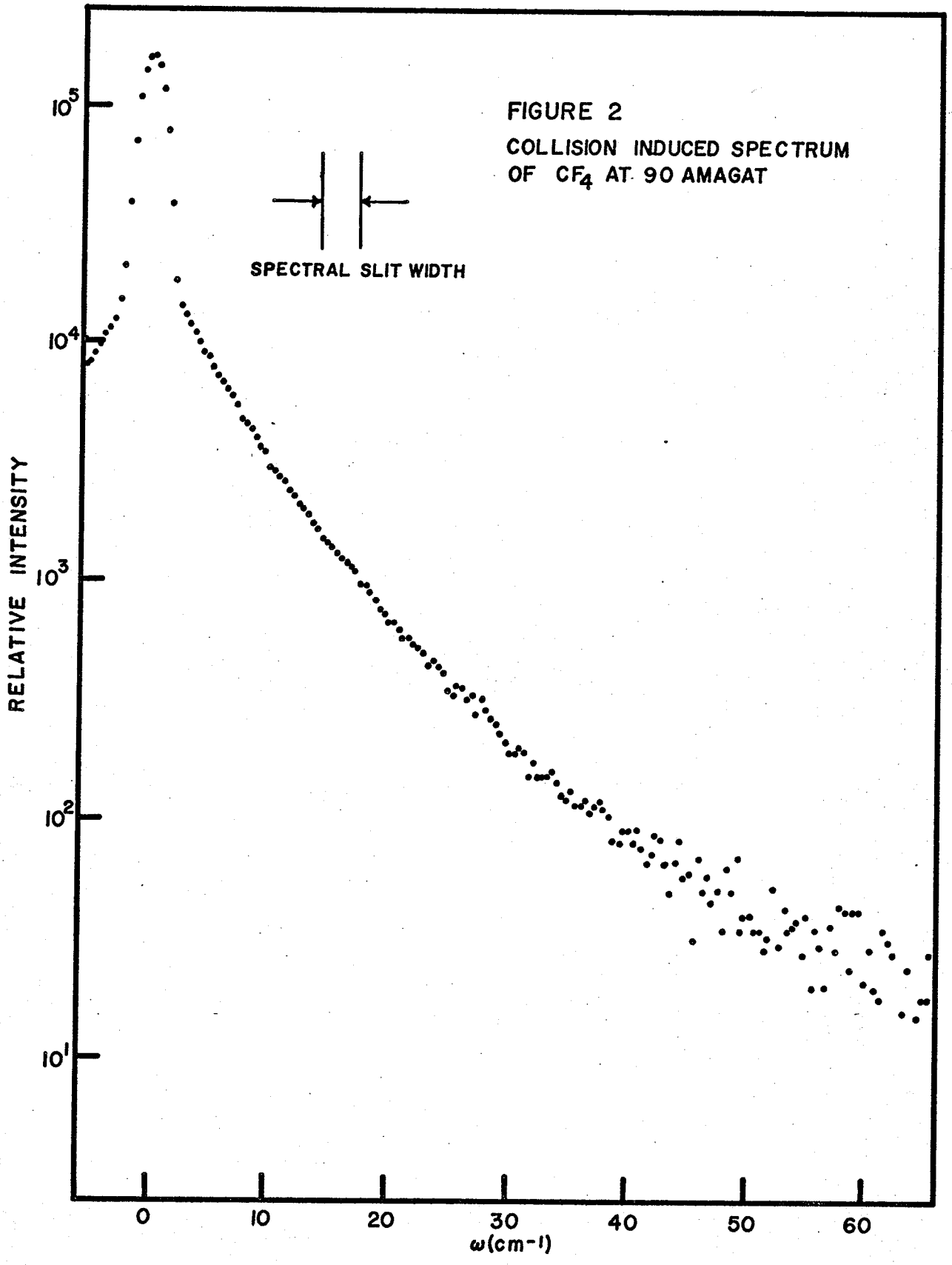
FIGURE 2
COLLISION INDUCED SPECTRUM
OF CF_4 AT 90 AMAGAT
SPECTRAL SLIT WIDTH
RELATIVE INTENSITY
10^5
10^4
10^3
10^2
10^1
0
10
20
30
40
50
60
ω(cm-1)

interactions with its neighbours. The difference between the polarizability of a collection of non-interacting molecules and that of the molecules when each is distorted by its neighbours is the collision induced polarizability of the cluster. Its time dependence arises from the change of this distortion with changes of the intermolecular positions. The time evolution of the intermolecular coordinates depends, however, on the intermolecular potential. Thus, both the cluster polarizability coupling the incident light to the molecules and the many-body potential governing the dynamics of the encounters enter the problem. Unfortunately, both contribute to the observed scattering in such a manner that their separate effects are very difficult to untangle.

Some progress had apparently been made when it was suggested that the scattering from liquids could be accounted for by the Isolated Binary Collision (IBC) model, which assumes that binary collisions and a zero impact parameter are valid assumptions even at liquid densities.[13] The observed spectrum could then be described by a compact mathematical expression in which the roles of the cluster polarizability and the intermolecular potential were clearly displayed.[13,15] However, subsequent experiments,[16,19,20] and analytical and molecular dynamics calculations[17,18,21,22] have shown that the IBC model does not satisfactorily reproduce the observations and leads to ambiguous conclusions. In trying to account for the observed scattering from liquids, it is not clear whether the discrepencies between theory and experiment result from inadequacies in the model used for the induced polarizability, or from the neglect of many-body encounters.[18,21,22]

1.2 Models of the Polarizability Function

The mechanisms accounting for the induced polarizability may be classified according to whether they are long range or short range. While the distinction is not clear cut, it is useful.

The principal long range induction mechanism is the Dipole Induced Dipole interaction.[1,14] The incident light field induces an electric dipole moment in the sample molecules. A molecule, which finds itself in the field of neighbouring dipoles, has induced on it a small additional moment not in general in the direction of the field of the incident light. To lowest order (assuming point dipoles), the induced polarizability increment for a pair is totally anisotropic and $\beta(r)=6\alpha^2 r^{-3}$, where r is the intermolecular separation and α is the polarizability of an isolated molecule. At high densities the range of the interaction will extend several intermolecular spacings and correlations between the motions of several molecules must be taken into account in calculating the scattering due to this mechanism.[18]

Short range induction mechanisms include Electron Overlap[13] and Frame Distortion[13] where the electron clouds or the molecular frame, respectively, are distorted during collision with another molecule. The range of the interaction is expected to be so short that even at high densities, only few body encounters need be considered. In this limit, it is the trajectory near the turning point in the collision which determines the spectrum of scattered light, and the form of the induced polarizability is of lesser importance.[13,14] Indeed, very little is known about the form of $\beta(r)$ due to Electron Overlap and Frame Distortion. The polarizability distortion due to Electron Overlap is believed to vary as r^{-9} on the basis of a

calculation involving colliding metallic spheres.[23] The induced polarizability due to Frame Distortion is thought to be determined by the slope of the repulsive part of the intermolecular potential. For the 6-12 Lennard-Jones potential, this gives an effect varying as r^{-13}. Other interactions which are of relatively short range are second order DID, varying as r^{-6}, and higher multipolar interactions

One sees that very different information about the molecular motion is involved in calculations of the light scattering spectrum depending upon whether the long range or the short range induction mechanisms are more important. Detailed knowledge of the multi-particle distribution function is required for calculations involving the long range induction mechanisms, while scattering by short range interactions depends only on the trajectory while the molecules are in contact. In a liquid both long and short range mechanisms are expected to contribute. Furthermore, the qualitative features of the scattering spectrum may be reproduced by invoking either mechanism alone,[14,18,21] which further complicates the interpretation of the experimental results.

In gases at low density, the molecular encounters are primarily binary, and approximate pair potentials for simple molecules are availiable. The more complete knowledge of molecular dynamics in a gas permits the role played by the induced polarizability in the scattering process to be studied in a consistent manner. It is only when the form of the induced polarizability has been elucidated, that it will be possible to assess the relative importance of the cluster polarizability and the many-body potential in the problem of light scattering from dense fluids.

1.3 Present Investigation

In the present work, an attempt has been made to determine the form of the polarizability anisotropy by using collision induced scattering data for compressed gases. The rare gases have already been intensively studied in several laboratories and the logical extension is to study isotropic molecules. The molecules CF_4 and SF_6 have therefore been chosen for this investigation. The scattering data have been analyzed in terms of the spectral profile and the spectral moments in order to reach conclusions about the form of the polarizability anisotropy.

CHAPTER 2

EXPERIMENTAL METHOD

The apparatus used is typical of laser Raman studies. Linearly polarized light at 488 nm. from an argon-ion laser illuminates the sample, which is contained in a stainless steel pressure cell. The light scattered at 90 degrees is collected and analyzed by a scanning double monochromator. The light is detected using photon counting techniques and the results stored in the memory of a multichannel scaler (Figure 3).

The laser is a Coherent Radiation model 52 argon-ion laser with an internal prism permitting single line operation. The output power used during these experiments was about 500 mW. as measured by a Coherent Radiation model 212 power meter. The 488.0 nm. laser line was chosen over the equally bright 514.5 nm. line in order to optimize the scattered intensity, which increases as ν^4.

2.1 Gas Handling System

The pressure cell and associated high pressure equipment was constructed by the American Instrument Company (Aminco). The optical cell is furnished with three fused silica windows and is designed to contain pressures up to 750 atmospheres (Figure 4). In order to reduce stray light within the cell, a blackened liner is used. Some difficulty in making leak-free window seals was experienced initially, since these experiments were conducted at pressures much lower than for which the cell was designed - the maximum pressures used were about 70 atmospheres. It was found that gaskets cut from "Parafilm",

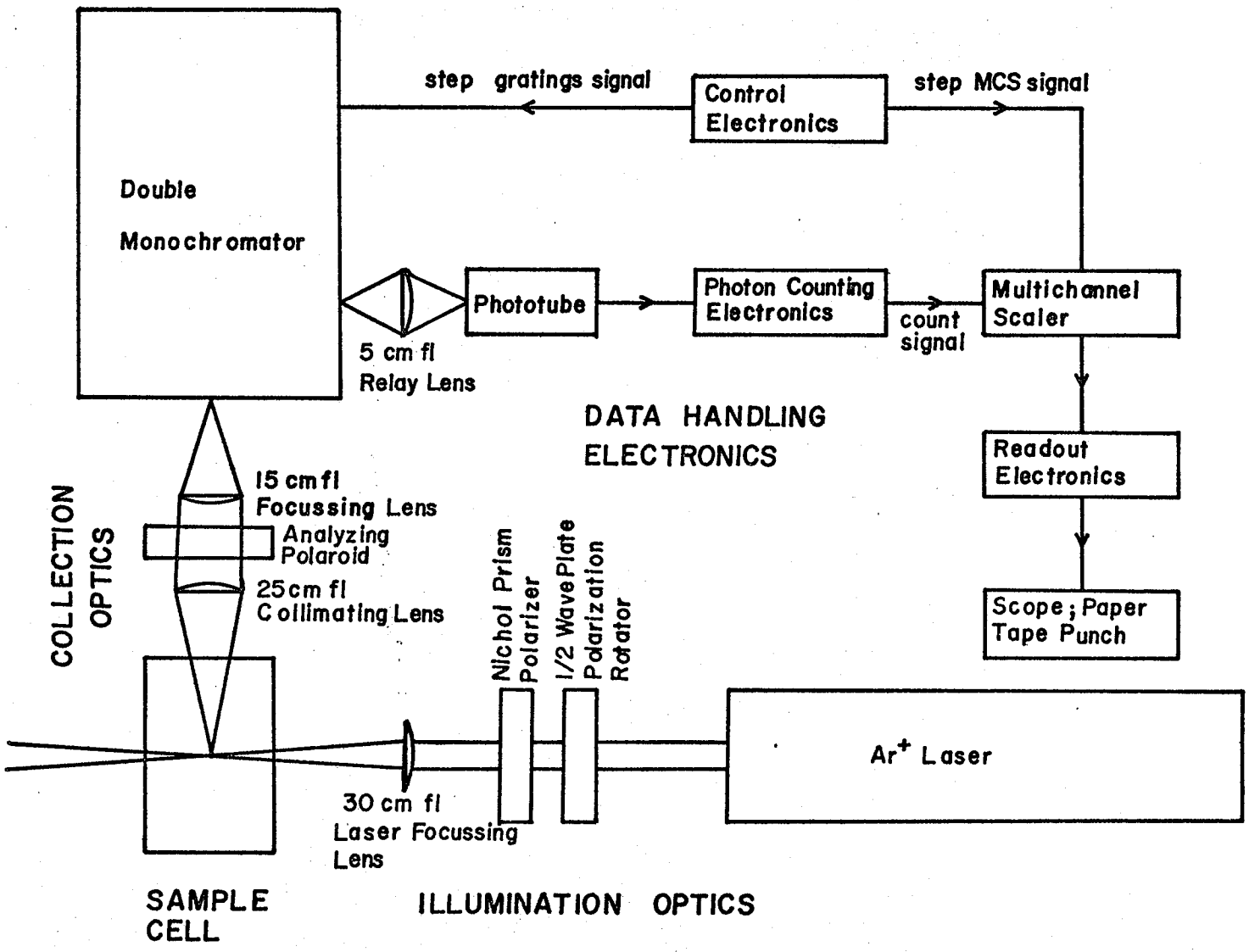

FIGURE 3

SCHEMATIC DIAGRAM OF THE EXPERIMENTAL APPARATUS

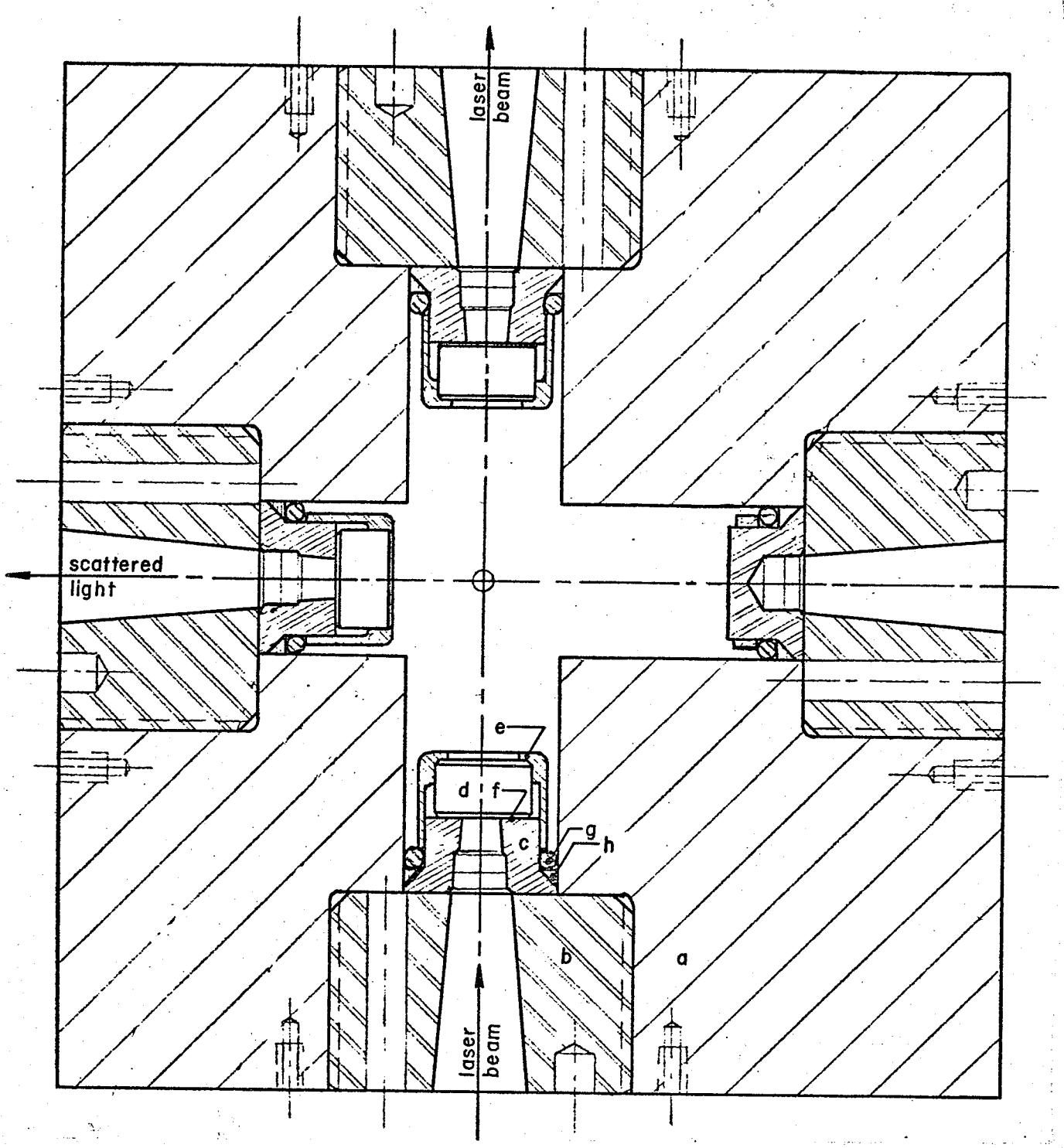

FIGURE 4

10000 PSI OPTICAL CELL

Drawn Full Scale

a) Cell Body – 316 S.S.
b) Threaded Cap – 304 S.S.
c) Seal Plug – 316 S.S.
d) Window – Fused Silica
e) Window Retainer – 316 S.S.
f) Low Pressure Gasket – Parafilm
g) O-Ring – Neoprene
h) Backup Ring – 17-4PH Hardened S.S.

with dimensions 14 mm. o.d. x 12 mm. i.d. x 0.005 inch thick, made very satisfactory seals.

The sample was introduced into the optical cell from another vessel (Aminco 41-19230) which served as a thermal compressor and permitted purification of the sample. In order to raise its pressure, gas from the cylinder was liquified in the cooled thermal compressor, which was then sealed off and allowed to warm up. The gases studied were CF_4 and SF_6. The CF_4 gas, as purchased from the Matheson Company Inc. (99.9% purity) contained a troublesome air impurity. In order to eliminate this trace of air, the raw CF_4 was condensed in the thermal compressor using liquid nitrogen as the coolant and the air was removed with a vacuum pump. The purity was considered adequate when neither the rotational nor vibration-rotational Raman spectrum of air was observable. The impurities in the SF_6 gas used (Matheson, 99.8% purity) were not as troublesome as those in the CF_4, and so the SF_6 samples did not require further purification.

The volumes of the optical cell and the thermal compressor were approximately 50 cc. and 100 cc. respectively. When filled, the system could be left for more than a week with no measurable leakage or contamination of the sample. Thus, the sample would be left undisturbed overnight in order that its temperature would stabilize and any dust would settle out before experimental measurements began.

The sample pressure was measured by a Heise, model CM-11170, 0-15000 psi. Bourdon tube gauge. The sample fill system is depicted schematically in Figure 5.

The density of the sample was calculated from its measured temperature and pressure using PVT data for the gases and solving for

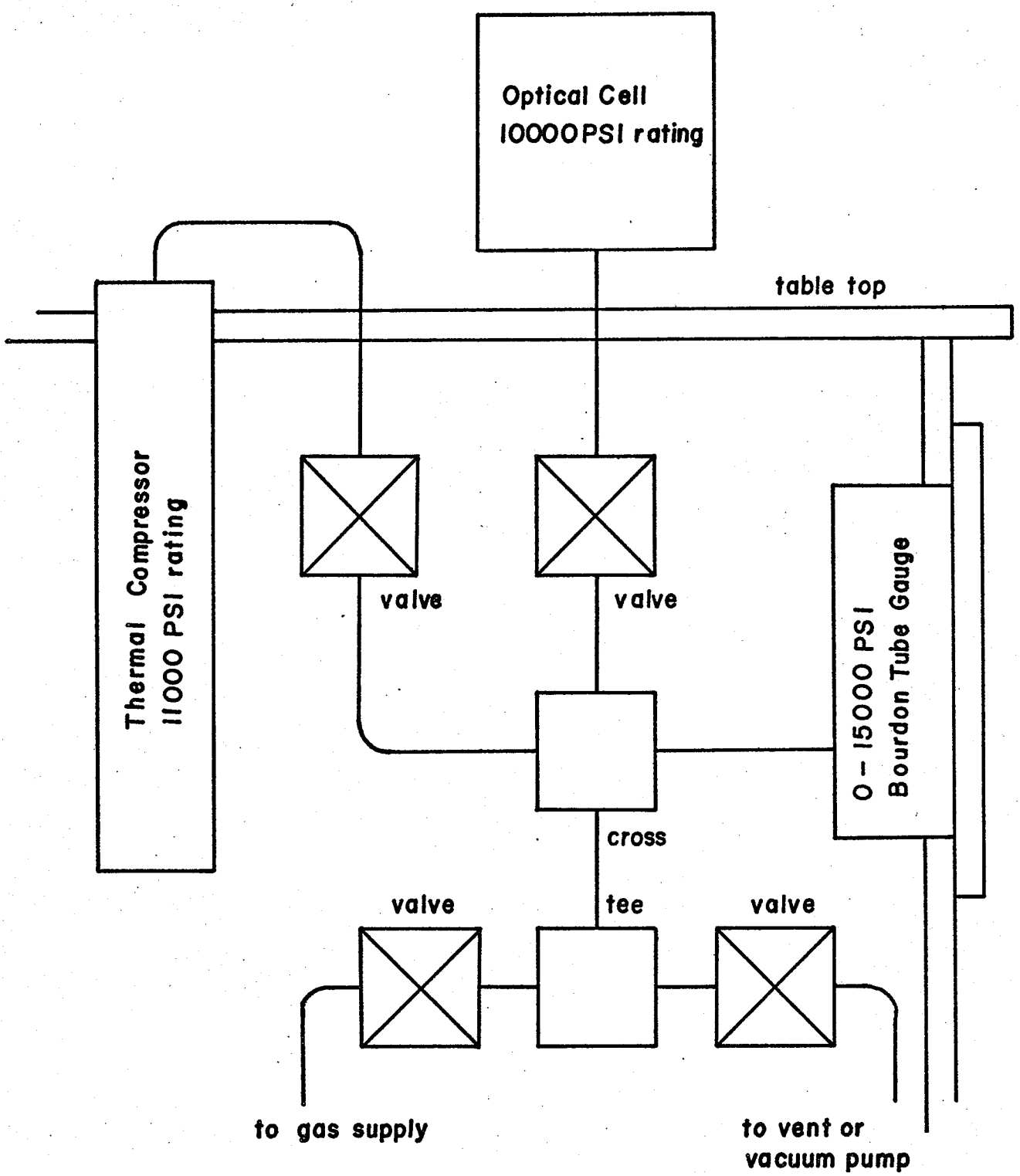

FIGURE 5

SAMPLE FILL SYSTEM

Interconnecting Tubing — 1/16" id 304 S.S. 100000 PSI rating
Valves and Fittings — 60000 PSI rating

the roots of the Beattie-Bridgeman equation of state[24,25,26] by an interative procedure[27] (eg. Appendix A3, Subroutine PVT). The experiments were performed with samples at 293 - 295 K. Pressures up to 70 atmosphere for CF_4 and 20 atmosphere for SF_6, corresponding to 96 Amagat and 27 Amagat, respectively, were used, which are within the range of densities where binary collisions predominate (ρ(Amagat)= ρ(P,T)/ ρ(STP)). The maximum densities of 96 and 27 Amagat correspond to 0.19 and 0.09 of liquid density at the normal boiling point for CF_4 and SF_6 respectively.[28]

2.2 Optical System

The beam from the laser is weakly focussed by a 30 cm. f.l. lens and then directed vertically through the sample cell by a right angle prism, so that the source region is parallel to the entrance slit of the monochromator. Focussing the beam allows for the more efficient transfer of light from the scattering source through the slit and aperture stop of the monochromator.[29,30] Before focussing, the laser beam is passed through a combination of quartz half-wave plate and Nichol prism polarizer. Rotation of the half-wave plate allows rotation of the plane of polarization of the light beam, while the polarizer removes the slight depolarization introduced by the half-wave plate.

Light scattered at 90 degrees to the direction of propagation of the incident beam is collected by an f/15 system. The speed of the collection system is limited chiefly by the small clear aperture of the pressure cell windows. An HN38 Polaroid in the collection arm is used to analyze the polarization of the scattered light.

Several polarization geometries may be obtained by rotating the half-wave plate or the Polaroid (Figure 6). Most experiments were done with the VH geometry. Ideally, this configuration permits observation of only the depolarized component of the scattered light, but such effects as incomplete extinction by the Polaroid, stress-induced birefringence in the pressure cell windows and depolarization by scattering from the rough walls of the sample cell allow "leakage" of about 10^{-3} of the polarized Rayleigh light within the acceptance cone of the collection system. This stray light is a problem when observing the depolarized spectrum near zero shift.

The spectral composition of the scattered light is analyzed by means of a Jarrell-Ash 25-100, one meter, f/8.7 double (subtractive mode) Czerny-Turner scanning monochromator.[31] The grating advance is controlled by a stepping motor actuating a cosecant arm, resulting in a drive which is linear in frequency and may be directly interfaced with digital electronics. Stepping the motor 20 times shifts the spectrum by 0.999 cm^{-1} with Jarrell-Ash number 1308 gratings installed. These gratings have 1180 grooves per mm. and are blazed at 500 nm. In the spectral region near 488 nm. the efficiency of the gratings varies slowly with frequency and is approximately equal for light polarized both parallel to and perpendicular to the rulings.

A double monochromator is used by reason of its superior stray light rejection. In a single monochromator, the mirrors and grating scatter light through small angles with respect to the direction of the reflected and diffracted beams as a result of small random surface imperfections. When a sharp spectral line is scanned at

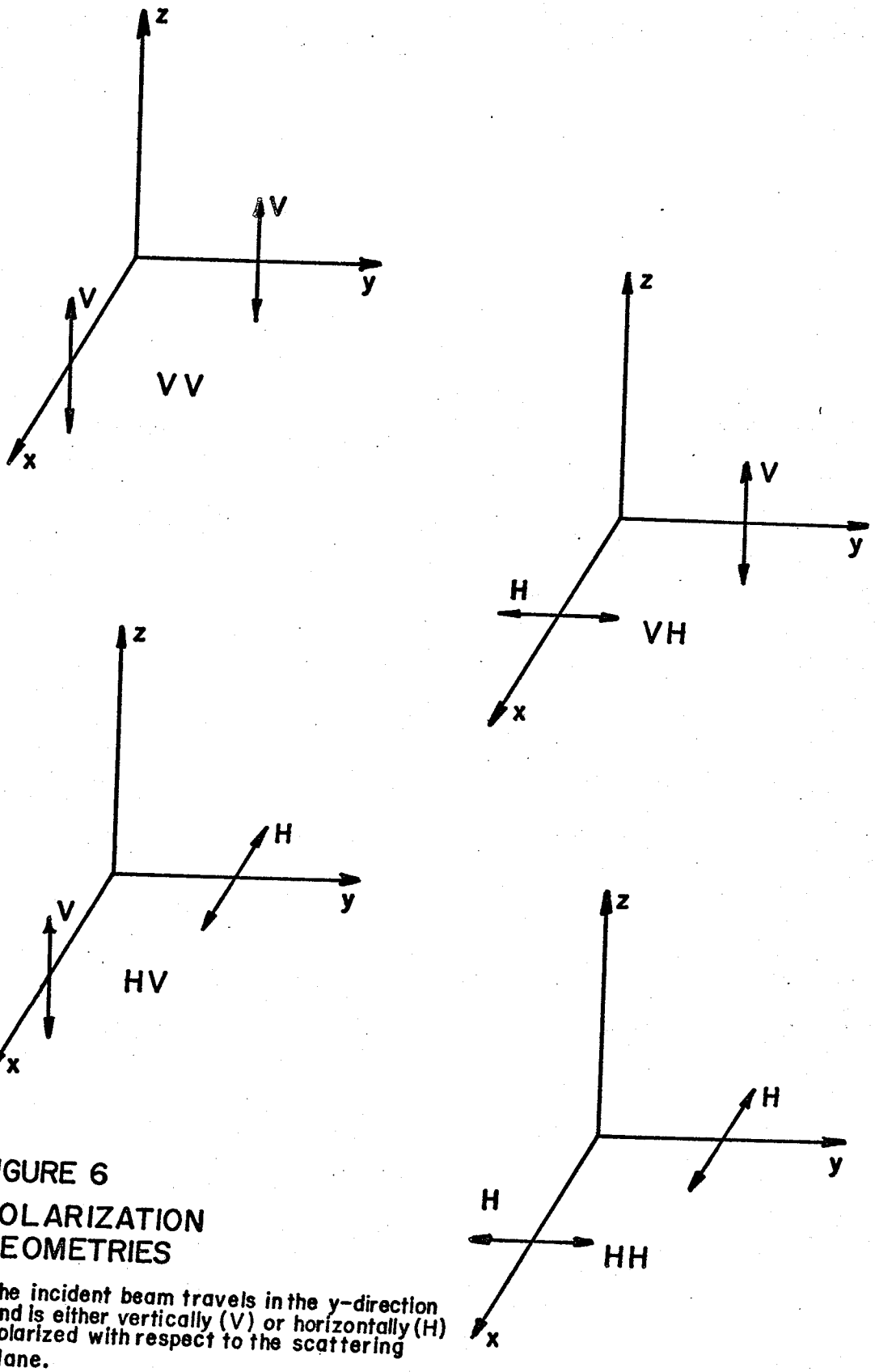

FIGURE 6

POLARIZATION GEOMETRIES

The incident beam travels in the y-direction and is either vertically (V) or horizontally (H) polarized with respect to the scattering plane.

The scattered light is observed in the x-direction and either the vertically or horizontally polarized component is selected.

high resolution this stray light appears as a broad tail about the line and it is tens of wavenumbers before the intensity of this tail falls below 10^{-5} of the intensity of the parent line. With a tandem monochromator the relative intensity of the tails falls below 10^{-5} of the parent line intensity within a few wavenumbers and below 10^{-10} within a few tens of wavenumbers.[31,32] Such extreme stray light rejection is necessary for measurements of the collision induced spectrum at small frequency shifts since the intensity of this scattering is several orders of magnitude less than that of the Rayleigh light that "leaks" into the monochromator past the analyzing polarizer.

The bandpass of the instrument, until it reaches its resolution limit of 0.1 cm^{-1}, is determined by the width of the slits. The attenuation of stray light begins only outside this bandpass. Therefore measurement of the Raman spectrum at small frequency shifts from the existing line demands narrow slits. However, for a broad featureless band, the fraction of light transmitted varies directly with the bandpass, which for best efficiency should be chosen no smaller than is necessary to prevent distortion of the spectrum. Since the collision induced spectrum is broad, featureless and very faint, this consideration demands wide slits. One the one hand, it is necessary to observe the shape of the depolarized spectrum to within a few wavenumbers of zero frequency shift. On the other hand, drifts and instabilities in the laser output and in alignment of the optics limits the duration of a scan to 3 hours. Noise resulting from the statistical fluctuations in the number of photons counted can only be reduced by increasing the flux of photons. The spectral slit

width of 2 cm^{-1} used for the measurements is a compromise between the more efficient utilization of the availiable light afforded by broader slits and the clearer separation of the Rayleigh and Raman components of the spectrum possible with narrower slits.

2.3 Detection System

The light transmitted by the monochromator is detected by a cooled RCA C31034 photomultiplier tube factory selected for low noise. This tube has a GaAs photocathode with a spectral response curve almost flat from 300 to 900 nm. With this tube, the measured overall system response is smoothly varying and constant to within a few percent over the 100 cm^{-1} region usually scanned in the experiments. Since the collision induced spectrum varies much more rapidly than the instrumental relative response, no significant distortion of the shape of the spectrum is introduced by omitting this correction.

The usefulness of the spectral measurements depends ultimately on whether the signal to noise ratio of the data is sufficient for the analysis to which it will be subjected. For relatively intense sources, the signal to noise ratio is determined by the statistical fluctuations in the signal. For very weak sources, the limiting factor becomes the noise introduced by the detector itself. Measurements of the profile of collision induced light scattering requires operation, to a large extent, in the weak signal regime. For this reason the noise performance of the detector assumes critical importance.

The noise from a phototube operating in the photon counting mode

appears as pulses at the anode which are not correlated to photons incident on the photocathode. At high temperatures, the principal noise source for the phototube used is thermionic emission of electrons from the photocathode. The dark count rate due to this source follows Richardson's law and is conveniently reduced by cooling the tube to -30 degrees C. in a Peltier effect cooler (Products For Research 83-055, which also incorporates electromagnetic shielding and biasing arrangements for the tube). The distribution of pulse amplitudes, with the tube operating in the dark at this temperature, contains a small peaked component due to electrons emitted from the photocathode, and an overlapping component due to other noise sources.[33,34]

Since the pulse height spectra of the noise pulses and the photo-electron pulses are different, the signal to noise ratio may be enhanced by discriminating against pulses of certain amplitudes. After recording pulse height spectra with and without light incident on the photocathode, the method due to Young[34] is used to determine the portion of the pulse height spectrm which should be retained for optimum signal to noise at low light levels (Appendix A1). Then the window of the SCA is set so as to permit only pulses having the desired amplitudes to be counted. With optimum discriminator levels, the dark count rate is about 2 counts per second.

The arrangement of the electronics used to process the photomultiplier pulses during an experiment and during setting of discriminator levels is shown in Figures 7a and 7b, respectively. The preamplifier is a FET-input charge sensitive type designed so that the additional noise introduced by the preamplifier is negligible

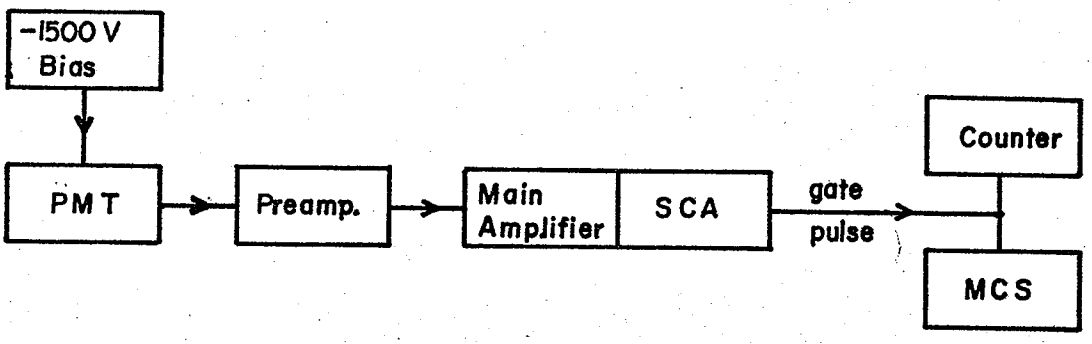

FIGURE 7a
ELECTRONICS FOR PROCESSING THE PHOTOMULTIPLIER OUTPUT PULSES

Bias Supply — Fluke 415B
Photomultiplier Tube (PMT) — RCA 31034
Main Amplifier and Single Channel Analyzer (SCA) — Ortec 486
Counter — General Radio 1192-B
Multichannel Scaler (MCS) — Nuclear Data ND-1200 Analyzer System

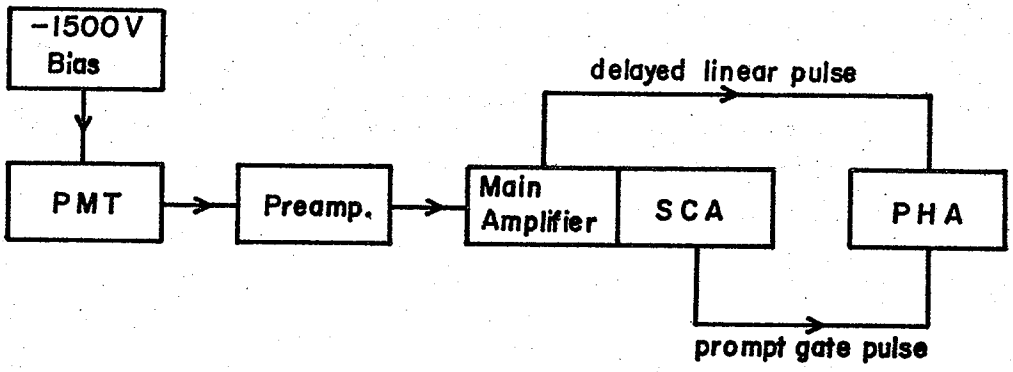

FIGURE 7b
ELECTRONICS FOR SETTING THE DISCRIMINATOR LEVELS

Pulse Height Analyzer (PHA) — Nucear Data ND-1200 Analyzer System

compared to that of the phototube (Figure 8). The remaining components are standard nuclear instrumentation modules.

The ND-1200 Analyzer system consists of an analog to digital converter (ND-560), data handling unit with 1024 channel memory, display oscilliscope and paper tape output interface. The system may be operated in a pulse height analysis mode while setting discriminator levels, or in a multichannel scaling mode when recording a scattered light spectrum.

To record a spectrum, the gratings of the monochromator and the channel advance of the MCS are stepped sychronously by clock signals derived from a 1 MHz crystal oscillator, while the photo-electron pulses are applied to the count input of the MCS. The dispersion of the spectrum recorded in the MCS is then simply determined from the number of grating steps taken during one channel advance. The dispersion used when collecting collision induced spectra was 10 channels/cm^{-1} (for convenience, not all the points have been plotted in the spectra of Figures 2, 9 and 12). The origin of the frequency scale is determined from the channel in which the peak of the Rayleigh line occurs. During aquisition of the spectrum, the count rate is displayed on a General Radio 1192B counter-timer. The background count rate is determined with the same instrument and used later as a correction to the scattering spectrum when computations are performed.

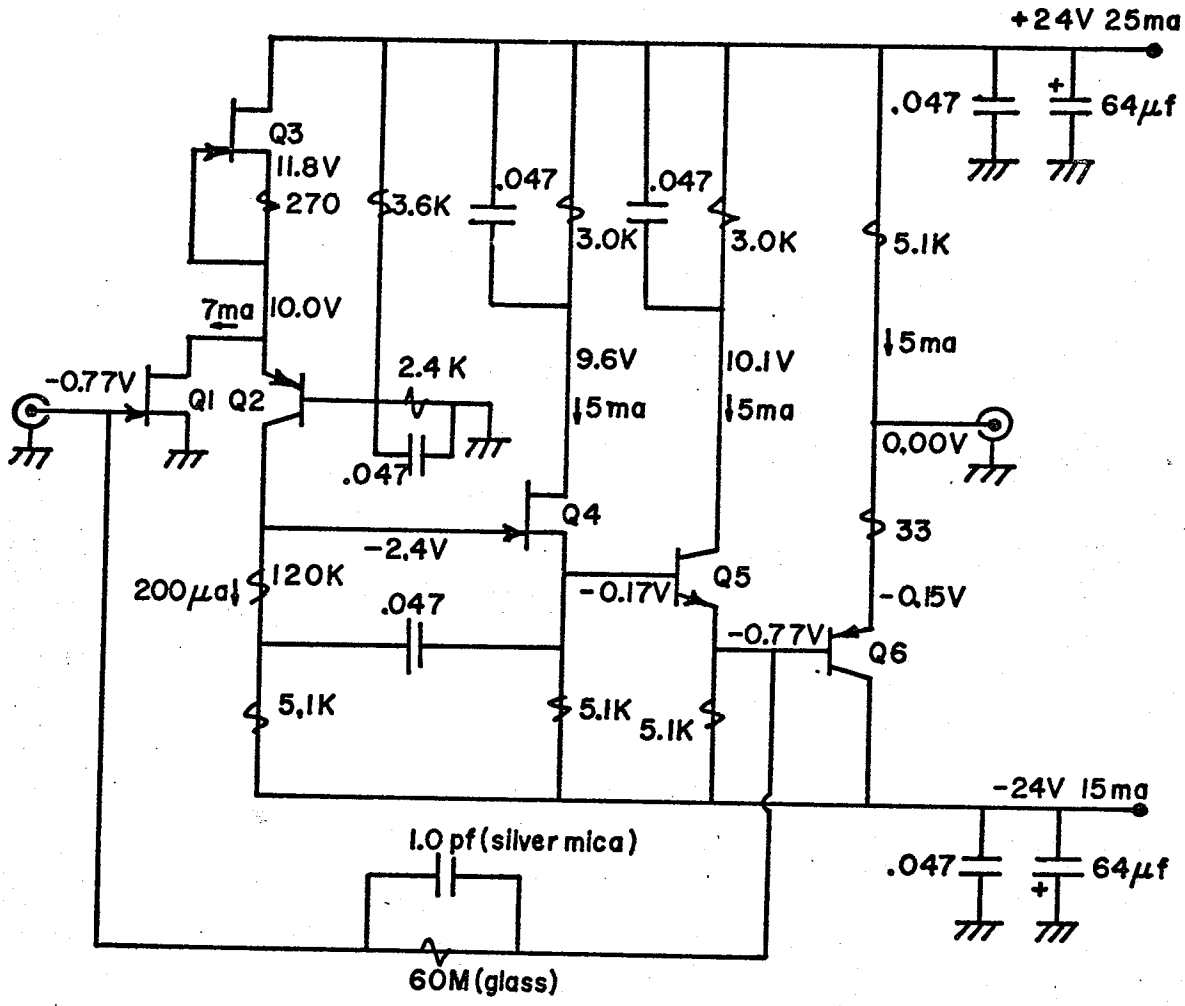

FIGURE 8

CHARGE SENSITIVE PREAMPLIFIER

Q1, Q3, Q4 are MPF 102 Si n-channel FET's.
Q2, Q5, Q6 are Si BJT's with $\beta > 100$.
Q1 and Q2 form a cascode pair and Q3 acts as a constant current source permitting a relatively large current in Q1, for high g_m, and a small current in Q2, for low noise.
Q4 is a source follower which bootstraps the load resistor of the cascode.
Q5 is an emitter follower which drives the output buffer and the feedback loop.
Q6 is an emitter follower which provides a low impedance output.

CHAPTER 3

LINE SHAPE ANALYSIS

The collision induced spectrum has been analyzed in terms of its line shape for two reasons. Firstly, when an appropriate representation has been found, the line shape function provides a concise summary of the data. Secondly, the discription in terms of a frequency spectrum allows many general features of the scattering mechanism to be obtained by inspection. Thus, the lineshape analysis is useful for providing the starting point for more detailed considerations of the scattering spectrum.

3.1 Method

The spectra from CF_4 and SF_6 have a shape which is typical of the profile of collision induced scattering obtained from atoms and isotropic molecules. At low densities, the intensity falls off nearly exponentially with frequency shift from the exciting line. At higher densities, a second exponential component appears. At the highest densities, the break point between the first and second component becomes less distinct and a logarithmic plot of the intensity profile shows a continuous curve rather than two separate slopes (Figure 9). Because of their shape, we have chosen to analyze the spectra in terms of functions exponential in frequency.

The simplest function of this type is $I(\omega)=A \exp(-\omega/\omega_o)$ where A and ω_o are the parameters, describing the shape of the spectrum, which are to be determined. This expression varies non-linearly with the parameter ω_o so that the nonlinear least squares

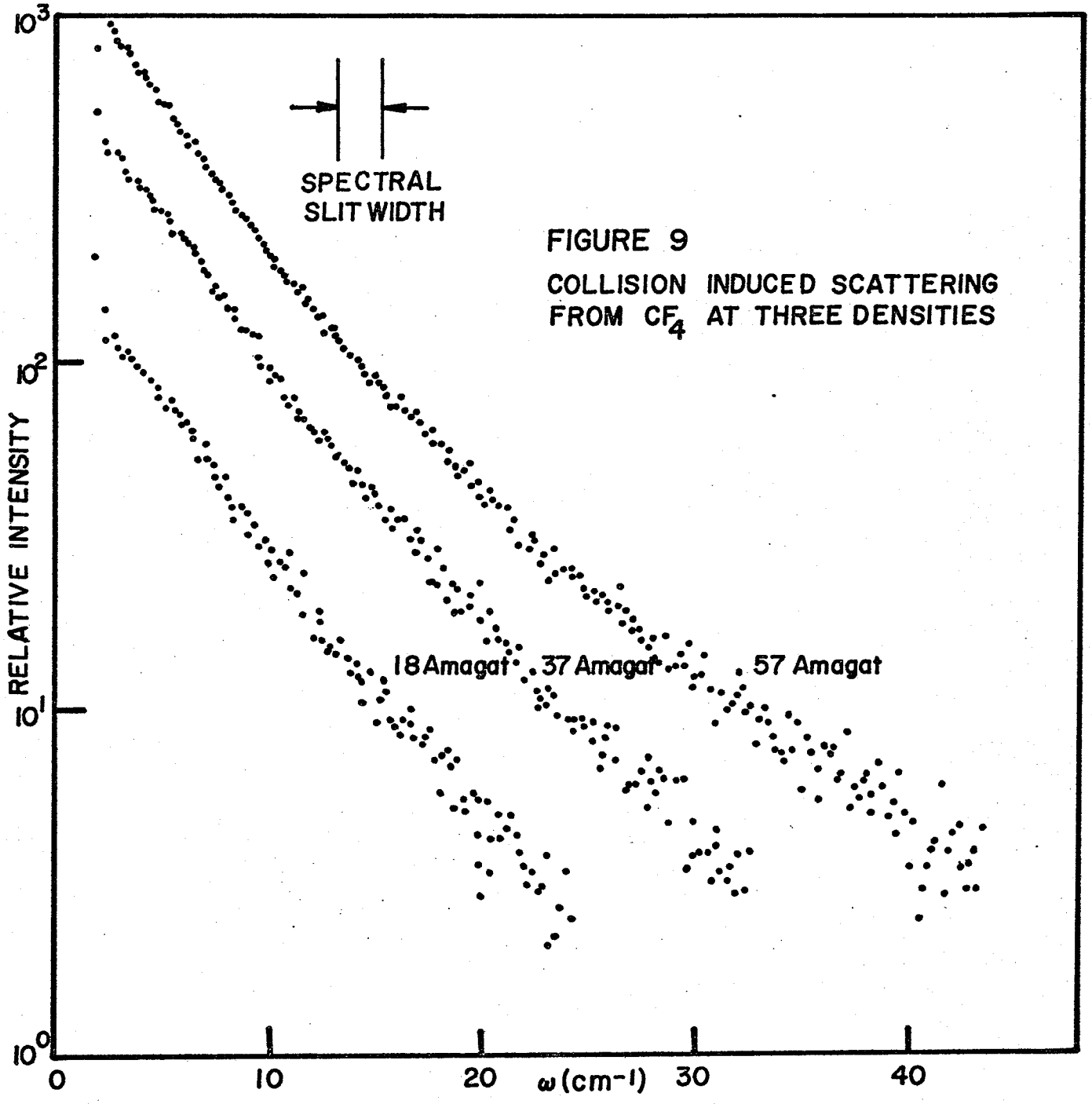

FIGURE 9

COLLISION INDUCED SCATTERING FROM CF_4 AT THREE DENSITIES

procedure has been adopted.[35,36] An initial guess of the parameter values is made and the Taylor expansion of the test function is evaluated about this point. Only terms up to first order in the parameters are retained and the resulting linearized test function is fitted to the data by the usual linear least squares technique. The revised parameter estimates are substituted for the initial guesses and the whole process repeated until some convergence criterion is satisfied. The weights for the data are obtained by assuming Gaussian counting statistics. Thus, if a point represents N counts, its weight is simply 1/N. The quality of the fit is judged by the χ^2-test.

The chief difficulty in extending this procedure to more complicated test functions is in arriving at initial parameter estimates which result in convergence. The program in Appendix A2 is designed to fit functions of the form:

$$F(x;A,a,B,b)=A \exp ax + B \exp bx$$

or

$$F(x;A,a)=A \exp ax$$

to the data.

3.2 CF_4 - Low Frequencies

Since the collision induced spectra obtained from isotropic molecules resemble those from the rare gases, except that the appearance of the second exponential component in the high frequency tail occurs at much lower densities, it seems that analysis of the low frequency scattering due to CF_4 in the same manner as for the rare gases might be profitable.

Fleury has studied collision induced light scattering from the rare gases (Ar, Ne, Kr, Xe) over a wide range of density and temperature.[37,38] Assuming an exponential representation for the spectrum,

$$I(\omega) = C \exp(-\omega/\omega_o)$$

and determining ω_o directly from the slope of the spectrum, he finds that in all cases ω_o can be represented by an expression:

$$\omega_o = \frac{A}{2\pi c}\left(\frac{\epsilon}{M\sigma^2}\right)^{\frac{1}{2}}\left(\frac{kT}{\epsilon}\right)^{\frac{1}{2}}\left[1 + \left(\frac{B\sigma^3\rho}{M}\right)^2\right] \qquad (3.1)$$

where M is the mass of the atom, ρ is the density and σ and ϵ are the parameters in the Lennard-Jones potential. With values of 3.0 ± 0.1, and 2.0 ± 0.1, respectively, for the dimensionless parameters A and B, this expression was found to produce excellent agreement with observations covering $0.7 < kT/\epsilon < 4$ and $0.05 < \rho\sigma^3/M < 1$ in Ar, Kr, and Xe.[38] This represents an extention to high frequency dynamics of the corresponding states principle (CSP), which asserts that the thermodynamic and transport coefficients for systems with the same form of intermolecular potential scale directly with the parameters of the potential. (The present experiments cover the range $1.5 < kT/\epsilon < 1.9$ and $0.03 < \rho\sigma^3/M < 0.3$ in CF_4 and SF_6.)

Fleury's expression carrys additional weight since Mahan has been able to show that the parameter A should be exactly equal to 3 in the case of a hard sphere gas.[39] The ρ^2 term, however, has not been explained and appears to be purely empirical in nature.

We have analyzed our data in a similar fashion by fitting an exponential function of the form $I(\omega) = C \exp(-\omega/\omega_o)$ over the frequency range 5 - 20 cm^{-1} using the non-linear least squares technique.

The lower limit of 5 cm^{-1} is chosen to minimize interference by the Rayleigh line, while the upper limit of 20 cm^{-1} is dictated by the appearance of the second exponential component at about 20 cm^{-1}. The single exponential function is not a very good representation of the spectrum and the reduced χ^2 for the fits was in the range 2-7. The results of this analysis are shown in Figure 10 where ω_o is plotted against density for a number of spectra.

For CF_4, eq. (3.1) predicts that

$$\omega_o = 5.65\ (1 + 3.14 \times 10^{-5} \rho^2)\ cm^{-1} \qquad (3.2)$$

with ρ expressed in Amagat units, and where $\epsilon/k = 152.5$ K (Kelvin) and $\sigma = 4.70$ Å have been substituted. When an expression of the form of eq. (3.1) is fitted to the data of Figure 10, the result is:

$$\omega_o = (4.92 \pm 0.03)\ (1 + (3.24 \pm 0.26) \times 10^{-5} \rho^2)\ cm^{-1} \qquad (3.3)$$

which is in good agreement with the prediction of eq. (3.2). The quadratic curve, however, does not fit the data very well, the standard deviation being 0.15 cm^{-1}. Particularily at low densities, the data is better represented by an expression linear in density:

$$\omega_o = (4.63 \pm 0.04)\ (1 + (3.32 \pm 0.20) \times 10^{-3} \rho)\ cm^{-1} \qquad (3.4)$$

with a lower standard deviation of 0.11 cm^{-1}.

Nevertheless, the good agreement between eq. (3.2) and eq. (3.3) leads one to conclude that the extended CSP links CF_4 and the rare gases, and that the Lennard-Jones potential is a good approximation to the true intermolecular potential for CF_4. Mac Cormack and Schneider reached the same conclusion based on their compressibility data for CF_4.[25]

The agreement of the analysis for CF_4 with Fleury's scaling law also suggests that the same scattering mechanism is operating in CF_4

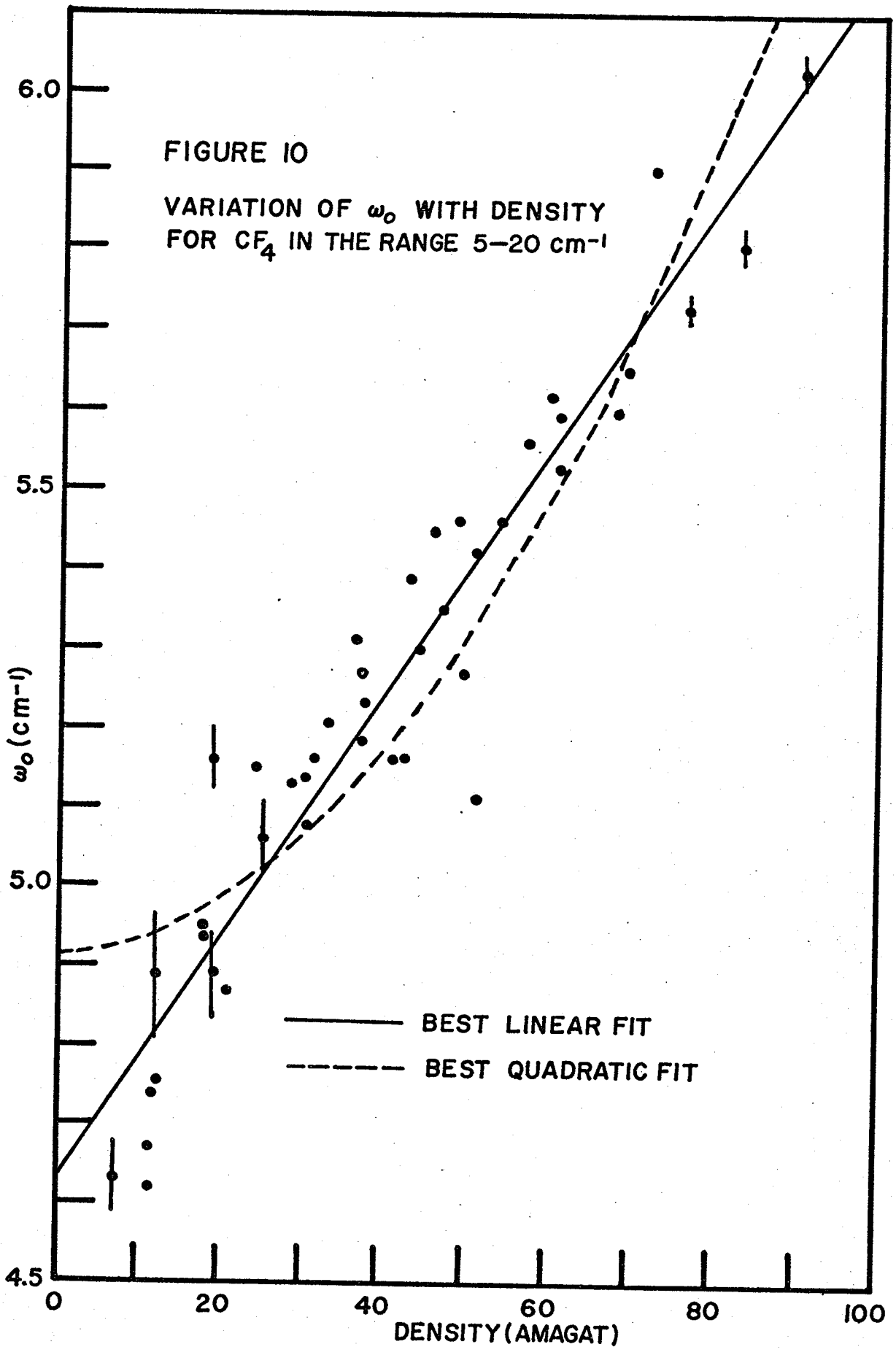

FIGURE 10

VARIATION OF ω_o WITH DENSITY FOR CF_4 IN THE RANGE 5–20 cm^{-1}

as in the rare gases. For the rare gases at low frequencies and at low densities, the DID interaction is believed to be the most important scattering mechanism.[1,18,41] Thus it is to be also expected that the DID interaction is the predominant scattering mechanism for CF_4 at low frequency and low density.

3.3 CF_4 - Total Profile

Since a second slope appears at high frequencies as the density is increased, an expression which is the sum of two exponential functions, $I(\omega) = A \exp(-\omega/\omega_1) + B \exp(-\omega/\omega_2)$ was also fitted to the spectra. The fits extend over the range 5-45 cm^{-1}. The lower limit is again chosen to minimize interference by the Rayleigh line, and the upper limit is selected to allow the fits to be made over a reasonable density range. At lower densities the tail disappears completely by 45 cm^{-1} and this determines the upper limit for all the fits, even though the tail extends up to 70 cm^{-1} at the highest densities. The values of ω_1 and ω_2 depend upon the range chosen, but their variation with density does not change greatly. The quality of the fits is excellent, with reduced χ^2 in the range 1.0-1.1. Figure 11 shows the variation of ω_1 and ω_2 with density.

If the exponentials are extrapolated to zero frequency and integrated from zero to infinity, then the contribution of each to the total integrated intensity is obtained. The ratio of the intensities I_1/I_2 is also plotted in Figure 11. The ratio is about 2.5 and decreases slowly with increasing density, demonstrating that the second exponential is becoming more important.

Since ω_2 is larger than ω_1, the time duration of the interaction

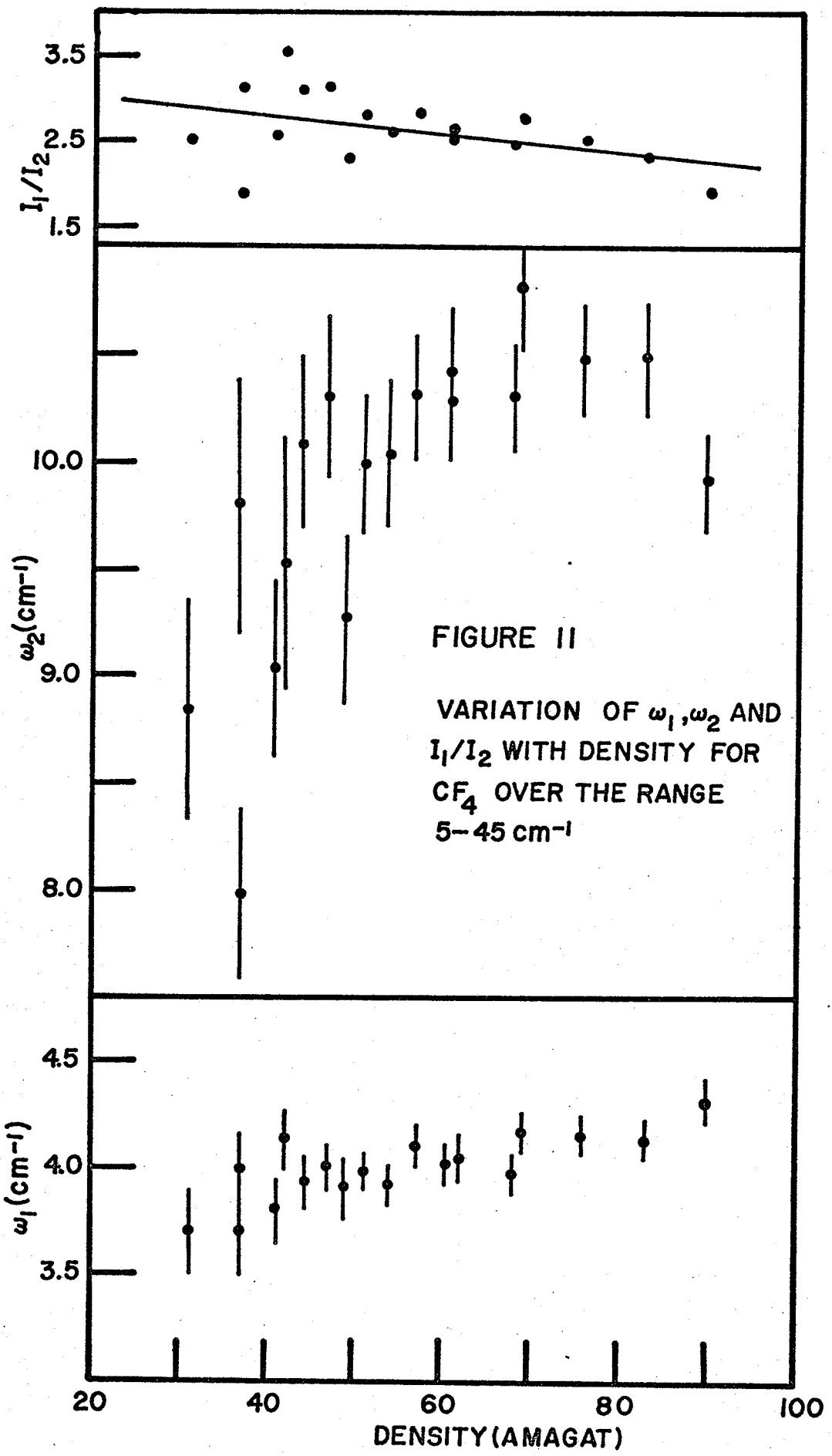

FIGURE 11

VARIATION OF ω_1, ω_2 AND I_1/I_2 WITH DENSITY FOR CF_4 OVER THE RANGE 5–45 cm^{-1}

giving rise to ω_2 must be shorter than for ω_1. There are several possible mechanisms for explaining the second exponential component. However, even rough calculations show that two of the possibilities, second order DID and octupolar effects, are several orders of magnitude too weak to account for the observed high frequency scattering.[40] This leaves only models based on close encounters. Bucaro and Litovitz, in their treatment of collision induced scattering from liquids, developed the IBC model in which the scattering is due entirely to close encounters.[13] They calculated a collision time, using a method due to Nikitin,[42] which is determined solely by the dynamics and is independent of the nature of the interaction inducing $\beta(r)$. The characteristic frequency, ω_o, is found to be approximated by:

$$\omega_o \doteq \frac{6}{2\pi^2 c\sigma}\left(\frac{2kT}{M}\right)^{\frac{1}{2}}\left[1 - \frac{2}{\pi}\arctan\left(\frac{2\epsilon}{kT}\right)^{\frac{1}{2}}\right]^{-1} \quad \text{cm}^{-1}. \qquad (3.5)$$

This expression gives a value of $\omega_o = 10.3$ for CF_4 which compares very favorably with the value of ω_2 determined from our data - the value of ω_2 increases sharply at low densities and then levels off at a value of 10.5 cm^{-1} (Figure 11). The initial increase is believed to be spurious and arises because the high frequency tail at low densities is too weak for reliable measurements to be made. In this case, the fitting program is not able to determine the correct parameters for the second exponential and tends to return values which make it merely a scalar multiple of the more intense low frequency component.

A conclusion that the shape of the high frequency tail in CF_4 is determined principally by the intermolecular potential would agree with the results of analytical calculations[14] and computer experiments[43]

on the rare gases. These investigations have used only the DID induction mechanism, which also indicates that it is not necessary to introduce additional interactions to account for the high frequency tail.

3.4 SF_6

The spectra obtained from SF_6 (eg. Figure 12) are similar to those obtained from CF_4, and the analysis proceeds in a fashion completely analogous to that described for CF_4.

The SF_6 spectra were first fitted with a single exponential over the range 2.5 - 9.0 cm^{-1}. Again, the lower bound is necessary to exclude contributions from the strong Rayleigh scattering, and the upper limit is set at the place where the second exponential component becomes important. The value of $\omega_o = 3.03 \pm 0.14$ cm^{-1} is obtained and no systematic variation with density is apparent. The fits are generally poor because of the strong curvature of the profile, with reduced χ^2 in the range 1.5 - 3.0.

Substitution of ϵ/k = 200.9 K and σ = 5.51 Å into eq. (3.1) yields the prediction that:

$$\omega_o = 3.73\ (1 + 3.02 \times 10^{-5} \rho^2)\ cm^{-1}. \qquad (3.6)$$

The value of ω_o predicted by eq. (3.6) varies only about 5% over the density range studied, which is smaller than the scatter of the experimentally determined values of ω_o. The agreement between eq. (3.6) and the experimental results suggests that the scattering at low frequencies is predominantly through the DID mechanism.

Next the SF_6 spectra were fitted by a sum of exponentials over the range 2.5 - 27.5 cm^{-1}. These fits are much better, with a

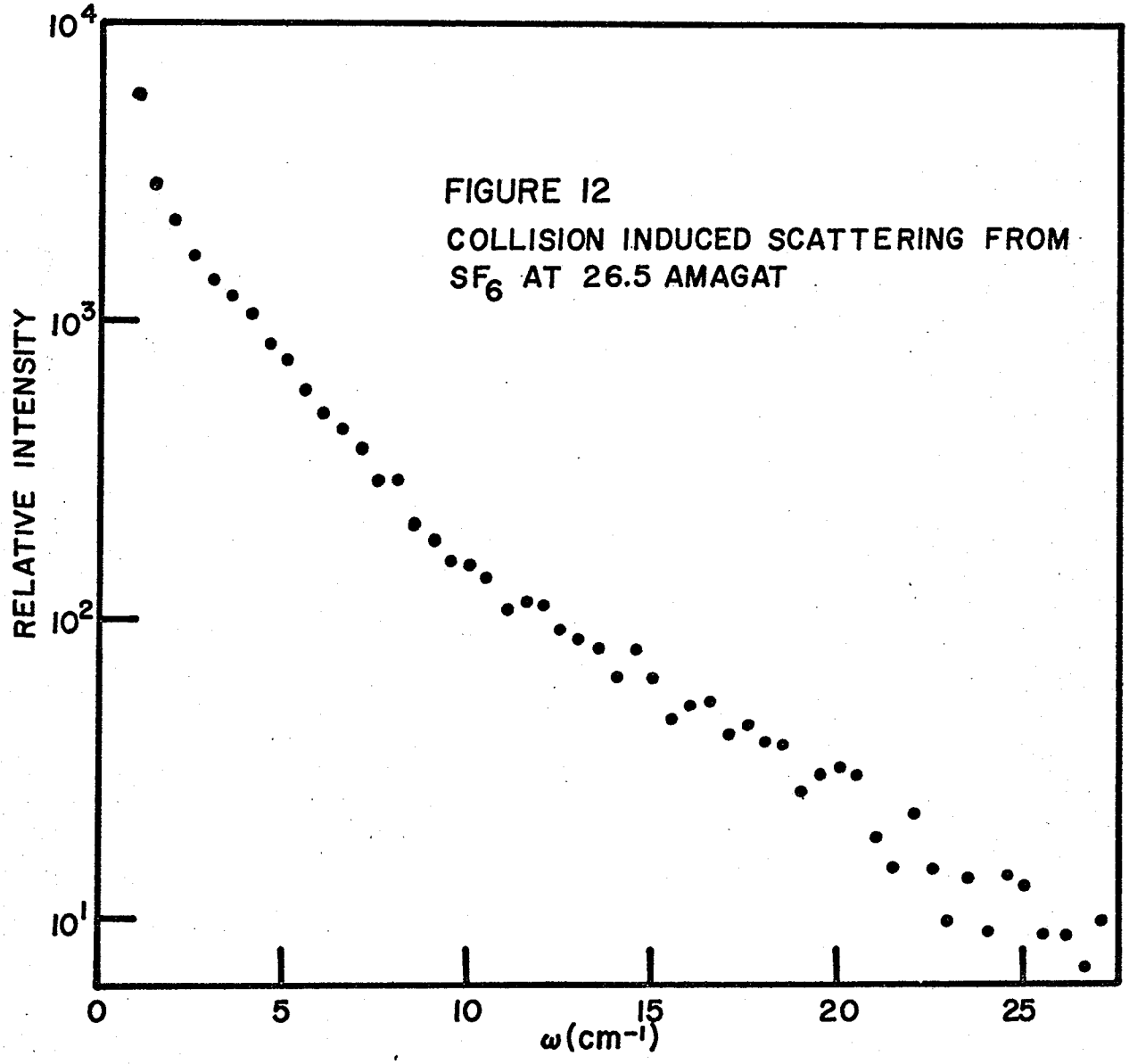

FIGURE 12

COLLISION INDUCED SCATTERING FROM SF_6 AT 26.5 AMAGAT

reduced χ^2 of about 1.2. The result of this procedure is $\omega_1 = 2.42 \pm 0.13$ cm^{-1} and $\omega_2 = 6.76 \pm 0.33$ cm^{-1}. The ratio of integrated intensities I_1/I_2 is 3.75 ± 0.43. The first exponential component is larger for SF_6 than CF_4 (I_1/I_2 is about 2.5 for CF_4) but otherwise the discription of the profiles is very similar. The ratio of the frequencies ω_2/ω_1 is 2.80 for SF_6 and 2.64 for CF_4, and the frequencies themselves, ω_1 and ω_2, scale with $(M\sigma^2)^{\frac{1}{2}}$ between the two cases.

Intensity considerations again exclude all models but that of close collisions for explaining the high frequency tail. Equation (3.5), in the case of SF_6, predicts $\omega_o = 7.45$ cm^{-1} which agrees well with the experimental value $\omega_2 = 6.76$ cm^{-1}. This indicates that the high frequency scattering for SF_6 is determined by the shape of the intermolecular potential alone, as also seems to be the case for the rare gases and CF_4.

CHAPTER 4

MOMENT ANALYSIS

Analysis of collision induced spectra in terms of moments is attractive for two reasons. Firstly, the experimental quantities to be measured are clearly specified. Secondly, theoretical calculations of the moments of the spectral distribution are more conveniently formulated and performed than the corresponding direct calculations of the line shape. The moment analysis[44,45] follows the method of McTague, Levine and Birnbaum.[12,41,46]

4.1 Method

If one considers only pairwise interactions and correlations in a fluid composed of optically isotropic molecules, the scattered intensity due to the induced polarizability becomes simply:

$$I(\omega) = (2\pi)^{-1} \int_{-\infty}^{\infty} J(t) \exp(-i\omega t)\, dt \qquad (4.1)$$

$$J(t) = \frac{V^2 \rho^2 k_i^4 I_i}{2\,(4\pi R_o)^2} \; F(t) \qquad (4.2)$$

$$F(t) = \langle \alpha(0)\,\alpha(t)\;(\hat{n}_i \cdot \hat{n}_f)^2 \rangle + \langle \beta(0)\,\beta(t)\,P_2(\cos\theta) \rangle \left[(45)^{-1}\,(3 + (\hat{n}_i \cdot \hat{n}_f)^2)\right]. \qquad (4.3)$$

Here V is the volume of the scattering source, ρ is the number density of molecules in the source, k_i is the magnitude of the propagation vector of the incident light, I_i is the incident intensity, R_o is the distance from the source to the observation point and, $\hat{n}_i$ and $\hat{n}_f$ are the unit polarization vectors of the incident and scattered light. The ensemble averages involve the spherical and anisotropic

parts of the induced polarizability, $\alpha(r)$ and $\beta(r)$ respectively, which become functions of time through the variation of the intermolecular separation, r(t). They are defined by

$$\alpha(r) = 1/3\ (\alpha_{\parallel} + 2\alpha_{\perp}) - 2\alpha \qquad (4.4)$$

$$\beta(r) = \alpha_{\parallel} - \alpha_{\perp} \qquad (4.5)$$

where $\alpha_{\parallel}$ and $\alpha_{\perp}$ are the polarizabilities of the pair of colliding molecules parallel and perpendicular to the intermolecular axis, and α is the scalar polarizability of an isolated molecule. P_2 is the second Legendre polynomial and θ is the angle between the directions of the intermolecular axis at times 0 and t.

The scattering due to $\alpha(r)$ is expected to be much weaker than that due to $\beta(r)$,[12] and by performing experiments with the VH polarization geometry, F(t) is reduced to:

$$F(t) = (15)^{-1} \langle \beta(0)\beta(t)\ P_2(\cos\theta) \rangle . \qquad (4.6)$$

Consideration of $\alpha(r)$ will therefore be omitted in the following discussion. The proportionality constant, determined by the experimental parameters in the expression for $I(\omega)$, will also be suppressed by working with the spectral distribution function $D(\omega)$.

Thus, the observed spectral distribution for the depolarized scattering is related to the anisotropic part of the pair polarizability through the Fourier transform:

$$D_{\beta}(\omega) = \int_{-\infty}^{\infty} dt\ \exp(-i\omega t)\, \phi_{\beta}(t) \qquad (4.7)$$

$$\phi_{\beta}(t) = V \langle \beta(0)\beta(t)\ P_2(\cos\theta) \rangle \qquad (4.8)$$

where $D(\omega)$ is the normalized spectral distribution function and $\phi(t)$ is the classical correlation function.

Taking the inverse Fourier transform of eq. (4.7) we obtain the following expression for $\phi_{\beta}(t)$ in terms of $D_{\beta}(\omega)$:

$$\phi_\beta(t) = (2\pi)^{-1} \int_{-\infty}^{\infty} D_\beta(\omega) \exp(i\omega t)\, d\omega . \qquad (4.9)$$

Expanding both sides of this expression in a Taylor series about t=0, one has:

$$\phi_\beta(t) = \sum_{n=0}^{\infty} \frac{t^n}{n!} \left[\frac{d^n}{dt^n} \phi_\beta(t) \right]_{t=0} \equiv \sum_{n=0}^{\infty} \frac{t^n}{n!} \phi_\beta^{(n)}(0)$$

$$= (2\pi)^{-1} \sum_{n=0}^{\infty} \frac{(it)^n}{n!} \int_{-\infty}^{\infty} \omega^n D_\beta(\omega)\, d\omega . \qquad (4.10)$$

Comparing coefficients of corresponding terms and using the fact that the correlation function is even in time, one obtains the following relations between derivatives of the correlation function at t=0 and the moments of the spectral distribution:

$$\phi_\beta^{(2n)}(0) = (2\pi)^{-1} (-1)^n \int_{-\infty}^{\infty} \omega^{2n} D_\beta(\omega)\, d\omega . \qquad (4.11)$$

Now the expression (4.8) may be used to evaluate the moments $\phi_\beta^{(2n)}(0)$ in terms of $\beta(r)$. The results for the first three are:[12,41,47,48]

$$\phi_\beta^{(0)}(0) = 4\pi \int_0^{\infty} \beta^2(r)\, g(r)\, r^2\, dr \qquad (4.12)$$

$$\phi_\beta^{(2)}(0) = -4\pi \frac{kT}{\mu} \int_0^{\infty} \left[\left(\frac{d\beta}{dr} \right)^2 + 6 \left(\frac{\beta}{r} \right)^2 \right] g(r)\, r^2\, dr \qquad (4.13)$$

$$\phi_\beta^{(4)}(0) = 4\pi \left\{ \left(\frac{kT}{\mu} \right)^2 \int_0^{\infty} \left[72 \left(\frac{\beta}{r^2} \right)^2 + 8 \left(\frac{1}{r} \frac{d\beta}{dr} \right)^2 - \frac{36}{r^2} \beta \frac{d^2\beta}{dr^2} + \frac{4}{r} \frac{d\beta}{dr} \frac{d^2\beta}{dr^2} + 3 \left(\frac{d^2\beta}{dr^2} \right)^2 \right]^2 g(r)\, r^2\, dr \right.$$

$$- \frac{kT}{\mu^2} \int_0^{\infty} \left[\left(\frac{d\beta}{dr} \frac{dV}{dr} \right) \left(2 \frac{d^2\beta}{dr^2} + \frac{4}{r} \frac{d\beta}{dr} - \frac{36}{r^2} \beta \right) + 48 \frac{\beta^2}{r^3} \frac{dV}{dr} \right] g(r)\, r^2\, dr + \frac{1}{\mu^2} \int_0^{\infty} \left(\frac{d\beta}{dr} \frac{dV}{dr} \right)^2 g(r)\, r^2\, dr \left. \right\} . \qquad (4.14)$$

In the above, μ is the reduced mass of the colliding pair and g(r) is the radial distribution function defined by:

$$g(r) = \exp(-V(r)/kT) \tag{4.15}$$

where V(r) is the intermolecular pair potential. By use of the above expressions, one may evaluate parameters in a model of the pair polarizability anisotropy, $\beta(r)$.

Several forms for $\beta(r)$ have been suggested.[22,41,48] It is clear from the analysis performed in Chapter 3, of the collision induced spectra in terms of the line shape, that the DID mechanism is of importance for CF_4, SF_6 and the rare gases. However, on the basis of the same analysis, no definite conclusions could be drawn about the importance or the form of any additional contributions to $\beta(r)$. The induction mechanisms, other than DID, mentioned in the introductory chapter were of short range. For this reason we have chosen a model for $\beta(r)$ of the form:

$$\beta(r) = \frac{6\alpha^2}{r^3} + \frac{B}{r^p} \tag{4.16}$$

where $6\alpha^2 r^{-3}$ is the contribution due to the DID mechanism and the $B\,r^{-p}$ term is an empirical approximation representing all other interactions. B and p are the parameters to be determined in the analysis and it is expected that the second contribution to $\beta(r)$ will be of much shorter range than the DID term.

Having chosen the form of the model for $\beta(r)$ one may evaluate the expressions for the moments. Upon representing the intermolecular potential by the Lennard-Jones 6-12 potential, and substituting eq. (4.16) into eq. (4.12) and (4.13), one arrives at the following relations:

$$\phi_\beta^{(0)}(0) = 4\pi \left\{ 36\,\alpha^4 \sigma^{-3} \int_0^\infty x^{-4}\, g(x)\, dx + 12\,\alpha^2\, B\, \sigma^{-p} \int_0^\infty x^{-(1+p)}\, g(x)\, dx + B^2\, \sigma^{3-2p} \int_0^\infty x^{2(1-p)}\, g(x)\, dx \right\} \quad (4.17)$$

$$\phi_\beta^{(2)}(0) = -4\pi\left(\frac{kT}{\mu}\right) \left\{ 15(6\alpha^2)^2 \sigma^{-5} \int_0^\infty x^{-6}\, g(x)\, dx + 36\,\alpha^2\, B(p+2)\, \sigma^{-(2+p)} \int_0^\infty x^{-(3+p)}\, g(x)\, dx + B^2\,(p^2+6)\, \sigma^{1-2p} \int_0^\infty x^{-2p}\, g(x)\, dx \right\} \quad (4.18)$$

where $x = r/\sigma$ (4.19)

$$g(x) = \exp\left(\frac{-4\epsilon}{kT} \left(x^{-12} - x^{-6} \right) \right) \quad (4.20)$$

and σ and ϵ are the parameters in the Lennard-Jones potential. Equation (4.16) may also be rewritten so that the parameters to be solved for, p and y, are both dimensionless:

$$\beta(x) = 6\,\alpha^2 \sigma^{-3} \left(x^{-3} + (y/6)\, x^{-p} \right) \quad (4.21)$$

where $y/6 = B\,\alpha^{-2} \sigma^{3-p}$. (4.22)

The moments $\phi_\beta^{(0)}(0)$ and $\phi_\beta^{(2)}(0)$ are computed from the data by using eq. (4.11). In order to determine $\beta(r)$, one must now find the values of B and p which satisfy eq. (4.17) and eq. (4.18) simultaneously.

If we specify p, the integrals occurring in eq. (4.17) and eq. (4.18) may be evaluated numerically (or from tables).[49] When this is done, each equation becomes a simple quadratic in B. The roots of eq. (4.17) and eq. (4.18) will not in general be the same. Therefore, the RHS's are evaluated for discrete values of p over the range $2 < p < 16$ and a search is made for pairs of equations, with the same p value, which are solved by approximately the same values of B.

Then, in the neighbourhood of the corresponding p values, the method of inverse interpolation with a fourth order polynomial was used to find the values of B and p exactly solving the system of equations. The computations were performed using the program of Appendix A3. The system of eq. (4.17) and eq. (4.18) generally yields two solutions and to distinguish between them either comparison of calculated and measured values of the higher moments or a resort to physical considerations must be employed.

4.2 Application to the Present Data

In applying the method of moments to the present data, two difficulties arise. Firstly, relative rather than absolute intensities have been measured. Following the procedure of Levine and Birnbaum,[41] we have used the relation between the integrated intensity of the scattered light and the second virial Kerr coefficient, B_K[12,41,50,51]

$$B_K = \frac{8\pi^2 N_o^2}{405\ kT} \int_o^\infty \beta_o(r)\beta_\omega(r)\ g(r)\ r^2\ dr \qquad (4.23)$$

where N_o is Avogadro's number, and $\beta_o(r)$ and $\beta_\omega(r)$ are the induced polarizability anisotropies at frequencies 0 and ω. The integral is almost the same as the one that appears in eq. (4.12) for the zeroth moment so that B_K measurements can be used to normalize the data. Unfortunately, this procedure is not without its problems. Recently, it has been found that the discrepencies between theory and experiment do not behave consistently for depolarized light scattering and the Kerr effect, even in the case of the rare gases.[52,53] The relative difference between calculations of B_K based on the DID

model and experimental measurements of B_K increases linearly with increasing atomic number for Ar, Kr, and Xe. The corresponding relative differences between theory and experiment for the total Rayleigh depolarization ratio decrease linearly with atomic number. One reason may be that B_K depends on $\beta_o(r)\beta_\omega(r)$ while light scattering depends on $\beta_\omega^2(r)$. For the rare gases the values of $\beta_o(r)$ and $\beta_\omega(r)$ are almost equal. In the case of a large molecule such as CF_4 and SF_6, they may differ significantly. Consequently, the normalization procedure we have adopted must be considered approximate.

The second difficulty is that measurements were not made over the whole range of ω from zero to infinity. The high frequency part of the spectrum could not be reliably measured because the light signal there is too small compared to the noise. That part of the spectrum is increasingly more important as higher moments are considered. At the other end of the range, the spectrum near zero shift is not accessible because of the strong Rayleigh scattering which overlaps the depolarized spectrum in this region. Because of the exponential-like nature of the spectrum, this portion of the spectrum makes a large contribution to the integrated intensity, though not to any of the higher moments. However, because of the way in which the intensity has been normalized, an error in the relative integrated intensity is effectively carried over, in equal measure, to the other moments. In order to account for the low frequency and high frequency ends of the spectrum we have extrapolated the observed profile to zero and infinity using the two-exponential fits obtained in the lineshape analysis. Appendix A4 contains the program used for computing the experimental values of the moments, using data from

the observed profile directly and incorporating the extrapolations where necessary. Since the sum of exponentials model used in fitting to the spectra does not accurately represent the data over the whole observed frequency range, it is clear that systematic errors can be expected in the extrapolation. In fact, it has been suggested that a completely different functional form, the squared Lorentzian, $I(\omega) \propto (1 + (\tau\omega/2)^2)^{-2}$, is appropriate for discribing the collision induced profile.[54] Despite these problems, it has been confirmed that the extrapolation does not lead to gross errors.[55]

4.3 CF_4

In solving for the parameters in $\beta(x)$ of eq. (4.21) for CF_4, the data of Table 1 were used. When the moment analysis was carried out, two sets of parameters p and y were obtained at all densities. For the set with the smaller value of p, in the range 3-5, y was always negative; for the other set, p was in the range 7-9 and y was always positive. Over the range of 50-100 Amagat in density, the solutions obtained were essentially independent of density. Below 50 Amagat however, the average values of p and y returned by the analysis decreased sharply and the results of experiments at any given density became totally irreproduceable. At low densities, the frequency range over which the spectrum was observable was so restricted that it no longer adequately represented the complete profile and the moment analysis failed. The average values of the parameters, for densities above 50 Amagat where the moment analysis was successful, are (i) $p = 4.05 \pm 0.1$ and $y/6 = -2.85 \pm 0.03$ and

TABLE 1 - COMPARISON OF RARE GAS AND MOLECULAR DATA

Gas	B_K (10^{+12}esu) expt [a]	B_K (10^{+12}esu) calc [a]	σ(Å) [b]	ϵ/k (K) [b]	α(Å^3) [a]	α^o(Å^3) [a]	M(amu)	$\phi^{(0)}$ [c] (Å^9)	$-\phi^{(0)}/\phi^{(2)}$ [c] (10^{-26}sec^2)
Ar	4.1±0.6	5.6	3.41	119.8	1.642	1.663	40	3.02±4.4	12.5
Kr	16±14	26	3.60	171	2.484	2.517	84	93.5±13.9	12.5
Xe	65±22	140	4.10	221	4.045	4.113	131	468±69	19.8
CF_4	37.7±3.6	25.2	4.70	152.5	2.85	3.85	88	270±30	17.6
SF_6	300±40	170	5.51	200.9	4.470	6.505	146	2170±290	98.4

a) from references 50 and 51, measured at 632.8 nm.

b) rare gas data from J. O. Hirshfelder, G. F. Curtis, R. B. Bird, Molecular Theory of Gases and Liquids (Wiley, New York, 1954); CF_4 and SF_6 data from refernces 24 and 25

c) rare gas results from reference 41; for CF_4 and SF_6 $\phi^{(0)}$ is calculated from the experimental Kerr effect data of references 50 and 51 using eq. (4.12) and eq. (4.23); $-\phi^{(0)}/\phi^{(2)}$ is determined from the author's data using eq. (4.11)

(ii) $p = 8.51 \pm 0.2$ and $y/6 = 0.757 \pm 0.02$. Thus, the two possible forms of the polarizability function are:

$$\beta(x) = 6\alpha^2\sigma^{-3}\left(x^{-3} - 2.85\, x^{-4.05} \right) \qquad (4.24)$$

$$\beta(x) = 6\alpha^2\sigma^{-3}\left(x^{-3} - 0.757\, x^{-8.51} \right). \qquad (4.25)$$

In order to distinguish between these two forms, the obvious test is to see if both give reasonable values for the higher moments. When the RHS's of eq. (4.12) and eq. (4.14) are evaluated with p=4.05, one obtains $\phi^{(4)} / \phi^{(0)} = 3.38 \times 10^{50}\ \text{sec}^{-4}$. With $p = 8.51$ the result is $\phi^{(4)} / \phi^{(0)} = 4.36 \times 10^{50}\ \text{sec}^{-4}$. In order to estimate the fourth moment from our data, we elected to work with the function fitted to the profile in the lineshape analysis, rather than to use directly the measured intensities which are not precisely known for large frequency shifts. Since the fitted function lies below the experimental points at high frequencies, the value of $\phi^{(4)} / \phi^{(0)} = 1.1 \times 10^{50}\ \text{sec}^{-4}$ obtained upon integration is expected to be a lower bound. This value is compatible with both possible forms of $\beta(x)$.

While the forms of eq. (4.24) and eq. (4.25) appear to be quite different, Figure 13 demonstrates that over the physically accessible range of $x > x_o$ the corresponding curves for $\beta^2(x)$ are almost indistinguishable (x_o is the distance of closest approach at the specified temperature).

The difficulty in discerning between the two forms arises because light scattering measurements are sensitive to $\beta^2(x)$ rather than $\beta(x)$. Without knowledge of the sign of $\beta(x)$, only measurements of greater precision will enable one to separate the two curves of Figure 13.

It is useful to compare the results for CF_4 with the results

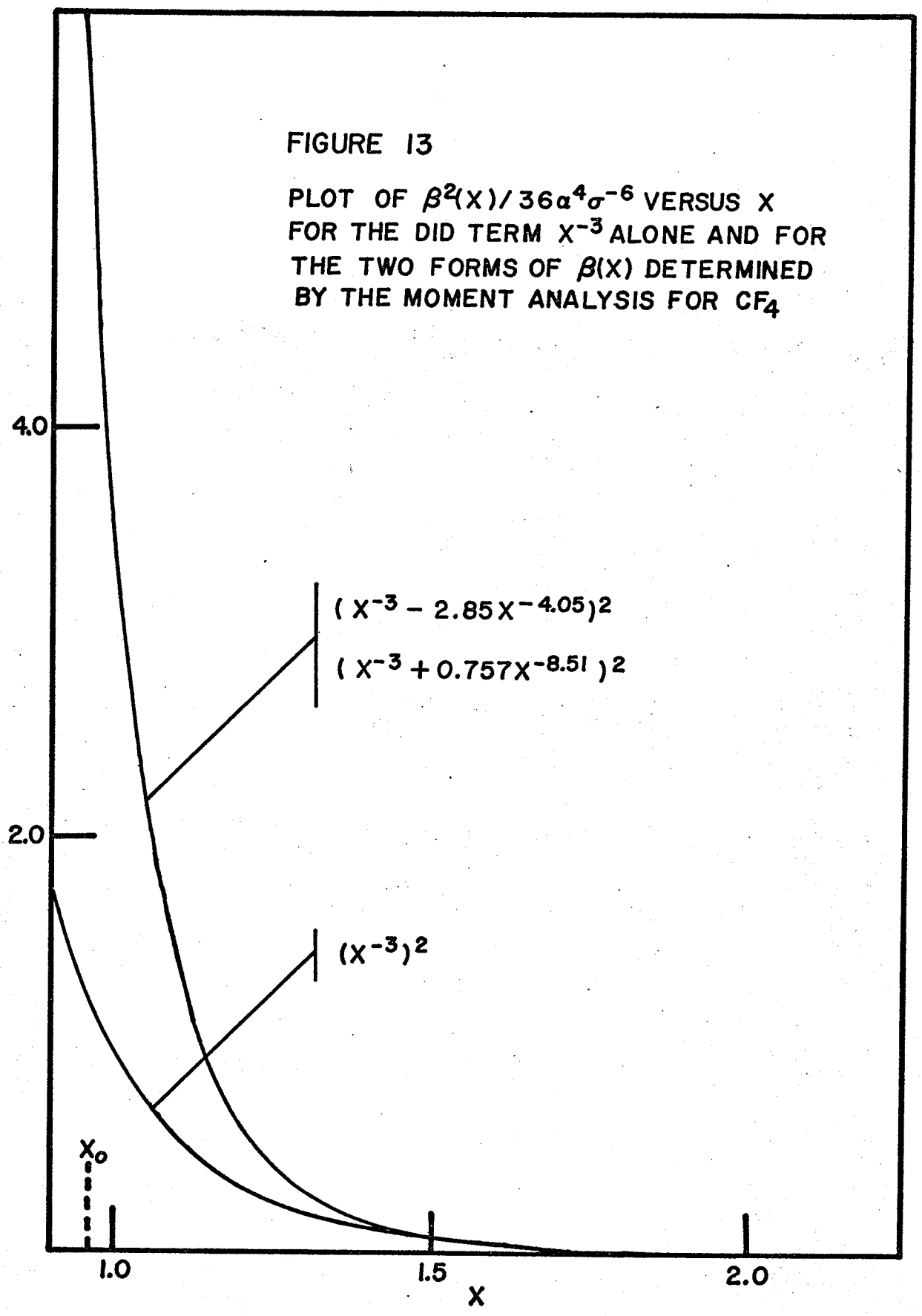

FIGURE 13

PLOT OF $\beta^2(X)/36\alpha^4\sigma^{-6}$ VERSUS X FOR THE DID TERM X^{-3} ALONE AND FOR THE TWO FORMS OF $\beta(X)$ DETERMINED BY THE MOMENT ANALYSIS FOR CF_4

summarized in Table 2, obtained in the analysis of the rare gases. The tabulated values were obtained using a Lennard-Jones potential and a model for $\beta(x)$ with a term $(y/6)\ x^{-p}$. In all cases a long range and a short range solution appears. For the rare gases, the correction to the polarizability function is always negative and always decreases the magnitude of $\beta(x)$ in the region $x > x_o$. This is in agreement with the Kerr effect data, where the experimental value of B_K is always smaller than the value calculated using the DID model. For CF_4, the additional term may be positive or negative, but in either case the correction increases the magnitude of $\beta(x)$, again in agreement with the Kerr effect data. Levine and Birnbaum [41] in their analysis of Ar, Kr, and Xe, anticipated that the correction to the polarizability would be of short range, and accordingly dismissed the long range solutions as physically unreasonable. However, Lallemand[48] has performed an extensive analysis for argon in which he has considered the Kihara, Barker-Pompe, Dymond-Alder and Lennard-Jones 6-16 potentials as well as treating both $(y/6)\ x^{-p}$ and $\exp(-x/d)$ as possible forms for the second term of $\beta(x)$. In all cases, the short range solution gave fourth and sixth moments which were too large and, in contradiction to the reasoning of Levine and Birnbaum, it was discarded in favor of the long range term.

Recently, calculations of increasing sophistication have been done to determine the polarizability of triplet H_2 [56,57], He_2 [58,59,60] and Ar_2 [61]. Lallemand's conclusion seems to be supported by the results of these detailed calculations. The SCF Hartree-Fock calculation of O'Brien et al[59] for He_2 returns values of $\beta(x)$ which

TABLE 2 - MOMENT ANALYSIS RESULTS

Gas	p	y/6
Ar [a]	6.5	- 0.223
	11.1	- 0.330
Kr [a]	9.2	- 0.847
	3.5	-
Xe [a]	9.6	- 0.957
	3.5	-
Ar [b]	4.15	- 0.23
	10.75	- 0.51
CF_4	4.05	- 2.85
	8.51	+ 0.757
SF_6	2.88	- 3.0
	2.82	+ 0.91

a) Levine and Birnbaum, reference 41

b) Lallemand, reference 48

may be represented by a DID term and an exponential in x. In the region near $r = \sigma$, the exponential varies approximately as r^{-6}. For the rare gases, the evidence points towards the long range solution as the correct one.

There is evidence in favor of the short range contribution as well. A short range solution is consistent with previous work on liquids with the IBC model.[16,20,62] For isotropic molecules an induced polarizability varying as r^{-9} seems to produce best agreement with the data, though there are ambiguities in the interpretation of the results.

It is not clear that $\beta(r)$ for CF_4 should behave just as $\beta(r)$ for the rare gases. The decrease of $\beta(r)$ with decreasing r in the rare gases seems to be associated with the strong repulsive interaction due to overlapping closed shells. For CF_4, $\beta(r)$ increases over the DID contribution indicating that the induction mechanism is not the same or that additional, more important mechanisms are operating. It is clear, however, that the long range solutions obtained in the moment analysis of CF_4 must not be cast lightly aside in favor of the short range solutions which are identified with the Electron Overlap and Frame Distortion induction mechanisms.

4.4 SF_6

The SF_6 moment analysis was carried out in the same way as the CF_4 moment analysis. The value of $-\phi^{(0)}/\phi^{(2)}$ obtained from the spectra decreases slightly with increasing density and the average value of $98.4 \pm 6.4 \times 10^{-26}$ sec^2 was used. Table 1 contains the other data used in the SF_6 analysis. Both $\phi^{(0)}$ and $-\phi^{(0)}/\phi^{(2)}$

are much larger for SF_6 than for CF_4 or any of the rare gases. Carrying out the analysis, we get two solutions but neither has a term of short range:

$$\beta(x) = 6\alpha^2\sigma^{-3}\left(x^{-3} - 3.0\,x^{-2.88}\right) \qquad (4.26)$$

or

$$\beta(x) = 6\alpha^2\sigma^{-3}\left(x^{-3} + 0.91\,x^{-2.82}\right). \qquad (4.27)$$

There is no need to calculate the higher moments in an effort to distinguish between the two - except for the sign, eq. (4.26) and eq. (4.27) are essentially identical for all x. The second term amounts to approximately doubling the value of the coefficient in the DID model. This agrees with the Kerr effect data, where the experimental B_K is almost twice as large as the one calculated from the DID model.

Triki et al[63] and Watson and Rowell[64] have found the point dipole approximation inappropriate in their studies of SF_6, and the present result must be taken as further evidence for the breakdown of the point dipole approximation. For a large molecule such as SF_6 the polarizability distribution within the molecule may have to be considered. Theimer and Paul[65] have treated depolarized light scattering using a polarizability density function and Triki[63] has found good agreement between depolarization ratio measurements and theory with this model.

CHAPTER 5

CONCLUSIONS

5.1 Results

The method of moments is shown to be a powerful technique, allowing direct evaluation of the form $\beta(r)$ from scattering data. Thus far, the method has some prominent drawbacks. Firstly, it is sensitive only to $\beta^2(r)$ so that information about the sign of $\beta(r)$ cannot be obtained. Secondly, two solutions are obtained. In order to distinguish between them more precise data, which will permit the accurate measurement of higher moments, are necessary. Thirdly, systematic errors are introduced by the use of Kerr effect data to normalize the measured intensity and by the need to extrapolate the measured profile. Absolute intensity measurements and measurements over a larger frequency range must be made to eliminate these troubles.

The analysis of CF_4 and SF_6, on the basis of the line profile and through the method of moments, indicates that the short range induction mechanisms do not play the role originally assumed for them. The mechanisms of Electron Overlap and Frame Distortion were postulated in conjunction with the IBC model of liquids and were thought to be chiefly responsible for the scattering in the high frequency wings. It has been found that a short range interaction is not necessary to account for this scattering, which seems to be governed by the repulsive part of the intermolecular potential. The importance, and even the existence, of the short range induction mechanisms must be reassessed in this light.

The work on SF_6 has produced evidence for the breakdown of the point dipole DID model in the case of large molecules. The DID model has always been accepted as the starting point in any discussion of collision induced light scattering. The present results indicate that even for this most simple model the details of the size, shape, and structure of the interacting molecules must be taken into account.

The importance of the method of moments is enhanced by the failure of the present models of the polarizability. Moments seem to be one of the few techniques which allow one to analyze the data without assuming the form of $\beta(r)$ at the outset. As has been emphasized previously, it is only when reliable models of the polarizabiltiy anisotropy are available, that one will be able to obtain useful results on molecular dynamics in dense media.

5.2 Recommendations

Three extensions of the present work are recommended. The first is in the way of instrumental improvements. Absolute intensities may be measured by observing the intensity of the collision induced scattering relative to the intensity of a rotational Raman line of H_2 for which the absolute scattering cross section is known.[66] The extrapolation at low frequencies may be eliminated by reducing the intensity of the stray Rayleigh scattered light. This reduction may be achieved by attenuating the stray light with an I_2 absorption cell[67] or a Fabry-Perot interferometer,[68] or by re-designing the optics so that the stray light is not collected to begin with. Extrapolation at high frequencies may be eliminated,

and the overall noise in the spectra may be reduced by improved efficiency in the use of the scattered light. In this respect, the possibility of multiplexing, by means of an imaging detector is being investigated.

The second extension is to make measurements which provide independent or additional information. One may observe the density dependence of the total depolarization ratio and of the depolarization ratio as a function of frequency. With a larger range of density, the relative importance of many-body effects at low and intermediate densities may be determined. By measuring the polarized and depolarized scattering, the observation of $\alpha(r)$ may be possible. Performing experiments over a wider range of temperatures permits one to vary the intermolecular collision parameters. Performing the moment analysis at different temperatures will provide a self-consistency check on the analysis and will allow more precise determination of the form of $\beta(r)$. The additional information may also be used to assess the accuracy of the empirical potentials used to describe the true intermolecular potential. Besides physically altering the temperature, one may effectively vary the temperature by studying other molecules. Changing the molecule under study has the same effect as changing the temperature at which the experiment is performed, since different molecules will be at different reduced temperatures.

The third extension of the present work will be improved calculations. Three body correlations may be accounted for and will allow more accurate comparison of theory and experiment.[18,66] New methods for calculating the induced polarizability in the collison

of complicated molecules are appearing.[70] It will be useful in two respects to attempt these calculations of the polarizability. They will allow detailed comparison of theory and experiment for specific molecules, and they will yield an increased insight into the general behavior of the induced polarizability.

REFERENCES

1. M. Thibeau, B. Oksengorn and B. Vodar, J. Phys. (Paris) 29, 287 (1968)
2. M. Thibeau and B. Oksengorn, J. Phys. (Paris) 30, 47 (1969)
3. M. Thibeau, G. C. Tabisz, B. Oksengorn and B. Vodar, J. Quant. Spectrosc. Radiat. Transfer 10, 839 (1970)
4. H. B. Levine and G. Birnbaum, Phys. Rev. Lett. 20, 439 (1968)
5. J. P. McTague and G. Birnbaum, Phys. Rev. Lett. 21, 661 (1968)
6. J. P. McTague, P. A. Fleury and D, B. DuPré, Phys. Rev. 188, 303 (1969)
7. J. I. Bersten, R. E. Slusher and C. M. Surko, Phys. Rev. Lett. 25, 1739 (1970)
8. W. S. Gernall, H. E. Howard-Lock and B. P. Stoicheff, Phys. Rev. A 1, 1288 (1970)
9. V. Volterra, J. A. Bucaro and T. A. Litovitz, Phys. Rev. Lett. 26, 55 (1970)
10. P. M. Lallemand, Phys. Rev. Lett. 25, 1079 (1970)
11. P. Lallemand, J. Phys. (Paris) 32, 119 (1971)
12. J. P. McTague and G. Birnbaum, Phys. Rev. A 3, 1376 (1971)
13. J. A. Bucaro and T. A. Litovitz, J. Chem. Phys. 54, 3846 (1971)
14. J. I. Gersten, Phys. Rev. A 4, 98 (1971)
15. H. K. Shin, J. Chem. Phys. 56, 2617 (1972)
16. G. C. Tabisz, W. R. Wall and D. P. Shelton, Chem. Phys. Lett. 15, 387 (1972)
17. R. A. Pasmanter, R. Sampson and A. Ben-Reuven, Chem. Phys. Lett. 16, 470 (1972)
18. W. M. Gelbart, J. Chem. Phys. 57, 699 (1972)

19. G. C. Tabisz, W. R. Wall, D. P. Shelton and J. H. K. Ho, Advances in Raman Spectroscopy, Vol. 1, Heyden and Son, London (1973)

20. J. H. K. Ho and G. C. Tabisz, Can. J. Phys. 51, 2025 (1973)

21. W. M. Gelbart, Depolarized Light Scattering by Simple Fluids, (unpublished)

22. B. J. Berne, M. Bishop and A. Rahman, J. Chem. Phys. 58, 2696 (1973)

23. M. R. Vukcevich, 1971, private communication quoted in reference 13

24. K. E. MacCormack and W. G. Schneider, J. Chem. Phys. 19, 845 (1951)

25. K. E. MacCormack and W. G. Schneider, J. Chem. Phys. 19, 849 (1951)

26. D. R. Douslin, R. H. Harrison, R. T. Moore and J. P. McCullough, J. Chem. Phys. 35, 1375 (1961)

27. R. G. Stanton, Numerical Methods for Science and Engineering, Prentice-Hall, Englewood Cliffs, New Jersey (1961)

28. C. D. Hodgman, Handbook of Chemistry and Physics, 44th Edition, Chemical Rubber Publishing Company, Cleveland, Ohio (1963)

29. J. J. Barrett and N. I. Adams, J. Opt. Soc. Am. 58, 311 (1968)

30. R. L. Schwiesow, J. Opt. Soc. Am. 59, 1285 (1969)

31. C. D. Allemand, Applied Optics, 9, 1304 (1970)

32. D. O. Landon and A. J. Mitteldorf, Spex Speaker (Spex Industries, Metuchen, N. J.) 17, 1 (1972)

33. A. H. Sommer, Photoemissive Materials, Wiley, New York, N. Y. (1968)

34. A. T. Young, Applied Optics 8, 2431 (1969)

35. E. M. Pugh and G. H. Winslow, The Analysis of Physical Measurements, Addison-Wesley, Reading, Mass. (1966)

36. J. H. Wilkinson, The Algebraic Eigenvalue Problem, Carendon Press, Oxford (1965)

37. P. A. Fleury, W. B. Daniels and J. M. Worlock, Phys. Rev. Lett. 27, 1493 (1971)

38. P. A. Fleury, J. M. Worlock and H. L. Carter, Phys. Rev. Lett. 30, 591 (1973)

39. G. D. Mahan, Phys. Lett. 44A, 287 (1973)

40. D. P. Shelton, M. S. Mathur and G. C. Tabisz, Phys. Rev. A 11, 834 (1975)

41. H. B. Levine and G. Birnbaum, J. Chem. Phys. 55, 2914 (1971)

42. E. E. Nikitin, Opt. Spectrosc. 6, 93 (1959)

43. B. J. Alder, H. L. Strauss and J. J. Weis, J. Chem. Phys. 59, 1002 (1973)

44. D. P. Shelton and G. C. Tabisz, Phys. Rev. A 11, 1571 (1975)

45. D. P. Shelton and G. C. Tabisz (to be published)

46. H. B. Levine, J. Chem. Phys. 56, 2455 (1972)

47. P. Lallemand, C. R. Acad. Sc. Paris 273, 89 (1971)

48. P. Lallemand, J. Phys. (Paris) 33, Colloque 1, 257 (1972)

49. A. D. Buckingham and J. A. Pople, Trans. Faraday Soc. 51, 1173 (1955)

50. A. D. Buckingham and D. A. Dunmur, Trans. Faraday Soc. 64, 1776 (1968)

51. A. D. Buckingham and B. J. Orr, Trans. Faraday Soc. 65, 673 (1969)

52. A. Triki, B. Oksegorn and B. Vodar, C. R. Acad. Sc. Paris 277, 411 (1973)

53. B. Oksengorn, C. R. Acad. Sc. Paris 279, 275 (1974)

54. B. Simic-Glavaski, D. A. Jackson and J. G. Powles, Phys. Lett. 34A, 255 (1971)

55. D. J. G. Irwin and A. D. May, Can. J. Phys. 50, 2174 (1972)

56. D. B. DuPré and J. P. McTague, J. Chem. Phys. 50, 2024 (1969)

57. A. D. Buckingham, P. H. Martin and R. S. Watts, Chem. Phys. Lett. 21, 186 (1973)

58. A. D. Buckingham and R. S. Watts, Mol. Phys. 26, 7 (1973)

59. E. F. O'Brien, V. P. Gutschick, V. McKoy and J. P. McTague, Phys. Rev. A 8, 690 (1973)

60. P. J. Fortune and P. R. Certain, J. Chem. Phys. 61, 2620 (1974)

61. P. Lallemand, D. David and B. Bigot, Mol. Phys. 27, 1029 (1974)

62. H. E. Howard-Lock and R. S. Taylor, Can. J. Phys. 52, 2436 (1974)

63. A. Triki, B. Oksengorn and B. Vodas, C. R. Acad. Sc. Paris, 274, 783 (1972)

64. R. C. Watson and R. L. Rowell, J. Chem. Phys. 61, 2666 (1974)

65. O. Theimer and R. Paul, J. Chem. Phys. 42, 2508 (1965)

66. F. Barocchi and J. P. McTague (to be published in Phys. Lett. A)

67. G. Hibler, J. Lippert and W. L. Peticolas, Spex Speaker (Spex Industries, Metuchen, N. J.) 16, 10 (1971)

68. W. Proffitt, L. M. Fraas, P. Cervenka and S. P. S. Porto, Applied Optics 10, 531 (1971)

69. H. I. Ralph and C. G. Gray, Mol. Phys. 27, 1683 (1974)

70. D. F. Heller, R. A. Harris and W. M. Gelbart, J. Chem. Phys. 62, 1947 (1975)

APPENDIX A

COMPUTER PROGRAMS

APPENDIX A1

SET DISCRIMINATOR LEVELS

MAIN

```
0001                COMMON/AREA1/PLOT(128),NPTS
0002                COMPLEX*16 DECK1
0003                REAL*4 X(1024),D(512),S(512),R(512),Q(512),SMTH(5)
0004                EQUIVALENCE (X(1),S),(X(513),D)
                C
                C READ IN DATA
                C
0005              102 FORMAT(A8,A8)
0006                READ(5,102)DECK1
0007              100 FORMAT(F6.0,9F7.0)
0008                READ(5,100)(X(I),I=1,1024)
                C
                C PRINT OUT DATA
                C
0009                DO 105 I=1,512
0010                S(I)=S(I)-D(I)/10.
0011              105 CONTINUE
0012                DO 115 I=1,100
0013                PLOT(I)=0.
0014                DO 120 J=1,5
0015                PLOT(I)=PLOT(I)+S(J+5*(I-1))
0016              120 CONTINUE
0017              115 CONTINUE
0018                NPTS=100
0019                CALL GRAPH
0020                WRITE(6,125)
0021              125 FORMAT('1'/'0',10X,
                   C 'SINGLE PHOTOELECTON PULSE HEIGHT DISTRIBUTION'/'0')
0022                WRITE(6,130)(PLOT(I),I=1,100)
0023              130 FORMAT(' ',10X,5E18.6)
0024                DO 135 I=1,100
0025                PLOT(I)=0.
0026                DO 140 J=1,5
0027                PLOT(I)=PLOT(I)+D(J+5*(I-1))
0028              140 CONTINUE
0029              135 CONTINUE
0030                CALL GRAPH
0031                WRITE(6,145)
0032              145 FORMAT('1'/'0',10X,'DARK PULSE HEIGHT DISTRIBUTION'/'0')
0033                WRITE(6,130)(PLOT(I),I=1,100)
0034                DO 150 I=1,100
0035                IF(PLOT(I).LT.1.)GO TO 148
0036                PLOT(I)=ALOG(PLOT(I))
0037                GO TO 150
0038              148 PLOT(I)=0.
0039              150 CONTINUE
0040                CALL GRAPH
0041                WRITE(6,155)DECK1
0042              155 FORMAT('1'/'0',10X,'LOG PLOT--DARK PULSE HEIGHT DISTRIBUTION'/
                   C '0',10X,'DATA FROM ',A8,A8/'0')
                C
                C COMPUTE R(I)
                C
0043                DO 11) I=1,512
0044                R(I)=0.
0045                IF(D(I).EQ.0.)GO TO 110
0046                R(I)=2.*S(I)/D(I)
0047              110 CONTINUE
                C
                C MOVING FIVE POINT LEAST SQUARES SMOOTH
                C
0048                K=I+2
0049                DO 160 I=1,508
```

MAIN

```
0050                DO 165 J=1,5
0051                SMTH(J)=R(I+J)
0052            165 CONTINUE
0053                R(K)=(12.*(SMTH(2)+SMTH(4))+17.*SMTH(3)-3.*(SMTH(1)+SMTH(5)))/35.
0054            160 CONTINUE
                C
                C COMPUTE Q(I) AND FIND INTERSECTION  OF Q(I) AND R(I)
                C
0055                SN=0.
0056                DN=0.
0057                N=512
0058                DO 152 I=1,512
0059                Q(I)=0.
0060                IF(N.LT.(513-I))GO TO 152
0061                SN=SN+S(513-I)
0062                DN=DN+D(513-I)
0063                IF(DN.EQ.0.)GO TO 152
0064                Q(513-I)=SN/DN
0065            152 CONTINUE
0066                I=200
0067            170 I=I-1
0068                IF(Q(I).LT.R(I))GO TO 170
0069                J=200
0070            175 J=J+1
0071                IF(R(J).GT.R(I))GO TO 175
0072                N=J
0073                SN=0.
0074                DN=0.
0075                DO 180 I=1,512
0076                Q(I)=0.
0077                IF(N.LT.(513-I))GO TO 180
0078                SN=SN+S(513-I)
0079                DN=DN+D(513-I)
0080                IF(DN.EQ.0.)GO TO 180
0081                Q(513-I)=SN/DN
0082            180 CONTINUE
0083                I=200
0084            190 I=I-1
0085                IF(Q(I).LT.R(I))GO TO 190
0086                J=200
0087            195 J=J+1
0088                IF(R(J).GT.R(I))GO TO 195
0089                ILWR=I
0090                IUPR=J
0091                N=IUPR-ILWR
0092                TD=0.
0093                TS=0.
0094                DO 200 I=1,N
0095                TD=TD+D(I+ILWR)
0096                TS=TS+S(I+ILWR)
0097            200 CONTINUE
0098                FS=0.
0099                DO 202 I=1,512
0100                FS=FS+S(I)
0101            202 CONTINUE
0102                FS=TS/FS
0103                TD=TD/1000.
                C
                C OUTPUT OF RESULTS
                C
0104                DO 205 I=1,100
0105                PLOT(I)=0.
0106                DO 210 J=1,5
```

```
0107              PLOT(I)=PLOT(I)+R(J+5*(I-1))
0108          210 CONTINUE
0109          205 CONTINUE
0110              CALL GRAPH
0111              WRITE(6,215)
0112          215 FORMAT('1'/'0',10X,'R'/'0')
0113              WRITE(6,130)(PLOT(I),I=1,100)
0114              DO 225 I=1,100
0115              PLOT(I)=0.
0116              DO 230 J=1,5
0117              PLOT(I)=PLOT(I)+Q(J+5*(I-1))
0118          230 CONTINUE
0119          225 CONTINUE
0120              CALL GRAPH
0121              WRITE(6,235)
0122          235 FORMAT('1'/'0',10X,'Q'/'0')
0123              WRITE(6,130)(PLOT(I),I=1,100)
0124              WRITE(6,250)ILWR,IUPR
0125          250 FORMAT('1'/'0',10X,'CHANNEL NUMBER OF LOWER DISCRIMINATOR LEVEL',
                 C I4/'0',10X,'CHANNEL NUMBER OF UPPER DISCRIMINATOR LEVEL',I4/'0')
0126              WRITE(6,260)TD,FS
0127          260 FORMAT('0',10X,'OPTIMUM DARK COUNT RATE=',F8.4,'HERTZ'/
                 C '0',10X,'FRACTION OF SIGNAL USED AT OPTIMUM=',F8.5/'0')
0128              WRITE(6,270)DECK1
0129          270 FORMAT('0',10X,2A8)
0130              STOP
0131              END
```

GRAPH

```
0001            SUBROUTINE GRAPH
                C
                C INPUT IS A REAL*4 VECTOR PLOT(128)
                C NPTS MAY BE 100 OR 128 POINTS
                C
0002            COMMON/AREA1/PLOT(128),NPTS
0003            REAL*4 MAX,MIN
0004            INTEGER*4 IPLOT(128,2)
0005            LOGICAL*1 LINE(128)/128*' '/
0006            LOGICAL*1 BLANK/' '/,STAR/'*'/
                C
                C FIND MAX AND MIN
                C
0007            MAX=PLOT(1)
0008            MIN=PLOT(1)
0009            DO 100 I=1,NPTS
0010            IF(PLOT(I).GT.MAX)MAX=PLOT(I)
0011          100 IF(PLOT(I).LT.MIN)MIN=PLOT(I)
                C
                C SCALE AND ROUND TO NEAREST INTEGER
                C
0012            IF(MAX.EQ.MIN)GO TO 121
0013            SCALE=50./(MAX-MIN)
0014            GO TO 122
0015          121 SCALE=0.
0016          122 IBSLN=-SCALE*MIN
0017            DO 120 I=1,NPTS
0018            PLOT(I)=PLOT(I)*SCALE+IBSLN
0019            IPLOT(I,1)=PLOT(I)
0020            IF((IPLOT(I,1)+1.-PLOT(I)).LT.0.5)IPLOT(I,1)=IPLOT(I,1)+1
0021          120 IPLOT(I,2)=I
                C
                C SORT
                C
0022          142 ISORT=0
0023            N=NPTS-1
0024            DO 140 I=1,N
0025            IF(IPLOT(I,1).LT.IPLOT(I+1,1))GO TO 141
0026            GO TO 140
0027          141 ITEMP1=IPLOT(I,1)
0028            ITEMP2=IPLOT(I,2)
0029            IPLOT(I,1)=IPLOT(I+1,1)
0030            IPLOT(I,2)=IPLOT(I+1,2)
0031            IPLOT(I+1,1)=ITEMP1
0032            IPLOT(I+1,2)=ITEMP2
0033            ISORT=1
0034          140 CONTINUE
0035            IF(ISORT.EQ.1)GO TO 142
                C
                C PLOT
                C
0036            WRITE(6,200)
0037            IF(NPTS.EQ.100)WRITE(6,205)
0038            IF(NPTS.EQ.128)WRITE(6,206)
0039            L=1
0040            DO 180 K=1,52
0041            M=0
0042            DO 181 I=L,NPTS
0043            IF(I.GT.NPTS)GO TO 182
0044            IF(IPLOT(I,1).EQ.(52-K))GO TO 183
0045          182 GO TO 184
0046          183 J=IPLOT(I,2)
0047            LINE(J)=STAR
```

GRAPH

```
0048          181 M=M+1
0049          184 IF(NPTS.EQ.100)WRITE(6,210)(LINE(J),J=1,100)
0050              IF(NPTS.EQ.128)WRITE(6,211)(LINE(J),J=1,128)
0051              IF(NPTS.EQ.100.AND.IBSLN.EQ.(52-K))WRITE(6,215)
0052              IF(NPTS.EQ.128.AND.IBSLN.EQ.(52-K))WRITE(6,216)
0053              DO 185 N=1,NPTS
0054          185 LINE(N)=BLANK
0055          180 L=L+M
0056              IF(NPTS.EQ.100)WRITE(6,205)
0057              IF(NPTS.EQ.128)WRITE(6,206)
0058              WRITE(6,220)MAX,MIN
0059          200 FORMAT('1'/'0')
0060          205 FORMAT(' ',18X,10('+---------'),'+-')
0061          206 FORMAT(' ',2X,13('+---------'))
0062          210 FORMAT(' ',18X,'|',100A1,'|')
0063          211 FORMAT(' ',2X,'|',128A1,'|')
0064          215 FORMAT('+',18X,10('+---------'),'+-')
0065          216 FORMAT('+',2X,13('+---------'))
0066          220 FORMAT('0',30X,'MAXIMUM VALUE=',E14.7,5X,'MINIMUM VALUE=',
             C E14.7/'0')
0067              RETURN
0068              END
```

APPENDIX A2

FIT EXPONENTIAL

TO DATA

MAIN

```
0001            COMMON/AREA1/PLOT(128),NPTS
0002            REAL*4 XY(800,4),V(1024),C(40)
0003            READ(5,200)(V(J),J=1,1024)
0004            READ(5,200)(C(J),J=1,40)
0005            READ(5,205)VCENT
0006        200 FORMAT(10F8.1)
0007        205 FORMAT(F8.3)
0008            IPEAK=VCENT
0009            M=800
0010            DO 110 I=1,M
0011            J=I+IPEAK+25
0012            XY(I,1)=(J-IPEAK)/10.
0013            XY(I,2)=V(J)
0014        110 XY(I,3)=1./(XY(I,2)+9.)
0015            AB=24.2299E3
0016            AL=-0.239456
0017            BB=3.04670E3
0018            BL=-0.0935379
0019            PL=0.
0020            QL=0.
0021            CALL TWOEXP(AB,AL,BB,BL,PL,QL,XY,M,ITER)
0022            DO 130 I=1,100
0023            PLOT(I)=0.
0024            DO 135 J=1,8
0025        135 PLOT(I)=PLOT(I)+XY(I+(J-1)*8,4)
0026        130 CONTINUE
0027            NPTS=100
0028            CALL GRAPH
0029            STOP
0030            END
```

TWOEXP

```
01              SUBROUTINE TWOEXP(AB,AL,BB,BL,PL,QL,XY,M,ITER)
02              REAL*8 A(4,4),T(4,4),B(4),Y(4),X(4),R(4),XSOLN(4)
03              REAL*4 XY(M,4)
          C THE MODEL IS AB*XY(I,1)**PL*EXP(AL*XY(I,1))+BB*XY(I,1)**QL*EXP(BL*XY(I,1))
          C THE PARAMETERS TO BE OPTIMIZED ARE 'AB','AL','BB' AND 'BL'
          C XY(I,1) CONTAINS THE VALUES OF THE INDEPENDENT VARIABLE
          C XY(I,2) CONTAINS THE MEASURED VALUE CORRESPONDING TO XY(I,1)
          C XY(I,3) CONTAINS THE WEIGHT OF THE MEASUREMENT XY(I,2)
          C XY(I,4) CONTAINS THE RESIDUALS XY(I,2)-(FITTED FUNCTION AT XY(I,1))
          C THE SUBROUTINE SLVEQN(A,T,B,Y,X,R,XSOLN,N) IS REQUIRED
04              N=4
05              DO 100 ITER=1,20
          C INITIALIZE A(I,J) AND B(I) TO ZERO
06              DO 115 I=1,N
07              DO 120 J=1,N
08            120 A(I,J)=0.D0
09            115 B(I)=0.D0
          C COMPUTE A(I,J) AND B(I)
10              DO 125 I=1,M
11              F1=AB*XY(I,1)**PL*EXP(AL*XY(I,1))
12              F2=BB*XY(I,1)**QL*EXP(BL*XY(I,1))
13              F11=F1**2*XY(I,3)
14              F12=F1*F2*XY(I,3)
15              F22=F2**2*XY(I,3)
16              BM=(XY(I,2)-F1-F2)*XY(I,3)
17              A(1,1)=A(1,1)+F11
18              A(1,2)=A(1,2)+F11*XY(I,1)
19              A(1,3)=A(1,3)+F12
20              A(1,4)=A(1,4)+F12*XY(I,1)
21              A(2,2)=A(2,2)+F11*XY(I,1)**2
22              A(2,3)=A(2,3)+F12*XY(I,1)
23              A(2,4)=A(2,4)+F12*XY(I,1)**2
24              A(3,3)=A(3,3)+F22
25              A(3,4)=A(3,4)+F22*XY(I,1)
26              A(4,4)=A(4,4)+F22*XY(I,1)**2
27              B(1)=B(1)+BM*F1
28              B(2)=B(2)+BM*F1*XY(I,1)
29              B(3)=B(3)+BM*F2
30              B(4)=B(4)+BM*F2*XY(I,1)
31            125 CONTINUE
32              A(1,1)=A(1,1)/AB**2
33              A(1,2)=A(1,2)/AB
34              A(1,3)=A(1,3)/(AB*BB)
35              A(1,4)=A(1,4)/AB
36              A(2,3)=A(2,3)/BB
37              A(3,3)=A(3,3)/BB**2
38              A(3,4)=A(3,4)/BB
39              A(2,1)=A(1,2)
40              A(3,1)=A(1,3)
41              A(4,1)=A(1,4)
42              A(3,2)=A(2,3)
43              A(4,2)=A(2,4)
44              A(4,3)=A(3,4)
45              B(1)=B(1)/AB
46              B(3)=B(3)/BB
          C SOLVE A(I,J)*XSOLN(J)=B(I)
47              CALL SLVEQN(A,T,B,Y,X,R,XSOLN,N)
          C COMPUTE THE CURRENT ESTIMATES OF THE PARAMETERS
48              AB=AB+XSOLN(1)
49              AL=AL+XSOLN(2)
50              BB=BB+XSOLN(3)
51              BL=BL+XSOLN(4)
52              WRITE(6,200)ITER
```

```
0053          200 FORMAT('0',10X,I10)
0054              WRITE(6,205)(XSOLN(I),I=1,4)
0055          205 FORMAT('0',10X,4D18.6)
0056              WRITE(6,210)AB,AL,BB,BL
0057          210 FORMAT('0',10X,4E18.6)
            C TEST FOR EXIT
0058              TEST=(XSOLN(1)/AB)**2+(XSOLN(2)/AL)**2+(XSOLN(3)/BB)**2
                 C +(XSOLN(4)/BL)**2
0059              TEST=SQRT(TEST)
0060              IF(TEST.LT.5.0E-06)GO TO 150
0061          100 CONTINUE
0062          150 CONTINUE
            C COMPUTE THE RESIDUALS
0063              DO 130 I=1,M
0064          130 XY(I,4)=XY(I,2)-AB*XY(I,1)**PL*EXP(AL*XY(I,1))
                 C -BB*XY(I,1)**QL*EXP(BL*XY(I,1))
0065              CHISQ=0.
0066              DO 135 I=1,M
0067          135 CHISQ=CHISQ+XY(I,4)**2*XY(I,3)
0068              WRITE(6,215)CHISQ
0069          215 FORMAT('0',10X,E18.6)
0070              RETURN
0071              END
```

SLVEQN

```
01          SUBROUTINE SLVEQN(A,T,B,Y,X,R,XSOLN,N)
02          IMPLICIT REAL*8(A-H,O-Z)
03          REAL*8 A(N,N),T(N,N),B(N),Y(N),X(N),R(N),XSOLN(N)
      C
      C SOLVE  A(I,J)*X(J)=B(I)
      C
      C A(I,J) MUST BE A REAL, SYMMETRIC MATRIX.
      C CHOLESKY DECOMPOSITION IS USED TO FACTOR A(I,J)INTO T(I,J)*T(J,I),
      C WHERE T(I,J) IS A REAL LOWER TRIANGULAR MATRIX.
      C THE NECESSARY AND SUFFICIENT CONDITION FOR THIS TO BE POSSIBLE IS THAT
      C DET(A(I,J)) IS POSITIVE DEFINITE. AFTER TRIANGULATION, BACK SUBSTITUTION IS
      C USED TO OBTAIN THE SOLUTION. AN ITERATIVE LOOP IS PROVIDED TO ALLOW THIS
      C SOLUTION TO BE IMPROVED IF NECESSARY.
      C THE ARRAY AREA IS 4*N**2+10*N BYTES
      C
      C COMPUTE T(I,J), THE LOWER TRIANGULAR FACTOR OF A(I,J)
04          DO 100 K=1,N
      C COMPUTE THE KTH DIAGONAL ELEMENT
05          JSTART=K+1
06          ISTOP=K-1
07          SUM=0.D0
08          IF(K.EQ.1)GO TO 110
09          DO 105 I=1,ISTOP
10        105 SUM=SUM+T(K,I)**2
11        110 T(K,K)=DSQRT(A(K,K)-SUM)
12          IF(K.EQ.N)GO TO 100
      C COMPUTE THE KTH COLUMN AND SET THE ELEMENTS ABOVE THE DIAGONAL TO ZERO
13          DO 115 J=JSTART,N
14          SUM=0.D0
15          IF(K.EQ.1)GO TO 125
16          DO 120 I=1,ISTOP
17        120 SUM=SUM+T(J,I)*T(K,I)
18        125 T(J,K)=(A(J,K)-SUM)/T(K,K)
19          T(K,J)=0.D0
20        115 CONTINUE
21        100 CONTINUE
      C THIS ENTRY POINT IS USED TO COMPUTE INVERSE(A(I,J)) WITHOUT RECOMPUTING T(I,J)
22          ENTRY SOLVEB(B)
      C INITIALIZE THE LOOP
23          DO 130 I=1,N
24          R(I)=B(I)
25        130 XSOLN(I)=0.D0
      C START OF THE LOOP
26          DO 195 ITER=1,1
      C SOLVE THE EQUATIONS T(I,J)*Y(J)=B(I)
27        135 DO 140 K=1,N
28          Y(K)=R(K)
29          IF(K.EQ.1)GO TO 150
30          ISTOP=K-1
31          DO 145 I=1,ISTOP
32        145 Y(K)=Y(K)-T(K,I)*Y(I)
33        150 Y(K)=Y(K)/T(K,K)
34        140 CONTINUE
      C SOLVE THE EQUATIONS T(J,I)*X(J)=Y(I)
35          DO 160 L=1,N
36          K=N-L+1
37          X(K)=Y(K)
38          IF(K.EQ.N)GO TO 170
39          ISTART=K+1
40          DO 165 I=ISTART,N
41        165 X(K)=X(K)-T(I,K)*X(I)
42        170 X(K)=X(K)/T(K,K)
43        160 CONTINUE
```

```
                C COMPUTE THE CURRENT APPROXIMATION TO XSOLN
0044                 DO 180 I=1,N
0045               180 XSOLN(I)=XSOLN(I)+X(I)
                C COMPUTE THE RESIDUAL VECTOR R(I)
0046                 DO 185 I=1,N
0047                 SUM=0.DO
0048                 DO 190 J=1,N
0049               190 SUM=SUM+A(I,J)*XSOLN(J)
0050               185 R(I)=B(I)-SUM
                C RETURN TO STMT 135 TO PERFORM THE NEXT ITERATION
0051               195 CONTINUE
0052                 RETURN
0053                 END
```

GRAPH

```
0001            SUBROUTINE GRAPH
                C
                C INPUT IS A REAL*4 VECTOR PLOT(128)
                C NPTS MAY BE 100 OR 128 POINTS
                C
0002            COMMON/AREA1/PLOT(128),NPTS
0003            REAL*4 MAX,MIN
0004            INTEGER*4 IPLOT(128,2)
0005            LOGICAL*1 LINE(128)/128*' '/
0006            LOGICAL*1 BLANK/' '/,STAR/'*'/
                C
                C FIND MAX AND MIN
                C
0007            MAX=PLOT(1)
0008            MIN=PLOT(1)
0009            DO 100 I=1,NPTS
0010            IF(PLOT(I).GT.MAX)MAX=PLOT(I)
0011          100 IF(PLOT(I).LT.MIN)MIN=PLOT(I)
                C
                C SCALE AND ROUND TO NEAREST INTEGER
                C
0012            IF(MAX.EQ.MIN)GO TO 121
0013            SCALE=50./(MAX-MIN)
0014            GO TO 122
0015          121 SCALE=0.
0016          122 IBSLN=-SCALE*MIN
0017            DO 120 I=1,NPTS
0018            PLOT(I)=PLOT(I)*SCALE+IBSLN
0019            IPLOT(I,1)=PLOT(I)
0020            IF((IPLOT(I,1)+1.-PLOT(I)).LT.0.5)IPLOT(I,1)=IPLOT(I,1)+1
0021          120 IPLOT(I,2)=I
                C
                C SORT
                C
0022          142 ISORT=0
0023            N=NPTS-1
0024            DO 140 I=1,N
0025            IF(IPLOT(I,1).LT.IPLOT(I+1,1))GO TO 141
0026            GO TO 140
0027          141 ITEMP1=IPLOT(I,1)
0028            ITEMP2=IPLOT(I,2)
0029            IPLOT(I,1)=IPLOT(I+1,1)
0030            IPLOT(I,2)=IPLOT(I+1,2)
0031            IPLOT(I+1,1)=ITEMP1
0032            IPLOT(I+1,2)=ITEMP2
0033            ISORT=1
0034          140 CONTINUE
0035            IF(ISORT.EQ.1)GO TO 142
                C
                C PLOT
                C
0036            WRITE(6,200)
0037            IF(NPTS.EQ.100)WRITE(6,205)
0038            IF(NPTS.EQ.128)WRITE(6,206)
0039            L=1
0040            DO 180 K=1,52
0041            M=0
0042            DO 181 I=L,NPTS
0043            IF(I.GT.NPTS)GO TO 182
0044            IF(IPLOT(I,1).EQ.(52-K))GO TO 183
0045          182 GO TO 184
0046          183 J=IPLOT(I,2)
0047            LINE(J)=STAR
```

```
0048          181 M=M+1
0049          184 IF(NPTS.EQ.100)WRITE(6,210)(LINE(J),J=1,100)
0050              IF(NPTS.EQ.128)WRITE(6,211)(LINE(J),J=1,128)
0051              IF(NPTS.EQ.100.AND.IBSLN.EQ.(52-K))WRITE(6,215)
0052              IF(NPTS.EQ.128.AND.IBSLN.EQ.(52-K))WRITE(6,216)
0053              DO 185 N=1,NPTS
0054          185 LINE(N)=BLANK
0055          180 L=L+M
0056              IF(NPTS.EQ.100)WRITE(6,205)
0057              IF(NPTS.EQ.128)WRITE(6,206)
0058              WRITE(6,220)MAX,MIN
0059          200 FORMAT('1'/'0')
0060          205 FORMAT(' ',18X,10('+---------'),'+-')
0061          206 FORMAT(' ',2X,13('+---------'))
0062          210 FORMAT(' ',18X,'|',100A1,'|')
0063          211 FORMAT(' ',2X,'|',128A1,'|')
0064          215 FORMAT('+',18X,10('+---------'),'+-')
0065          216 FORMAT('+',2X,13('+---------'))
0066          220 FORMAT('0',30X,'MAXIMUM VALUE=',E14.7,5X,'MINIMUM VALUE=',
                 C E14.7/'0')
0067              RETURN
0068              END
```

ONEXP

```
0001            SUBROUTINE ONEXP(AB,AL,PL,XY,M,ITER)
0002            REAL*8 A(2,2),T(2,2),B(2),Y(2),X(2),R(2),XSOLN(2)
0003            REAL*4 XY(M,4)
              C THE MODEL IS AB*XY(I,1)**PL*EXP(AL*XY(I,1))
              C THE PARAMETERS TO BE OPTIMIZED ARE 'AB' AND 'AL'
              C XY(I,1) CONTAINS THE VALUES OF THE INDEPENDENT VARIABLE
              C XY(I,2) CONTAINS THE MEASURED VALUE CORRESPONDING TO XY(I,1)
              C XY(I,3) CONTAINS THE WEIGHT OF THE MEASUREMENT XY(I,2)
              C XY(I,4) CONTAINS THE RESIDUALS XY(I,2)-(FITTED FUNCTION AT XY(I,1))
              C THE SUBROUTINE SLVEQN(A,T,B,Y,X,R,XSOLN,N) IS REQUIRED
0004            N=2
0005            DO 100 ITER=1,20
              C INITIALIZE A(I,J) AND B(I) TO ZERO
0006            DO 115 I=1,N
0007            DO 120 J=1,N
0008          120 A(I,J)=0.D0
0009          115 B(I)=0.D0
              C COMPUTE A(I,J) AND B(I)
0010            DO 125 I=1,M
0011            F=AB*XY(I,1)**PL*EXP(AL*XY(I,1))
0012            FSQ=F**2*XY(I,3)
0013            BM=F*(XY(I,2)-F)*XY(I,3)
0014            A(1,1)=A(1,1)+FSQ
0015            A(1,2)=A(1,2)+XY(I,1)*FSQ
0016            A(2,2)=A(2,2)+XY(I,1)**2*FSQ
0017            B(1)=B(1)+BM
0018            B(2)=B(2)+BM*XY(I,1)
0019          125 CONTINUE
0020            A(1,1)=A(1,1)/AB**2
0021            A(1,2)=A(1,2)/AB
0022            A(2,1)=A(1,2)
0023            B(1)=B(1)/AB
              C SOLVE A(I,J)*XSOLN(J)=B(I)
0024            CALL SLVEQN(A,T,B,Y,X,R,XSOLN,N)
              C COMPUTE THE CURRENT ESTIMATES OF THE PARAMETERS
0025            AB=AB+XSOLN(1)
0026            AL=AL+XSOLN(2)
0027            WRITE(6,200)ITER
0028          200 FORMAT('0',10X,I10)
0029            WRITE(6,205)(XSOLN(I),I=1,2)
0030          205 FORMAT('0',10X,2D18.6)
0031            WRITE(6,210)AB,AL
0032          210 FORMAT('0',10X,2E18.6)
              C TEST FOR EXIT
0033            TEST=(XSOLN(1)/AB)**2+(XSOLN(2)/AL)**2
0034            TEST=SQRT(TEST)
0035            IF(TEST.LT.5.0E-06)GO TO 150
0036          100 CONTINUE
0037          150 CONTINUE
              C COMPUTE THE RESIDUALS
0038            DO 130 I=1,M
0039          130 XY(I,4)=XY(I,2)-AB*XY(I,1)**PL*EXP(AL*XY(I,1))
0040            CHISQ=0.
0041            DO 135 I=1,M
0042          135 CHISQ=CHISQ+XY(I,4)**2*XY(I,3)
0043            WRITE(6,215)CHISQ
0044          215 FORMAT('0',10X,E18.6)
0045            RETURN
0046            END
```

APPENDIX A3

MOMENT ANALYSIS

MAIN

```
0001                COMMON/AREA4/NRTS,P(4),BP(4)
0002                COMMON/AREA5/SIG,EPS,ALPHA,RMASS,TEMP
0003                COMMON/AREA6/PRES,RMIX,ATM,RHO,AMAG
0004                INTEGER*4 RUN,COUNT
                C
                C  'SIG' AND 'EPS' ARE THE LENNARD-JONES PARAMETERS
                C  'SIG' IS IN UNITS OF (ANGSTROM)
                C  'EPS' IS IN UNITS OF (DEGREE K)
                C  'ALPHA' IS THE POLARIZABILITY OF A SINGLE MOLECULE
                C  'ALPHA' IS IN UNITS OF (ANGSTROM**3)
                C  'RMASS' IS THE REDUCED MASS OF THE COLLIDING PAIR OF MOLECULES
                C  'RMASS' IS IN UNITS OF (AMU)
                C  'TEMP' IS IN UNITS OF (DEGREE K)
                C  'SMALLK' IS BOLTZMANN'S CONSTANT
                C  'SMALLK'=1.38054(ANGSTROM**2*SEC**-2/DEGREE K)
                C
0005                SIG=4.70
0006                EPS=152.5
0007                ALPHA=2.84907
0008                RMASS=44.0055
0009                TEMP=293.
0010                SMALLK=1.38054
                C
0011                CALL ARRAY
0012              999 READ(5,900,END=1000)RUN,RATIO,IPRES,RMIX,COUNT
0013              900 FORMAT(I4,F12.3,I8,F8.1,I8)
                  CRUN        RATIO    IPRES    RMIX    COUNT
0014                WRITE(6,901)
0015                WRITE(6,902)
0016                WRITE(6,903)RUN
0017              901 FORMAT(1H1)
0018              902 FORMAT(1H0,10X,'RUN NUMBER')
0019              903 FORMAT(1H+,10X,10X,I4)
0020                PRES=IPRES
0021                CF4=RMIX
0022                HE=100.0-RMIX
0023                CALL PVT
0024                PHI0=21.5053
0025                PHI2=0.25562E-03*RATIO*PHI0
0026                CALL SOLVE(PHI0,PHI2)
0027                CALL ROOTS
0028                WRITE(6,902)
0029                WRITE(6,903)RUN
0030                WRITE(6,904)
0031              904 FORMAT(1H0,10X,'THE TOTAL NUMBER OF COUNTS IN THE OBSERVED ',
                   C 'SPECTRUM AFTER SUBTRACTING THE BACKGROUND IS')
0032                RCOUNT=COUNT
0033                WT=RCOUNT/SQRT(RCOUNT)
0034                WRITE(6,905)COUNT,WT
0035              905 FORMAT(1H0,10X,I8,' COUNTS',10X,'WEIGHT=N/SQRT(N)=',F8.2)
0036                WRITE(6,906)PRES,ATM
0037              906 FORMAT(1H0,10X,'TOTAL PRESSURE=',F6.0,'(PSIG)=',F6.1,'(ATM)')
0038                WRITE(6,907)RHO,AMAG
0039              907 FORMAT(1H0,10X,'DENSITY OF CF4=',F8.5,'(MOLE/LITER)=',F10.6,
                   C '(AMAGAT)')
0040                WRITE(6,908)
0041                WRITE(6,909)CF4,HE
0042              908 FORMAT(1H0,10X,'THE MIXTURE CONTAINED')
0043              909 FORMAT(1H0,10X,'CF4 -',F6.1,'(MOLE PERCENT)',5X,'HE -',F6.1,
                   C '(MOLE PERCENT)')
0044                WRITE(6,910)PHI0,PHI2
0045              910 FORMAT(1H0,10X,'PHI0=',F8.4,5X,'PHI2=',F8.4)
0046                WRITE(6,911)
```

MAIN

```
0047          911 FORMAT(1HO,10X,'THE SOLUTIONS ARE AT')
0048              DO 940 I=1,NRTS
0049              Y=BP(I)*SIG**(3.-P(I))/ALPHA**2
0050              WRITE(6,912)P(I),BP(I),Y
0051          912 FORMAT(1HO,10X,'P=',F6.2,5X,'B=',E15.7,5X,
     C 'Y=B*SIGMA**(3-P)/ALPHA**2=',E15.7)
0052          940 CONTINUE
0053              GO TO 999
0054         1000 STOP
0055              END
```

PVT

```
0001            SUBROUTINE PVT
0002            COMMON/AREA6/PRES,RMIX,ATM,RHO,AMAG
              C  CALCULATES THE DENSITY OF CF4 IN CF4-HE MIXTURES AT 293 DEGREES K
0003            EPSL=1.0E-04
0004            R=(100.0-RMIX)/RMIX
0005            ATM=(PRES+14.6959)/14.6959
0006            A=24.04194*(R+1.)
0007            B=-2.286258+3.136725*R+0.535674*R**2
0008            C=0.169700
0009            D=-0.976956E-03
0010            RHO=ATM/A
0011        150 RHON=ATM/(A+B*RHO+C*RHO**2+D*RHO**3)
0012            IF(ABS(RHON-RHO).LT.EPSL)GO TO 151
0013            RHO=RHON
0014            GO TO 150
0015        151 AMAG=23.94676*RHO
0016            RETURN
0017            END
```

ROOTS

```
0001            SUBROUTINE ROOTS
0002            COMMON/AREA3/FUNC(30,4),SOLN(30,2)
0003            COMMON/AREA4/NRTS,P(4),BP(4)
0004            EPSL=0.1E-02
0005            K=0
0006            DO 800 J=1,4
0007            M=2
0008            IF(J.EQ.1.OR.J.EQ.2)M=1
0009            I=0
0010          801 I=I+1
0011            IF(I+1.GE.30)GO TO 800
0012            SGNA=SIGN(1.,FUNC(I,J))
0013            SGNB=SIGN(1.,FUNC(I+1,J))
0014            IF(SGNA.EQ.SGNB)GO TO 801
0015            IF(I-1.LT.1)GO TO 802
0016            IF(I+1.GT.30)GO TO 803
0017            N=4
0018            F0=FUNC(I-1,J)
0019            F1=FUNC(I,J)
0020            F2=FUNC(I+1,J)
0021            F3=FUNC(I+2,J)
0022            DF0=F1-F0
0023            DF1=F2-F1
0024            DF2=F3-F2
0025            DDF0=DF1-DF0
0026            DDF1=DF2-DF1
0027            DDDF0=DDF1-DDF0
0028            A=DDDF0/6.
0029            B=DDF0/2.-DDDF0/2.
0030            C=DDDF0/3.-DDF0/2.+DF0
0031            D=F0
0032            X=1.
0033          830 XN=(-1./A)*(B+C/X+D/X**2)
0034            IF(ABS(XN-X).LT.EPSL)GO TO 831
0035            X=XN
0036            GO TO 830
0037          831 CROSS=I-1+XN
0038            VALUE=CROSS/2.+1.5
0039            S0=SOLN(I-1,M)
0040            S1=SOLN(I,M)
0041            S2=SOLN(I+1,M)
0042            S3=SOLN(I+2,M)
0043            DS0=S1-S0
0044            DS1=S2-S1
0045            DS2=S3-S2
0046            DDS0=DS1-DS0
0047            DDS1=DS2-DS1
0048            DDDS0=DDS1-DDS0
0049            AA=DDDS0/6.
0050            BB=DDS0/2.-DDDS0/2.
0051            CC=DDDS0/3.-DDS0/2.+DS0
0052            DD=S0
0053            SOLNB=AA*XN**3+BB*XN**2+CC*XN+DD
0054            GO TO 805
0055          802 IF(I+1.GT.30)GO TO 804
0056            N=3
0057            F0=FUNC(I,J)
0058            F1=FUNC(I+1,J)
0059            F2=FUNC(I+2,J)
0060            DF0=F1-F0
0061            DF1=F2-F1
0062            DDF0=DF1-DF0
0063            A=DDF0/2.
```

```
0064            B=-DDF0/2.+DF0
0065            C=F0
0066            X=1.
0067        820 XN=(-1./A)*(B+C/X)
0068            IF(ABS(XN-X).LT.EPSL)GO TO 821
0069            X=XN
0070            GO TO 820
0071        821 CROSS=I+XN
0072            VALUE=CROSS/2.+1.5
0073            S0=SOLN(I,M)
0074            S1=SOLN(I+1,M)
0075            S2=SOLN(I+2,M)
0076            DS0=S1-S0
0077            DS1=S2-S1
0078            DDS0=DS1-DS0
0079            AA=DDS0/2.
0080            BB=-DDS0/2.+DS0
0081            CC=S0
0082            SOLNB=AA*XN**2+BB*XN+CC
0083            GO TO 805
0084        803 IF(I-1.LT.1)GO TO 804
0085            N=3
0086            F0=FUNC(I-1,J)
0087            F1=FUNC(I,J)
0088            F2=FUNC(I+1,J)
0089            DF0=F1-F0
0090            DF1=F2-F1
0091            DDF0=DF1-DF0
0092            A=DDF0/2.
0093            B=-DDF0/2.+DF0
0094            C=F0
0095            X=1.
0096        810 XN=(-1./A)*(B+C/X)
0097            IF(ABS(XN-X).LT.EPSL)GO TO 811
0098            X=XN
0099            GO TO 810
0100        811 CROSS=I-1+XN
0101            VALUE=CROSS/2.+1.5
0102            S0=SOLN(I-1,M)
0103            S1=SOLN(I,M)
0104            S2=SOLN(I+1,M)
0105            DS0=S1-S0
0106            DS1=S2-S1
0107            DDS0=DS1-DS0
0108            AA=DDS0/2.
0109            BB=-DDS0/2.+DS0
0110            CC=S0
0111            SOLNB=AA*XN**2+BB*XN+CC
0112            GO TO 805
0113        804 N=2
0114            F0=FUNC(I,J)
0115            F1=FUNC(I+1,J)
0116            CROSS=-F0/(F1-F0)
0117            VALUE=CROSS/2.+1.5
0118            S0=SOLN(I,M)
0119            S1=SOLN(I+1,M)
0120            DS0=S1-S0
0121            AA=DS0
0122            BB=S0
0123            SOLNB=AA*XN+BB
0124            GO TO 805
0125        805 K=K+1
0126            P(K)=VALUE
```

```
0127                BP(K)=SOLNB
0128                GO TO 801
0129            800 CONTINUE
0130                NRTS=K
0131                RETURN
0132                END
```

SOLVE

```
0001            SUBROUTINE SOLVE(PHI0,PHI2)
0002            COMMON/AREA2/COEF00,COEF01(30),COEF02(30),COEF20,COEF21(30),
               C COEF22(30)
0003            COMMON/AREA3/FUNC(30,4),SOLN(30,2)
0004            WRITE(6,506)
0005            P=2.0
0006            DO 401 I=1,30
0007            SQ0=COEF01(I)**2-4.*COEF02(I)*(COEF00-PHI0)
0008            DISC0=SQRT(SQ0)
0009            SQ2=COEF21(I)**2-4.*COEF22(I)*(COEF20-PHI2)
0010            DISC2=SQRT(SQ2)
0011            SOLNU0=(-COEF01(I)+DISC0)/(2.*COEF02(I))
0012            SOLNL0=(-COEF01(I)-DISC0)/(2.*COEF02(I))
0013            SOLNU2=(-COEF21(I)+DISC2)/(2.*COEF22(I))
0014            SOLNL2=(-COEF21(I)-DISC2)/(2.*COEF22(I))
0015            SOLN(I,1)=SOLNU0
0016            SOLN(I,2)=SOLNL0
0017            FUNC(I,1)=SOLNU0-SOLNU2
0018            FUNC(I,2)=SOLNU0-SOLNL2
0019            FUNC(I,3)=SOLNL0-SOLNU2
0020            FUNC(I,4)=SOLNL0-SOLNL2
0021            WRITE(6,503)P,SOLNU0,SOLNL0,SOLNU2,SOLNL2
0022        401 P=P+0.5
0023            WRITE(6,502)
0024            P=2.0
0025            DO 450 I=1,30
0026            WRITE(6,503)P,FUNC(I,1),FUNC(I,2),FUNC(I,3),FUNC(I,4)
0027        450 P=P+0.5
0028        502 FORMAT(1H0,10X,'  P ',6X,'FUNCTION 1',8X,'FUNCTION 2',8X,
               C 'FUNCTION 3',8X,'FUNCTION 4')
0029        503 FORMAT(1H ,10X,F4.1,4E18.7)
0030        506 FORMAT(1H0,10X,'  P ',6X,'SOLUTION 1',8X,'SOLUTION 2',8X,
               C 'SOLUTION 3',8X,'SOLUTION 4')
0031            RETURN
0032            END
```

ARRAY

```
0001              SUBROUTINE ARRAY
0002              COMMON/AREA2/COEF00,COEF01(30),COEF02(30),COEF20,COEF21(30),
                 C COEF22(30)
0003              COMMON/AREA5/SIG,EPS,ALPHA,RMASS,TEMP
0004              REAL INTGRL
0005              A=ALPHA**2
0006              EXPON=4.
0007              COEF00=36.*A**2*(1./SIG)**3*INTGRL(EXPON)
0008              EXPON=6.
0009              COEF20=540.*A**2*(1./SIG)**5*INTGRL(EXPON)
0010              P=2.0
0011              DO 301 I=1,30
0012              EXPON=1.+P
0013              COEF01(I)=12.*A*(1./SIG)**P*INTGRL(EXPON)
0014              EXPON=2.*P-2.
0015              COEF02(I)=(1./SIG)**(2.*P-3.)*INTGRL(EXPON)
0016              EXPON=3.+P
0017              COEF21(I)=36.*A*(P+2.)*(1./SIG)**(P+2.)*INTGRL(EXPON)
0018              EXPON=2.*P
0019              COEF22(I)=(P**2+6.)*(1./SIG)**(2.*P-1.)*INTGRL(EXPON)
0020          301 P=P+0.5
0021              WRITE(6,500)
0022              P=2.0
0023              DO 550 I=1,30
0024              WRITE(6,501)P,COEF00,COEF01(I),COEF02(I),COEF20,COEF21(I),
                 C COEF22(I)
0025          550 P=P+0.5
0026          500 FORMAT(1H1,10X,'  P ',8X,'COEF00',12X,'COEF01',12X,'COEF02',12X,
                 C 'COEF20',12X,'COEF21',12X,'COEF22')
0027          501 FORMAT(1H ,10X,F4.1,6E18.7)
0028              RETURN
0029              END
```

INTGRL

```
0001            REAL FUNCTION INTGRL(EXPON)
0002            COMMON/AREA5/SIG,EPS,ALPHA,RMASS,TEMP
0003            DIMENSION RESULT(4)
              C  EVALUATE INTEGRAL USING SIMPSONS RULE
0004            C=-4.*EPS/TEMP
0005            EPSL=1.0E-05
0006            UP=4.7
0007            ITER=0
0008            H=1./32.
0009          110 CONTINUE
0010            X=0.7
0011            INTGRL=FX(X,EXPON)
0012          100 CONTINUE
0013            X=X+H
0014            INTGRL=INTGRL+4.*FX(X,EXPON)
0015            IF(X.GE.(UP-H))GO TO 101
0016            X=X+H
0017            INTGRL=INTGRL+2.*FX(X,EXPON)
0018            GO TO 100
0019          101 X=X+H
0020            INTGRL=INTGRL+FX(X,EXPON)
0021            INTGRL=(H/3.)*INTGRL+((1./X)**(EXPON-1.)/(EXPON-1.))
                C -C*((1./X)**(EXPON+5.)/(EXPON+5)-(1./X)**(EXPON+11)/(EXPON+11))
0022            ITER=ITER+1
0023            RESULT(ITER)=INTGRL
0024            IF(ITER.EQ.1)GO TO 120
0025            IF(ITER.EQ.4)GO TO 130
0026            IF(ABS((RESULT(ITER)-RESULT(ITER-1))/RESULT(ITER)).LT.EPSL)GO
                1 TO 130
0027          120 H=H/2.
0028            GO TO 110
0029          130 CONTINUE
0030            WRITE(6,700)
0031            WRITE(6,701)EXPON,INTGRL
0032          700 FORMAT(1H ,10X,'EXPONENT=-',4X,5X,'INTEGRAL=')
0033          701 FORMAT(1H+,10X,10X,F4.1,5X,9X,E13.7)
0034            RETURN
0035            END
```

FX

```
0001                FUNCTION FX(X,EXPON)
0002                COMMON/AREA5/SIG,EPS,ALPHA,RMASS,TEMP
              C   GX AND FX WILL UNDERFLOW IF X.LT.(0.7)
0003                C=-4.*EPS/TEMP
0004                GX=EXP(C*((1./X)**12-(1./X)**6))
0005                FX=GX*((1./X)**EXPON)
0006                RETURN
0007                END
```

APPENDIX A4

CALCULATE MOMENTS OF SPECTRUM

```
STMT   SOURCE STATEMENT

    1 RDDECK   CSECT
    2          USING *,15
    3          B     *+12
    4          DC    AL1(4),CL7'DAVE'
    5          STM   14,12,12(13)
    6          BAL   14,*+76
    7          DROP  15
    8          USING *,13
    9          DC    18A(*-*)
   10          ST    13,4(14)
   11          ST    14,8(13)
   12          LR    13,14
   13 * READY TO START
   14          OPEN  CARD
   15+         CNOP  0,4 ALIGN LIST TO FULLWORD
   16+         BAL   1,*+8 LOAD REG1 W/LIST ADDR.
   17+         DC    AL1(128) OPTION BYTE
   18+         DC    AL3(CARD) DCB ADDRESS.
   19+         SVC   19 ISSUE OPEN SVC
   20 INITIAL  ZAP   ZEROMOM(8),=P'0'
   21          ZAP   SECMOM(8),=P'0'
   22 * INITIALIZE ZEROMOM AND SECMOM
   23 READLOOP GET   CARD,AREA
   24+READLOOP LA    1,CARD LOAD PARAMETER REG 1
   25+         LA    0,AREA LOAD PARAMETER REG 0
   26+         L     15,48(0,1) LOAD GET ROUTINE ADDR.
   27+         BALR  14,15 LINK TO GET ROUTINE
   28          CLC   =CL10' ',AREA+60
   29          BE    DATAPROC
   30          CLC   =C'RUN NO',AREA+60
   31          BE    LOADRNNO
   32 * CHANNEL NO IS THE SHIFT IN CHANNELS FROM THE RAYLEIGH LINE
   33          CLC   =C'CH NO FIRST PT',AREA+60
   34          BE    LOADCHNO
   35          CLC   =C'USE DATA BETWEEN',AREA+60
   36          BE    LOADSTSP
   37 * CHSTART MUST BE AT OR AFTER CHNO FIRST PT
   38 * USE DATA POINTS UP TO THE END OF DATA OR CHSTOP,WHICHEVER COMES FIRST
   39 * BUT CHSTOP MUST BE GIVEN A VALUE
   40          CLC   =C'DARK COUNT',AREA+60
   41          BE    LOADDARK
   42          CLC   =C'FIT PARAMETERS',AREA+60
   43          BE    LOADFIT
   44 * FIT PARAMETERS ARE AAMP,ASLOPE,BAMP,BSLOPE
   45 * THE FORM OF THE FIT IS  (AAMP/10)*EXP(-(ASLOPE/10**6)*W)+(BAMP/10)*
   46 *                              EXP(-(BSLOPE/10**6)*W)
   47          CLC   =C'RETURN',AREA+60
   48          BE    LOADR
   49          CLC   =C'FINISH',AREA+60
   50          BE    LOADF
   51          B     READLOOP
   52 * READ NEXT CARD IF THE PRESENT CARD CANNOT BE IDENTIFIED
   53 DATAPROC LA    10,0
   54          LA    9,AREA
   55 LOOP     MVC   TEMP1(6),0(9)
   56 * PICK OUT A SIX CHARACTER FIELD
   57          CLC   TEMP1(6),=CL6' '
   58          BE    READLOOP
   59 * READ NEXT CARD IF A DATA FIELD IS BLANK
   60          CP    CHNO(2),CHSTOP(2)
```

```
STMT   SOURCE STATEMENT

   61            BNL    READ_LOOP
   62 * READ NEXT CARD IF THE END CHANNEL HAS BEEN REACHED
   63            CP     CHNO(2),CHSTART(2)
   64            BL     NEXTPT
   65 * GO TO NEXT CHANNEL IF CHSTART HAS NOT BEEN REACHED
   66            PACK   TEMP2(8),TEMP1(6)
   67            SP     TEMP2(8),DARK(4)
   68            AP     ZEROMOM(8),TEMP2(8)
   69            ZAP    TEMP3(4),CHNO(2)
   70            MP     TEMP3(4),CHNO(2)
   71            MP     TEMP2(8),TEMP3(4)
   72            AP     SECMOM(8),TEMP2(8)
   73 NEXTPT     AP     CHNO(2),=P'1'
   74            LA     10,1(10)
   75            LA     9,6(9)
   76            C      10,=F'10'
   77            BNE    LOOP
   78            B      READ_LOOP
   79 * END OF DATA PROC SECTION
   80 * RESULTS ARE ZEROMOM,SECMOM,CHNO
   81 LOADRNNO   MVC    TEMP3(4),AREA
   82            PACK   TEMP2(8),TEMP3(4)
   83            CVB    3,TEMP2
   84            STH    3,RUN
   85            B      READ_LOOP
   86 LOADSTSP   MVC    TEMP3(4),AREA
   87            PACK   TEMP2(8),TEMP3(4)
   88            MVC    CHSTART(2),TEMP2+6
   89            CVB    3,TEMP2
   90            STH    3,CHST
   91            MVC    TEMP3(4),AREA+4
   92            PACK   TEMP2(8),TEMP3(4)
   93            MVC    CHSTOP(2),TEMP2+6
   94            B      READLOOP
   95 LOADCHNO   MVC    TEMP3(4),AREA
   96            PACK   TEMP2(8),TEMP3(4)
   97            MVC    CHNO(2),TEMP2+6
   98            B      READLOOP
   99 LOADDARK   MVC    TEMP3(4),AREA
  100            PACK   TEMP2(8),TEMP3(4)
  101            MVC    DARK(4),TEMP2+4
  102            CVB    3,TEMP2
  103            STH    3,BKGRND
  104            B      READLOOP
  105 LOADFIT    MVC    TEMP1(6),AREA+2
  106            PACK   TEMP2(8),TEMP1(6)
  107            CVB    3,TEMP2
  108            ST     3,AAMP
  109            MVC    TEMP1(6),AREA+10
  110            PACK   TEMP2(8),TEMP1(6)
  111            CVB    3,TEMP2
  112            ST     3,ASLOPE
  113            CLC    =CL16' ',AREA+16
  114            BE     FLAG
  115            MVC    TEMP1(6),AREA+18
  116            PACK   TEMP2(8),TEMP1(6)
  117            CVB    3,TEMP2
  118            ST     3,BAMP
  119            MVC    TEMP1(6),AREA+26
  120            PACK   TEMP2(8),TEMP1(6)
```

```
STMT   SOURCE STATEMENT

  121            CVB   3,TEMP2
  122            ST    3,BSLOPE
  123            B     NOFLAG
  124 FLAG       MVC   ONEXP(2),=H'1'
  125            MVC   BAMP,=F'0'
  126            MVC   BSLOPE,=F'2000'
  127            B     READ_LOOP
  128 NOFLAG     MVC   ONEXP(2),=H'0'
  129            B     READLOOP
  130 LOADR      L     15,ACONVERT
  131            BALR  14,15
  132            L     15,PRINTOUT
  133            BALR  14,15
  134            B     INITIAL
  135 LOADF      L     15,ACONVERT
  136            BALR  14,15
  137            L     15,PRINTOUT
  138            BALR  14,15
  139            B     FINISH
  140 CONVERT    ZAP   TEMP2(8),CHNO(2)
  141            CVB   3,TEMP2
  142            STH   3,CHN
  143            CVB   3,ZEROMOM
  144            ST    3,MOM0
  145            ZAP   TEMP0(9),SECMOM(8)
  146            DP    TEMP0(9),=PL2'100'
  147            ZAP   TEMP2(8),TEMP0(7)
  148            CVB   3,TEMP2
  149            ST    3,MOM2
  150            LA    1,=A(MOM0,MOM2,AAMP,ASLOPE,BAMP,BSLOPE,RUN,CHST,CHN,ONEXX
                       P,BKGRND)
  151            BR    14
  152 * CONSTANT AND STORAGE DEFINITIONS
  153 CARD       DCB   DSORG=PS,RECFM=F,LRECL=80,BLKSIZE=80,                    X
                       MACRF=(GM),DDNAME=CARDIN


  155+*                          DATA CONTROL BLOCK
  156+*
  157+CARD       DC    0F'0' ORIGIN ON WORD BOUNDARY

  159+*                          DIRECT ACCESS DEVICE INTERFACE

  161+           DC    BL16'0' FDAD,DVTBL
  162+           DC    A(0) KEYLE,DEVT,TRBAL

  164+*                          COMMON ACCESS METHOD INTERFACE

  166+           DC    AL1(0) BUFNO
  167+           DC    AL3(1) BUFCB
  168+           DC    AL2(0) BUFL
  169+           DC    BL2'0100000000000000' DSORG
  170+           DC    A(1) IOBAD

  172+*                          FOUNDATION EXTENSION

  174+           DC    BL1'00000000' BFTEK,BFLN,HIARCHY
  175+           DC    AL3(1) EODAD
  176+           DC    BL1'10000000' RECFM
  177+           DC    AL3(0) EXLST
```

```
STMT   SOURCE STATEMENT

 179+*                          FOUNDATION BLOCK

 181+           DC    CL8'CARDIN' DDNAME
 182+           DC    BL1'00000010' DFLGS
 183+           DC    BL1'00000000' IFLG
 184+           DC    BL2'0101000000000000' MACR

 186+*                          BSAM-BPAM-QSAM INTERFACE

 188+           DC    BL1'00000000' RER1
 189+           DC    AL3(1) CHECK, GERR, PERR
 190+           DC    A(1) SYNAD
 191+           DC    H'0' CIND1, CIND2
 192+           DC    AL2(80) BLKSIZE
 193+           DC    F'0' WCPO, WCPL, OFFSR, OFFSW
 194+           DC    A(1) IOBA
 195+           DC    AL1(0) NCP
 196+           DC    AL3(1) EOBR, EOBAD

 198+*                          QSAM INTERFACE

 200+           DC    A(1) RECAD
 201+           DC    H'0' QSWS
 202+           DC    AL2(80) LRECL
 203+           DC    BL1'00000000' EROPT
 204+           DC    AL3(1) CNTRL
 205+           DC    F'0' PRECL
 206+           DC    A(1) EOB
 207 PRINTOUT   DC    V(PRTOUT)
 208 ACONVERT   DC    A(CONVERT)
 209 AREA       DC    CL80' '
 210 ZEROMOM    DS    D
 211 SECMOM     DS    D
 212 TEMP2      DS    D
 213 TEMP1      DS    PL6
 214 CHNO       DS    PL2
 215 CHSTART    DS    PL2
 216 CHSTOP     DS    PL2
 217 TEMP3      DS    PL4
 218 MOMO       DS    F
 219 MOM2       DS    F
 220 DARK       DS    F
 221 AAMP       DS    F
 222 ASLOPE     DS    F
 223 BAMP       DS    F
 224 BSLOPE     DS    F
 225 DNEXP      DS    H
 226 RUN        DS    H
 227 CHST       DS    H
 228 CHN        DS    H
 229 BKGRND     DS    H
 230 BLANK      DS    H
 231 TEMPO      DS    PL9

 232 FINISH     L     13,4(13)
 233            LM    14,15,12(13)
 234            LM    1,12,24(13)
 235            END   RDDECK
 236                  =C'USE DATA BETWEEN'
 237                  =CL16' '
```

```
STMT   SOURCE STATEMENT

  238                =F'10'
  239                =F'0'
  240                =F'2000'
  241                =A(MOMO,MOM2,AAMP,ASLOPE,BAMP,BSLOPE,RUN,CHST,CHN,ONEXP,X
                     BKGRND)
  242                =CL10' '
  243                =C'RUN NO'
  244                =C'CH NO FIRST PT'
  245                =C'DARK COUNT'
  246                =C'FIT PARAMETERS'
  247                =C'RETURN'
  248                =C'FINISH'
  249                =CL6' '
  250                =H'1'
  251                =H'0'
  252                =PL2'100'
  253                =P'0'
  254                =P'1'
```

PRTOUT

```
0001          SUBROUTINE PRTOUT(MOM0,MOM2,AAMP,ASLOPE,BAMP,BSLOPE,RUN,CHST,CHN,
             C ONEXP,BKGRND)
0002          INTEGER*2 RUN,CHST,CHN,ONEXP,BKGRND
0003          INTEGER*4 MOM0,MOM2,AAMP,ASLOPE,BAMP,BSLOPE,FLAG,BKGD
0004          A=AAMP/10.0
0005          AW=ASLOPE/10.0**5
0006          B=BAMP/10.0
0007          BW=BSLOPE/10.0**5
0008          DM0=MOM0
0009          DM2=MOM2*100.0
0010          W1=CHST
0011          W2=CHN
0012          FLAG=ONEXP
0013          BKGD=BKGRND
0014          CFM0=A/AW+B/BW
0015          CFM2=2.0*A/AW**3+2.0*B/BW**3
0016          SEGMT0=(-A/AW)*(EXP(-AW*W2)-EXP(-AW*W1))+
             C (-B/BW)*(EXP(-BW*W2)-EXP(-BW*W1))
0017          SEGMT2=(-A/AW)*((W2**2-2.0*(AW*W2-1.0)/AW**2)*EXP(-AW*W2)-
             C (W1**2-2.0*(AW*W1-1.0)/AW**2)*EXP(-AW*W1))+
             C (-B/BW)*((W2**2-2.0*(BW*W2-1.0)/BW**2)*EXP(-BW*W2)-
             C (W1**2-2.0*(BW*W1-1.0)/BW**2)*EXP(-BW*W1))
0018          CFDM0=CFM0-SEGMT0+DM0
0019          CFDM2=CFM2-SEGMT2+DM2
0020          RATIOF=CFM2/CFM0
0021          RATIOD=CFDM2/CFDM0
0022          WRITE(6,100)
0023          WRITE(6,101)RUN
0024          WRITE(6,102)
0025          IF(FLAG.EQ.0)GO TO 20
0026       10 WRITE(6,96)
0027          WRITE(6,97)A,AW
0028          GO TO 30
0029       20 WRITE(6,98)
0030          WRITE(6,99)A,AW,B,BW
0031       30 WRITE(6,103)
0032          WRITE(6,104)CFM0,CFM2
0033          WRITE(6,108)
0034          WRITE(6,109)RATIOF
0035          WRITE(6,105)
0036          WRITE(6,106)
0037          WRITE(6,107)CHST,CHN,BKGD
0038          WRITE(6,103)
0039          WRITE(6,104)CFDM0,CFDM2
0040          WRITE(6,108)
0041          WRITE(6,109)RATIOD
0042          WRITE(6,110)
0043       96 FORMAT(1H0,10X,7X,'EXP(-',8X,'X)')
0044       97 FORMAT(1H+,F17.1,F13.6)
0045       99 FORMAT(1H+,F17.1,F13.6,F10.1,F13.6)
0046       98 FORMAT(1H0,10X,7X,'EXP(-',8X,'X)+',7X,'EXP(-',8X,'X)')
0047      100 FORMAT(1H-,10X,'RUN NUMBER')
0048      101 FORMAT(1H+,I24)
0049      102 FORMAT(1H0,10X,'USING ONLY THE FITTED CURVE')
0050      103 FORMAT(1H0,10X,'ZEROTH MOMENT',15X,'SECOND MOMENT')
0051      104 FORMAT(1H+,E38.7,E29.7)
0052      105 FORMAT(1H0,10X,'USING THE FITTED CURVE TO EXTRAPOLATE AND USING')
0053      106 FORMAT(1H0,10X,'DATA BETWEEN CHANNEL',5X,'AND CHANNEL',5X,
             C 'WITH BACKGROUND OF',5X,'COUNTS/CHANNEL')
0054      107 FORMAT(1H+,I34,I16,I23)
0055      108 FORMAT(1H0,10X,'SECOND MOMENT/ZEROTH MOMENT')
0056      109 FORMAT(1H+,E51.7)
0057      110 FORMAT(1H0)
```

```
0058                RETURN
0059                END
```

APPENDIX B

PUBLICATIONS

Reprinted from:

CHEMICAL PHYSICS LETTERS

Volume 15, No. 3, 15 August 1972

COLLISION-INDUCED LIGHT SCATTERING FROM LIQUID CCl_4 AND C_6H_{12}*

G.C. TABISZ, W.R. WALL and D.P. SHELTON

Department of Physics, University of Manitoba, Winnipeg, Manitoba R3T 2N2, Canada

pp. 387 – 391

NORTH-HOLLAND PUBLISHING COMPANY — AMSTERDAM

COLLISION-INDUCED LIGHT SCATTERING FROM LIQUID CCl_4 AND C_6H_{12}*

G.C. TABISZ, W.R. WALL and D.P. SHELTON
Department of Physics, University of Manitoba, Winnipeg, Manitoba R3T 2N2, Canada

Received 25 April 1972

Collision-induced light scattering was observed in pure CCl_4 and C_6H_{12} and in their mixtures. The intensity $I(\omega)$ in the high frequency wing was fitted to an expression, $I(\omega) \propto \omega^q \exp(-\omega/\omega_0)$ where q and ω_0 are variable parameters. It was found that the values of q and ω_0 are dependent upon the region of the profile over which the fit is made; possible interpretations are discussed.

1. Introduction

Collision-induced light scattering (CIS) is a newly-identified phenomenon which has increased the scope of the information obtainable about dense media by scattering methods [1–4]. While free, optically isotropic atoms or molecules do not depolarize light, an anisotropy can be induced in the total polarizability of a system of interacting atoms which produces a broad depolarized wing centred about the polarized Rayleigh line. Three models for the induction mechanism have been proposed based on studies of liquids and compressed gases.

(i) *Dipole-induced dipole (DID)* [1,2,5]: The anisotropy results from the interaction between electric dipoles induced in the atoms by the incident light. The total field acting on a given atom is the sum of this external light field and the internal field due to the induced dipoles in its neighbours. Orientational fluctuations in the net induced moment due to the atomic motion yield the depolarized scattering. This is a long-range interaction giving an effective pair polarizability which varies as r^{-3} where r is the distance between the atoms in a collision pair.

(ii) *Electron overlap (EO)* [3,4]. The distortion of the electron clouds during close encounters is responsible for the induced polarizability. Originally, the form $r^2 \exp(-ar^2)$ was proposed but recently**, an r^{-9} dependence has been derived in the case of argon.

(iii) *Frame distortion* [6]. Bucaro and Litovitz [7,8] have made an extensive study of CIS in atomic and molecular liquids and concluded that frame distortion during close collisions which gives a pair polarizability varying as r^{-13} is the principal induction mechanism in liquids composed of isotropic and non-isotropic molecules.

With the use of several simplifying assumptions, principally binary collisions with zero impact parameter, Bucaro and Litovitz were able to derive an expression for the intensity I in the wings as a function of frequency ω,

$$I(\omega) \propto \omega^{2[(m-7)/7]} \exp(-\omega/\omega_0) , \qquad (1)$$

where the induced incremental polarizability is given by

$$\Delta\alpha(r) \propto r^{-m} . \qquad (2)$$

The constant ω_0 is inversely proportional to a characteristic time associated with the duration of the interaction giving rise to $\Delta\alpha$.

In the analysis of their spectra, they assumed a value for m and determined the corresponding ω_0 from their data. As there is evidence from experiments on compressed gases [1,2] that the DID contribution diminishes at high densities, they assumed that, in the

* This work is supported by a grant from the National Research Council of Canada.

** M.R. Vukcevich, private communication quoted in ref. [6].

case of atomic liquids, the electron overlap effect predominates. They found that $m = 9$ in the case of argon and xenon and $m = 13$ in the case of molecular liquids gave values of ω_0 in agreement with their calculations. This work is an excellent attempt to categorize CIS in liquids while providing insight into the interaction mechanisms responsible for the scattering. Primarily, it shows that binary interactions remain important even in the liquid phase.

Gersten [9,10] has pointed out that in the spectra of compressed rare gases, different parts of the profile are affected by different details of the interaction.

Encouraged by the success of Bucaro and Litovitz but mindful that the complications envisaged by Gersten should apply to liquids as well as gases, we have repeated observations of the CIS spectra in pure CCl_4 and C_6H_{12}, as well as in mixtures, with the goal of further investigating the form of the spectral profile.

2. Experimental method

The experimental set-up is typical of laser Raman scattering studies. Light from an argon-ion laser (CRL 52) operating at about 3/4 watt at 4880 Å is passed through a half-wave plate and prism polarizer before being focussed in the sample cell. The light scattered at 90° is collected by an f/2 system and brought to a double scanning monochromator (Jarrell–Ash 25-100) having a spectral slit width of 1 cm^{-1}. The detector is a cooled EMI 6256B photomultiplier tube used in the photon-counting mode. With the discriminator levels set for an optimum signal-to-noise ratio at low light intensities, the dark count is 1/3 cpsec. The output is stored in a multichannel analyzer (Victoreen ST400M) whose channel advance is controlled by the stepping drive for the monochromator gratings. The geometry used is such that if the incident light is considered to travel in the x direction, polarized in the z direction, then observations are made in the z direction. All experiments are performed at 295°K.

3. Analysis of results

If a frame distortion origin for the induced polarizability is assumed, eq. (1) leads to a linear relationship between $\ln[I(\omega)/\omega^{12/7}]$ and ω with a slope $(-1/\omega_0)$. When this test is applied to the data, it is found that $\omega_0 = 12.1$ cm^{-1} for CCl_4 and 14.7 cm^{-1} for C_6H_{12} in excellent agreement with Bucaro and Litovitz (11.9 and 14.8 cm^{-1} respectively). The frequency range over which this linear relation holds is 30 to 80 cm^{-1} for CCl_4 and 30 to 120 cm^{-1} for C_6H_{12} (fig. 1).

Frame distortion may not however be the only interaction mechanism contributing to the scattering. It was noted that much of the high frequency tail of the CCl_4 could not be accounted for by the above method. When $m = 9$ was tried, a value consistent with an electron overlap interaction (at least for rare gas atoms), eq. (1) held over an increased frequency range, 20 cm^{-1} to 100 cm^{-1}. Moreover the quality of the fit was much improved over that with $m = 13$. This result led us to perform the analysis based on the following considerations.

All authors who have proposed mechanisms for collision-induced scattering conclude that the high frequency profile is described by an expression:

$$I(\omega) = f(\omega) \exp(-\omega/\omega_0) . \quad (3)$$

In the original model of Levine and Birnbaum, $f(\omega)$ is approximated by $\omega^{1/2}$; the more general function $\omega^{2[(m-7)/7]}$ shows clearly that the power of ω is a function of the induction process. Gersten [10] has emphasized that the exponential factor in (3) is model independent (although the value of ω_0 is not). The accurate determination of $f(\omega)$ should lead to meaningful information not available through the exponential. Because of the presence of this strong exponential factor, the exact form of $f(\omega)$ is difficult to extract from the experimental data.

In an effort to acquire some estimate of $f(\omega)$ directly from the observed spectra, we have assumed that the high frequency profile can be represented by:

$$I(\omega) \propto \omega^q \exp(-\omega/\omega_0) , \quad (4)$$

where both q and ω_0 are taken as variable parameters and made a least squares fit to the spectra by applying the technique of multiple regression. The results given in table 1 are averages over several spectra. The errors quoted represent one standard deviation. For C_6H_{12}, the fits in the range 25 cm^{-1} and 40 cm^{-1} to 100 cm^{-1} are the more significant as they are over a region sufficiently removed from the laser line to be

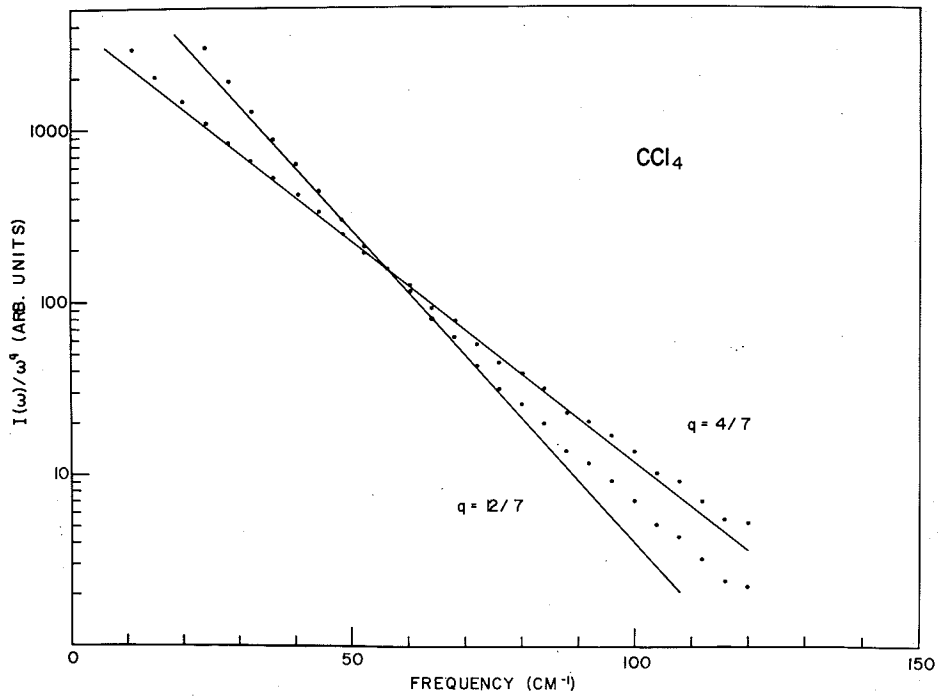

Fig. 1. $I(\omega)/\omega^q$ for the observed spectrum of CCl_4 at 293°K where q is 12/7 and 4/7 corresponding to $\Delta\alpha(r)$ varying as r^{-13} and r^{-9} respectively. Data points are shown only every 4 cm^{-1}.

Table 1
Parameters obtained from the least squares fit

	Range (cm^{-1})	q	Effective m	ω_0 (cm^{-1})	Standard error of estimate
CCl_4	16→ 85	0.49 ± 0.04	8.7 ± 0.13	17.0 ± 0.25	0.05
	16→105	0.22 ± 0.03	7.8 ± 0.12	19.1 ± 0.25	0.06
	16→125	0.15 ± 0.04	7.5 ± 0.13	19.6 ± 0.24	0.11
	40→100	−0.72 ± 0.19	4.5 ± 0.67	25.3 ± 1.9	0.09
C_6H_{12}	15→115	0.78 ± 0.05	9.7 ± 0.17	19.2 ± 0.32	0.11
	25→115	1.36 ± 0.07	11.7 ± 0.23	16.7 ± 0.28	0.10
	40→115	2.04 ± 0.13	14.1 ± 0.46	14.5 ± 0.33	0.10

free of contributions due to the permanent anisotropy of the molecule. The 'effective m' is determined by setting

$$q = (2/7)(m-7)\,. \qquad (5)$$

The standard error of estimate is calculated only over the range of the fit.

4. Discussion

The most striking result in table 1 is the fact that for both liquids, the values of q and ω_0 depend on the frequency region over which the fit is made. For C_6H_{12} the result in the range 40 to 115 cm^{-1} agrees with that of Bucaro and Litovitz. On the other hand,

for CCl_4, as more of the tail is included in the fit, the effective m decreases and ω_0 increases, nowhere approximating $m = 13$ or $\omega_0 = 11.9$ cm^{-1}.

The failure of eq. (1) to hold over the entire tail with one set of values for q and ω_0 indicates that more than one type of interaction is operative in the scattering. For C_6H_{12}, short-range effects seem to be important with frame distortion especially dominant beyond 40 cm^{-1}. The theory of Bucaro and Litovitz holds well in this case: basically a single short-range interaction. For CCl_4, both short- and long-range interactions contribute. Here the theory of Bucaro and Litovitz is not entirely applicable as their calculations of ω_0 are valid only near the turning point. Judging from the effective m values, the short-range part includes both electron overlap and frame distortion. The long-range interaction could be of the dipole-induced dipole type.

It should be recalled that because of symmetry effects, the intensity of the scattering through DID at liquid densities is much less than that predicted from an extrapolation of the gas results using a quadratic dependence on density; however it should not necessarily vanish. In liquids the DID interaction would be effective through rapid local fluctuations in the positions of molecules, not describable by the trajectory dynamics used to derive eq. (1). Thus the spectral profile due to DID would broaden as the density increases and it would be expected to contribute to the far wings of spectrum.

The ω_0 found for $40 < \omega < 100$ corresponds to a time of 2.1×10^{-13} sec which is of the order of magnitude of the time between collisions in a cell model for liquid CCl_4 [11]; the time between collisions would be the time characterizing these fluctuations in positions.

The values of ω_0 obtained from the spectra of mixtures in the range 40 to 100 cm^{-1} are plotted in fig. 2 as a function of CCl_4 concentration. A least squares fit to a polynomial in concentration shows that the variation of ω_0 with concentration can be well represented by a quadratic and a cubic term, the higher order and linear terms being negligible. Since ω_0 characterizes the spectral profile, this means that changes in the line shape occur roughly in the same way with concentration. The cell model used by Thibeau [1,2] to explain the results in gaseous argon at high pressures predicts a density dependence of the

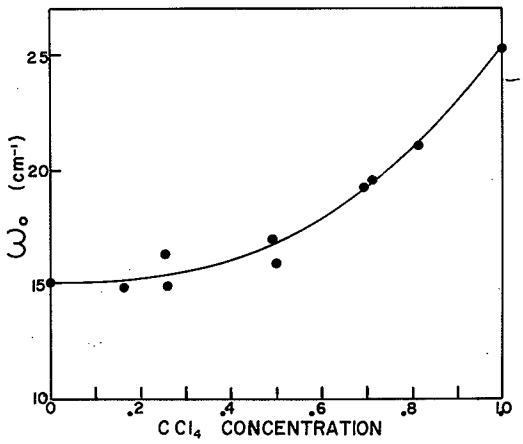

Fig. 2. The variation of ω_0 with the concentration of CCl_4 in the frequency range 40 to 100 cm^{-1}.

total intensity involving several terms of the form $(\rho/\rho_s)^x$ where x is between 2 and 3.3; ρ_s is the maximum density taken to be that of the solid. Therefore as one goes from pure C_6H_{12} which is of frame distortion origin to pure CCl_4, the concentration dependence of ω_0 is similar to the density dependence of the intensity for DID scattering in dense media. A thorough treatment of scattering from mixtures is complex and difficult to apply [12]; nevertheless this result appears to support the conclusion that the tail of the CCl_4 spectrum contains a contribution from DID scattering. In any event, the low power of the concentration dependence reaffirms that the scattering is due to interactions between a few molecules even in the liquid phase.

5. Summary

Based on the statistical accuracy of the data further speculation on the physical meaning of results in table 1 is uncertain. It is clear however that the values of q and ω_0 giving the best fit to the observed spectra change over the profile. This variation is attributable to the total induced polarizability being due to more than one type of interaction. For CCl_4, it appears that both short- and long-range forces are effective in the interaction; electron overlap, DID and frame distortion could all be contributing. On the other hand for C_6H_{12}, only the short-range interactions seem to be important.

References

[1] M. Thibeau, B. Oksengorn and B. Vodar, J. Phys. (Paris) 29 (1968) 287.
[2] M. Thibeau, G.C. Tabisz, B. Oksengorn and B. Vodar, J. Quant. Spectry. Radiative Transfer 10 (1970) 839.
[3] H.B. Levine and G. Birnbaum, Phys. Rev. Letters 20 (1968) 439.
[4] J.P. McTague and G. Birnbaum, Phys. Rev. Letters 21 (1968) 661.
[5] P. Lallemand, Phys. Rev. Letters 25 (1970) 1079; J. Phys. (Paris) 32 (1971) 10.
[6] H.S. Gabelnick and H.L. Strauss, J. Chem. Phys. 49 (1968) 2334.
[7] J.A. Bucaro and T.A. Litovitz, J. Chem. Phys. 54 (1971) 3846.
[8] J.A. Bucaro and T.A. Litovitz, J. Chem. Phys. 55 (1971) 3585.
[9] J.I. Gersten, R.E. Slusher and C.M. Surko, Phys. Rev. Letters 25 (1970) 1739.
[10] J.I. Gersten, Phys. Rev. A4 (1971) 98.
[11] F.J. Bartoli and T.A. Litovitz, J. Chem. Phys. 56 (1972) 413.
[12] S. Kielich, Chem. Phys. Letters 10 (1971) 516.

Reprinted from

ADVANCES IN RAMAN SPECTROSCOPY, VOLUME 1

(Proceedings of Third International Conference on Raman Spectroscopy, Reims, France, September 1972)

Heyden & Son Ltd., London

60. THE SPECTRAL PROFILE OF COLLISION-INDUCED LIGHT SCATTERING FROM SOME MOLECULAR LIQUIDS

G. C. Tabisz, W. R. Wall, D. P. Shelton and J. Ho
Department of Physics, University of Manitoba, Winnipeg, Manitoba, Canada

INTRODUCTION

Collision-induced light scattering (CIS) is a newly identified phenomenon which has increased the scope of the information obtainable about dense media by scattering methods.[1–4] While free, optically isotopic atoms or molecules do not depolarize light, an anisotropy can be induced in the total polarizability of a system of interacting atoms which produces a broad depolarized wing centred about the polarized Rayleigh line. Three models for the induction mechanism have been proposed based on studies of liquids and compressed gases.

(i) **Dipole-induced dipole (DID).**[1,2,5] The anisotropy results from the interaction between electric dipoles induced in the atoms by the incident light. The total field acting on a given atom is the sum of this external light field and the internal field due to the induced dipoles in its neighbours. Orientational fluctuations in the net induced moment due to the atomic motion yield the depolarized scattering. This is a long-range interaction giving an effective pair polarizability which varies as r^{-3} where r is the distance between the atoms in a collision pair.

(ii) **Electron Overlap (EO).**[3,4] The distortion of the electron clouds during close encounters is responsible for the induced polarizability. Originally, the form $r^2 \exp(-ar^2)$ was proposed but recently,[6] an r^{-9} dependence has been derived in the case of argon.

(iii) **Frame Distortion.**[7] Bucaro and Litovitz[8,9] have made an extensive study of CIS in atomic and molecular liquids and have concluded that frame distortion during close collisions which gives a pair polarizability varying as r^{-13} is the principal induction mechanism in liquids composed of isotropic and non-isotropic molecules.

With the use of several simplifying assumptions, principally binary collisions with zero impact parameter, Bucaro and Litovitz were able to derive an expression for the intensity I in the wings as a function of frequency ω

$$I(\omega) \propto \omega^{2[(m-7)/7]} \exp(-\omega/\omega_0) \qquad (1)$$

where the induced incremental polarizability is given by

$$\Delta\alpha(r) \propto r^{-m} \tag{2}$$

The constant ω_0 is inversely proportional to a characteristic time associated with the duration of the interaction giving rise to $\Delta\alpha$.

In the analysis of their spectra, they assumed a value for m and determined the corresponding ω_0 from their data. As there is evidence from experiments on compressed gases[1,2] that the DID contribution diminishes at high densities, they assumed that, in the case of atomic liquids, the electron overlap effect predominates. They found that $m = 9$ in the case of argon and xenon and $m = 13$ in the case of molecular liquids gave values of ω_0 in agreement with their calculations. This work is an excellent attempt to categorize CIS in liquids while providing insight into the interaction mechanisms responsible for the scattering. Primarily, it shows that binary interactions remain important even in the liquid phase.

Gersten[10,11] has pointed out that in the spectra of compressed rare gases, different parts of the profile are affected by different details of the interaction.

Encouraged by the success of Bucaro and Litovitz but mindful that the complications envisaged by Gersten should apply to liquids as well as gases, we have repeated observations of the CIS spectra in pure CCl_4 and C_6H_{12} with the goal of further investigating the form of spectral profile.

EXPERIMENTAL METHOD

The experimental set-up is typical of laser Raman scattering studies. Light from an argon-ion laser (CRL No. 52) operating at about 3/4 W at 4880 Å is passed through a half-wave plate and prism polarizer before being focused in the sample cell. The light scattered at 90° is collected by an $f/2$ system and brought to a double scanning monochromator (Jarrell–Ash No. 25–100) having a spectral slit width of 1 cm^{-1}. The detector is a cooled EMI 6256B photomultiplier tube used in the photon counting mode. With the discriminator levels set for an optimum signal-to-noise ratio at low light intensities, the dark count is 1/3 c.p.s. The output is stored in a multichannel analyser (Victoreen No. ST400M) whose channel advance is controlled by the stepping drive for the monochromator gratings. The geometry used is such that if the incident light is considered to travel in the x-direction, polarized in the z-direction, then observations are made in the z-direction. All experiments are performed at 295 K.

ANALYSIS OF RESULTS

If a frame distortion origin for the induced polarizability is assumed, Eqn. (1) leads to a linear relationship between $\ln (I(\omega)/\omega^{12/7})$ and ω with a slope $(-1/\omega_0)$. When this test is applied to the data, it is found that $\omega_0 = 11.9$ cm^{-1} for CCl_4 and 15.0 cm^{-1} for C_6H_{12} in excellent agreement with Bucaro and Litovitz (11.9 and 14.8 cm^{-1} respectively). The frequency range over which this linear relation holds is 30 to 80 cm^{-1} for CCl_4 and 30 to 120 cm^{-1} for C_6H_{12} (Fig. 1).

Frame distortion may not, however, be the only interaction mechanism contributing to the scattering. It was noted that much of the high frequency tail of the CCl_4 could not be accounted for by the above method. When $m = 9$ was tried, a value consistent with an electron overlap interaction (at least for rare gas atoms), Eqn. (1) held over an increased frequency range, 20 cm^{-1} to 100 cm^{-1}. Moreover the quality of the fit was much improved

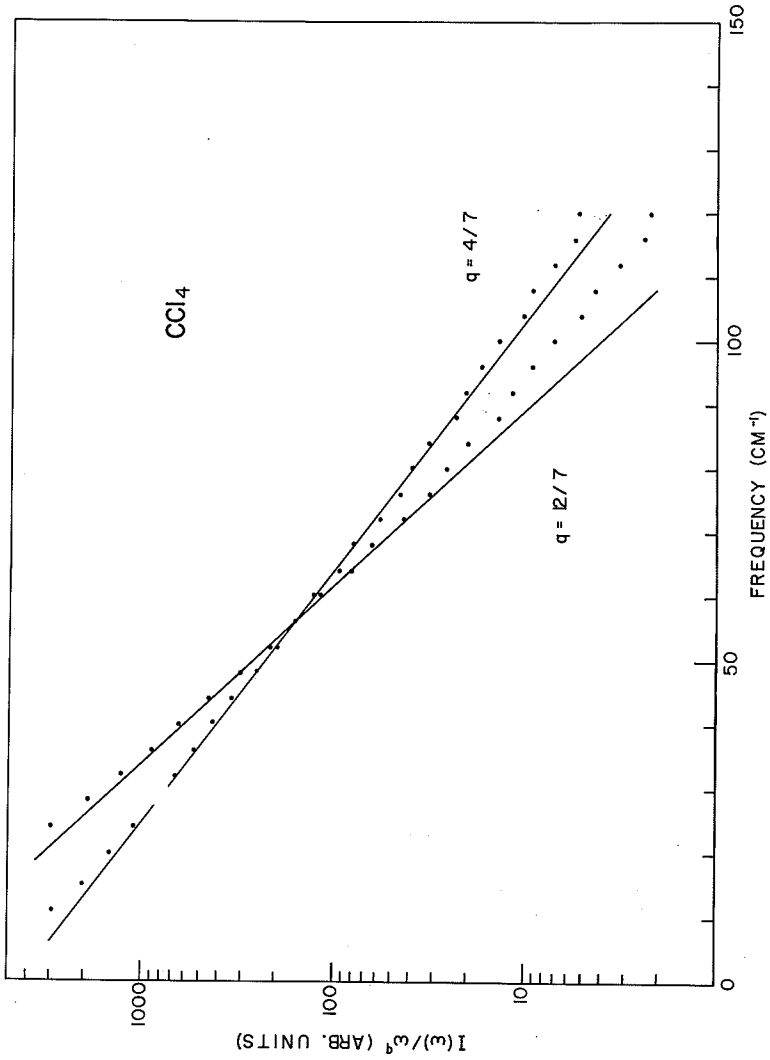

Fig. 1. $I(\omega)/\omega^q$ for the observed spectrum of CCl_4 at 295 K where q is 12/7 and 4/7 corresponding to $\Delta\alpha(r)$ varying as r^{-13} and r^{-9} respectively. Data points are shown only every 4 cm^{-1}.

Table 1. Parameters obtained from the least squares fit with Eqn. (4).

	Range (cm^{-1})	q	Effective m	ω_0 (cm^{-1})	S^2
CCl_4	16 → 100	0.36 ± 0.05	8.3 ± 0.2	18.0 ± 0.46	2.16
	30 → 80	0.74 ± 0.15	9.6 ± 0.5	15.2 ± 0.75	1.55
	40 → 100	0.11 ± 0.3	7.3 ± 1.1	19.2 ± 1.9	1.50
C_6H_{12}	16 → 100	0.28 ± 0.08	7.9 ± 0.28	23.1 ± 1.0	3.06
	30 → 80	0.71 ± 0.20	9.4 ± 0.68	20.3 ± 1.7	1.17
	40 → 100	1.73 ± 0.27	13.0 ± 0.98	15.0 ± 0.97	1.10
	40 → 120	1.68 ± 0.24	12.9 ± 0.84	15.2 ± 0.91	1.08

over that with $m = 13$. This result led us to perform the analysis based on the following considerations.

Most authors who have proposed mechanisms for collision-induced scattering conclude that the high frequency profile is described by an expression

$$I(\omega) = f(\omega) \exp(-\omega/\omega_0) \tag{3}$$

In the original model of Levine and Birnbaum, $f(\omega)$ is approximated by $\omega^{1/2}$; the more general function $\omega^{2[(m-7)/7]}$ shows clearly that the power of ω is a function of the induction process. Gersten[11] has emphasized that the exponential factor in Eqn. (3) is model independent (although the value of ω_0 is not). The accurate determination of $f(\omega)$ should lead to meaningful information not available through the exponential. Because of the presence of this strong exponential factor, the exact form of $f(\omega)$ is difficult to extract from the experimental data.

In an effort to acquire some estimate of $f(\omega)$ directly from the observed spectra, we have assumed that the high frequency profile can be represented by

$$I(\omega) \propto \omega^q \exp(-\omega/\omega_0) \tag{4}$$

where both q and ω_0 were taken as variable parameters and made a least squares fit to the spectra. The results given in Table 1 are averages over several spectra. The errors quoted represent a 99% confidence interval. For C_6H_{12}, the fits in the range 40 cm^{-1} to 120 cm^{-1} are the more significant as they are over a region sufficiently removed from the laser line to be free of contributions due to the permanent anisotropy of the molecule. The 'effective m' is determined by setting

$$q = (2/7)(m-7) \tag{5}$$

S^2 is χ^2 divided by the number of degrees of freedom.

DISCUSSION

The most striking result in Table 1 is the fact that for both liquids, the values of q and ω_0 depend on the frequency region over which the fit is made. For C_6H_{12} the result in the range 40 to 120 cm^{-1} agrees with that of Bucaro and Litovitz. On the other hand,

for CCl_4, as more of the tail is included in the fit, the effective m decreases and ω_0 increases, nowhere approximating $m = 13$ or $\omega_0 = 11.9\ cm^{-1}$.

The failure of Eqn. (1) to hold over the entire tail with one set of values for q and ω_0 indicates that more than one type of interaction is operative in the scattering. For C_6H_{12}, short-range effects seem to be important with frame distortion especially dominant beyond 40 cm^{-1}. The theory of Bucaro and Litovitz holds well in this case: basically a single short-range interaction. For CCl_4, both short- and long-range interactions contribute. Here the theory of Bucaro and Litovitz is not entirely applicable as their calculations of ω_0 are valid only near the turning point. Judging from the effective m values, the short-range part includes both electron overlap and frame distortion. The long-range interaction could be of the dipole-induced dipole type.

It should be recalled that because of symmetry effects, the intensity of the scattering through DID at liquid densities is much less than that predicted from an extrapolation of the gas results using a quadratic dependence on density; however it should not necessarily vanish. In liquids the DID interaction would be effective through rapid local fluctuations in the positions of molecules, not describable by the trajectory dynamics used to derive Eqn. (1). Thus the spectral profile due to DID would broaden as the density increases and it would be expected to contribute to the far wings of spectrum.

The ω_0 found for $40 < \omega < 100$ corresponds to a time of 2.8×10^{-13} s which is of the order of magnitude of the time between collisions in a cell model for liquid CCl_4;[12] the time between collisions would be the time characterizing these fluctuations in positions.

Table 2. Parameters obtained from the least squares fit with Eqn. (6).

	Range (cm^{-1})	B	C	S^2
CCl_4	16 → 100	0.50 ± 0.03	−0.59 ± 0.20	2.85
	30 → 80	0.76 ± 0.07	1.15 ± 0.46	1.56
	40 → 100	0.76 ± 0.07	0.10 ± 1.22	1.44
C_6H_{12}	16 → 100	0.37	−1.24	6.67
	30 → 80	0.56 ± 0.20	0.42 ± 1.3	1.34
	40 → 100	1.04 ± 0.16	3.61 ± 1.2	1.07
	40 → 120	0.99 ± 0.12	3.33 ± 0.87	0.98

Further analysis

The expression developed by Shin[13]

$$I(\omega) \propto \omega^A \exp(-B\omega^{12/19} + C\omega^{6/19}) \qquad (6$$

was also fitted to the data with A fixed for $m = 13$. The results are given in Table 2.

For CCl_4 beyond 30 cm^{-1}, the B is in excellent agreement with predictions (0.77) and while C is uncertain, the expected value (0.76) is bracketed. With C_6H_{12}, B and C are much larger than the model suggests (0.66 and 0.69). The quality of the fit for both liquids is comparable to that using Eqn. (4).

This result leads to the conclusion that frame distortion is important for CCl_4 in the far tail. Since Eqn. (6) is a more exact formulation within the binary collision model

than is Eqn. (1), it is more sensitive to the assumptions made. The neglect of the angular dependence of intermolecular forces in determining the collision trajectory may account for the discrepancy in the case of the non-spherical molecule C_6H_{12}.

While both the Bucaro and Litovitz and the Shin expressions can mathematically describe the observed spectra, the parameters required are not always in agreement with calculations and conflicting conclusions concerning the interaction arise. The question of the line shape in collision-induced scattering is still a problem.

REFERENCES

1 M. Thibeau, B. Oksengorn and B. Vodar, *J. Phys. (Paris)* **29**, 287 (1968).
2 M. Thibeau, G. C. Tabisz, B. Oksengorn and B. Vodar, *J. Quant. Spectry. Radiative Transfer* **10**, 839 (1970).
3 H. B. Levine and G. Birnbaum, *Phys. Rev. Letters* **20**, 439 (1968).
4 J. P. McTague and G. Birnbaum, *Phys. Rev. Letters* **21**, 661 (1968).
5 P. Lallemand, *Phys. Rev. Letters* **25**, 1079 (1970); *J. Phys. (Paris)* **32**, 10 (1971).
6 M. R. Vukcevich, private communication quoted in ref. 8.
7 H. S. Gabelnick and H. L. Strauss, *J. Chem. Phys.* **49**, 2334 (1968).
8 J. A. Bucaro and T. A. Litovitz, *J. Chem. Phys.* **54**, 3846 (1971).
9 J. A. Bucaro and T. A. Litovitz, *J. Chem. Phys.* **55**, 3585 (1971).
10 J. I. Gersten, R. E. Slusher and C. M. Surko, *Phys. Rev. Letters* **25**, 1739 (1970).
11 J. I. Gersten, *Phys. Rev.* A4, 98 (1971).
12 F. J. Bartoli and T. A. Litovitz, *J. Chem. Phys.* **56**, 413 (1972).
13 H. K. Shin, *J. Chem. Phys.* **56**, 2617 (1972).

Collision-induced light scattering by compressed CF_4 and CF_4-He mixtures*

D. P. Shelton, M. S. Mathur, and G. C. Tabisz
Department of Physics, University of Manitoba, Winnipeg, R3T 2N2, Canada
(Received 15 August 1974)

We have observed the collision-induced scattering from compressed CF_4 up to 70 atm and from CF_4-He mixtures at concentrations of 27%, 47%, and 48% CF_4, up to a total pressure of 155 atm. To describe the intensity distribution for pure CF_4, a single exponential function, $I = C\exp(-\omega/\omega_0)$, was fitted in the frequency range 5–20 cm^{-1}; the density dependence of ω_0 follows the scaling law derived by Fleury for rare-gas spectra. An expression involving the sum of two exponentials was fitted over a broader frequency range 5-45 cm^{-1}. It is argued that the expected intensity due to the second-order dipole-induced dipole interaction or to octupole effects is too small to account for the high-frequency tail. The shape of this tail indicates that it may arise from close encounters in which the collision time is determined principally by the intermolecular potential. The values of ω_0 determined from the spectra of the mixtures do not differ significantly from those obtained from pure CF_4. As the total pressure of the mixtures was varied, there were no sudden changes in the scattering analogous to the sharp increase of dielectric loss observed in the microwave absorption spectra and associated with the formation of dimers. In summary, the characteristics of the scattering closely resemble that from the rare gases.

INTRODUCTION

Collision-induced light scattering is essentially a translational Raman effect; the relative kinetic energy of a number of interacting molecules is altered in the scattering process. The scattering is due to a time-dependent polarizability $\Delta\alpha(t)$ induced in a cluster of interacting molecules.[1-3] The intensity distribution is then given by the Fourier transform of $\Delta\alpha(t)$,

$$I(\omega) \propto \left| \int \Delta\alpha(t) e^{i\omega t} dt \right|^2 . \quad (1)$$

Such scattering is usually observed as a broad, depolarized tail on the sharp, polarized Rayleigh line.[4] However, there have been recent reports of its occurrence in association with Raman vibrational bands.[5,6]

Since the effect exists solely because of collisions, its study, in principle, may yield information on intermolecular forces and molecular dynamics in dense media. The difficulty resides in separating the contribution in the observed scattering of the induced or cluster polarizability from that of the intermolecular potential governing the dynamics of the encounter.

Much activity has centered on the scattering from rare-gas systems.[1,3,4,7,8] The reason is simply that a free rare-gas atom has an isotropic polarizability, and consequently the scattering spectrum should be completely polarized; observed depolarized components are then entirely attributable to collision effects. Extensive studies, particularly by Fleury and his co-workers,[7,8] have been made of the gas, liquid, and solid phases of argon, xenon, and neon.

Two interaction mechanisms have been proposed to account for the induced polarizability. One is the dipole–induced-dipole (DID) interaction.[1,9,10] The external light field induces an electric dipole moment in the sample atoms. In turn, these induced dipoles interact with each other, yielding an effective pair polarizability which, to first order, is completely anisotropic and varies as r^{-3}, where r is the interatomic distance. The second mechanism is shorter in range and is caused by the overlapping of electron charge distributions during close collisions (EO).[2] In the case for helium, several calculations have been made of the dependence of the induced polarizability on interatomic distance using Hartree-Fock methods.[11,12]

Studies of the scattering from molecular systems have been concerned principally with the liquid phase.[13-15] In addition to the DID and EO mechanisms, a third is also possible. The internal degrees of freedom of the molecule can be important because a frame distortion of the molecules during collision can also give rise to an induced polarizability. Some progress had apparently been made when it was suggested[13,16] that the scattering from liquids could be accounted for by an isolated binary-collision model. The observed tail of the line profile could then be described by a compact mathematical expression in which the roles of the cluster polarizability and the intermolecular potential were clearly delineated. However, it has now been emphasized by experiment[15] and by computer calculations in molecular dynamics[17] that such a model does not satisfactorily reproduce the observed profile.

We have begun a study of collision-induced scattering from gaseous molecular systems in a re-

gime where a binary-collision model is more appropriate. In this paper, we report on the scattering from compressed CF_4, over a pressure range from 10 to 70 atm, and from CF_4-He mixtures at total pressures up to 155 atm.

CF_4 is a nonpolar spherical-top molecule of tetrahedral symmetry possessing an isotropic polarizability; it is a gas at room temperature and pressure. It has a collision-induced far-infrared absorption spectrum which is attributable to induction by the molecular octupole field.[18] In addition, in mixtures with helium, its microwave absorption spectrum displays an unusual behavior which has been associated with the formation of dimers.[19] Comparisons between the scattering, far-infrared, and microwave spectra will be useful in the analysis of the results.

EXPERIMENTAL METHOD

The apparatus used is typical of laser Raman studies. Linearly polarized light at 4880 Å from an argon-ion laser is focused by a lens (focal length 30 cm) on the sample contained within a stainless-steel pressure cell. The cell has three windows of fused silica and is capable of maintaining pressures up to 750 atm. A system of diaphragms and blackened cell walls serve to reduce stray light within the cell. The light scattered at 90° is collected by an $f/11$ system and focused on the entrance slit of a scanning double monochromator whose spectral slit width was 2 cm^{-1}. Photon-counting detection techniques are employed using a cooled RCA *C*31034 photomultiplier (PM) tube. With the discriminator levels set for an optimum signal-to-noise ratio at low light intensities, the dark count is 2–3 counts/sec. The output of the PM tube is stored in a multichannel analyzer whose channel advance is controlled by the stepping drive of the monochromator gratings. A half-wave plate and prism polarizer in the laser beam and a polarizer in the collection arm permit observations in several polarization geometries.

The CF_4 gas, purchased from the Matheson Company, Inc., had a purity of 99.7%. In order to remove a troublesome air impurity, the CF_4 sample was first frozen (the melting point is 89 K) at liquid-nitrogen temperatures in another pressure vessel which also served as a thermal compressor. As the sample was allowed to warm up to the boiling point (145 K), the oxygen and nitrogen impurities were pumped off. The degree of purification was determined by monitoring the rotational Raman scattering due to air. The helium used in the mixture was Matheson ultrahigh purity grade (99.999%).

Experiments were performed at 295 K. To remain within a pressure range where binary collisions predominate, the maximum pressure for the pure CF_4 observations was limited to 70 atm. The CF_4-He mixtures studied corresponded to 27%, 47%, and 48% CF_4 by density, with a maximum total pressure of 155 atm. The frequency range 0–75 cm^{-1} was scanned in all cases, although, at low pressures, the signal had fallen into the noise well before 75 cm^{-1}.

Amagat densities were calculated using the *P-V-T* data of MacCormack and Schneider[20] for CF_4 and Michels and Wouters[21] for He. Extrapolation of the CF_4 data for pressures above 50 atm was necessary. The partial densities of the components of the mixtures were determined following the method of Stephenson[22] and Cho.[23]

ANALYSIS OF RESULTS

Pure CF_4

Figure 1 shows the observed spectra for three densities plotted on a logarithmic intensity scale. Their general appearance is similar to spectra from the rare gases. At low density, the intensity falls off in a fashion closely exponential from the exciting frequency. As the density increases, a second slope is discernible at higher frequencies. At the highest densities studied, the identification of two distinct slopes becomes impossible, since the intensity profile curves over the entire frequency range. For gaseous argon, however, the second slope does not appear until densities of the order of the triple-point density are reached. Here, all the spectra have been taken under conditions well below the triple-point density for CF_4.

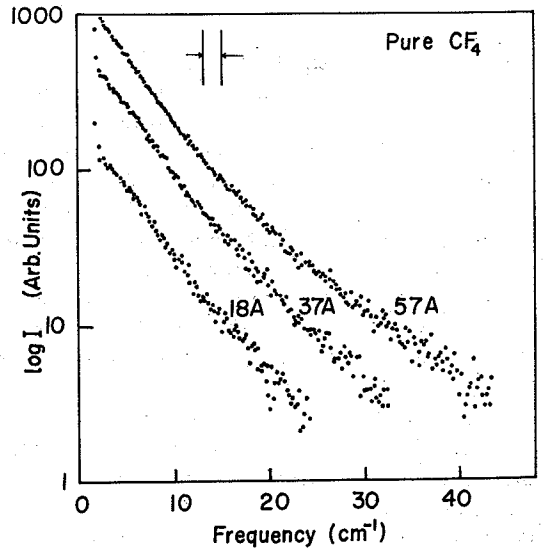

FIG. 1. Collision-induced scattering from pure CF_4 at three densities at 295 K. The vertical bars represent the spectral slit width of 2 cm^{-1}.

Because of this evolution in the shape of the spectrum, we have chosen to analyze the data in two ways: (i) by considering first a single slope and (ii) by treating two simultaneously.

Low frequencies—single exponential

Fleury and his co-workers have studied the collision-induced scattering from the rare gases (argon, neon, xenon, and krypton) over a wide range of density and temperature covering the gas, liquid, and solid phases. Assuming an exponential representation for the spectra,

$$I(\omega) = Ce^{-\omega/\omega_0}, \tag{2}$$

they determine ω_0 directly from the slope of their spectra and find that it can be represented in *all* cases by an expression

$$\omega_0 = \frac{A}{2\pi c}\left(\frac{\epsilon}{M\sigma^2}\right)^{1/2}\left(\frac{kT}{\epsilon}\right)^{1/2}\left[1+\left(\frac{B\sigma^3\rho}{M}\right)^2\right], \tag{3}$$

where M is the mass, ρ is the density, and σ and ϵ are the parameters in the Lennard-Jones potential. A and B are adjustable parameters, which they found to be 3.0 ± 0.1 and 2.0 ± 0.1, respectively. For gases above the triple-point density and for solids, the relevant slope is that at high frequency. In determining that Eq. (3) holds for several different atomic systems, they have extended the corresponding-states principle to high-frequency dynamics. The corresponding-states principle usually asserts that the thermodynamic and transport coefficients, for systems with the same form of the intermolecular potential, scale directly with the parameters of that potential.

To analyze our data in a similar manner, we have fitted our spectra by an expression of the form of Eq. (2) in the frequency range 5–20 cm^{-1} using nonlinear least-squares techniques. C and ω_0 were taken as adjustable. The starting point of 5 cm^{-1} was chosen as it is sufficiently removed from the laser frequency to make errors due to stray light small. The upper limit at 20 cm^{-1} is necessary because, as will be discussed in the following section, for the higher-density spectra, the second slope becomes important at about 20 cm^{-1}. In Fig. 2, ω_0 is plotted versus density for 43 different spectra. The error bars, shown at low and high densities, represent the estimated uncertainty in the determination of ω_0 by the fitting method. There is no significant difference between the values obtained for spectra taken with various polarization geometries.

For CF_4, Eq. (3) predicts that

$$\omega_0 = 5.65[1+(3.14\times10^{-5})\rho^2]\ cm^{-1}, \tag{4}$$

where ρ is expressed in amagat units, and $\epsilon/k = 152.5$ K and $\sigma = 4.70$ Å have been substituted.

When an expression of the form of Eq. (3) is fitted to the data in Fig. 2,

$$\omega_0 = (4.92\pm0.03)\{1+[(3.24\pm0.26)\times10^{-5}]\rho^2\}\ cm^{-1} \tag{5}$$

is found, which corresponds to $A = 2.62\pm0.02$ and $B = 2.03\pm0.05$. While these coefficients are in good agreement with the scaling law Eq. (3), the estimated standard deviation of the fit is 0.15 cm^{-1}, with discrepancies apparent, particularly at low density. Fitting a polynomial linear in density gives

$$\omega_0 = (4.63\pm0.04)\{1+[(3.32\pm0.20)\times10^{-3}]\rho\}\ cm^{-1} \tag{6}$$

with a lower estimated standard deviation of 0.11 cm^{-1}. Thus over the restricted density range of this study, a linear dependence of ω_0 on ρ gives a slightly better description of the data than does a quadratic expression.

Nevertheless, from the good agreement between Eq. (4) and Eq. (5), it may be concluded that the extended corresponding-states principle links the rare gases and CF_4 and that the Lennard-Jones potential is a good approximation to the true intermolecular potential for CF_4 for describing the dynamics effective in collision-induced scattering. Based upon their compressibility data, MacCormack and Schneider[20] also concluded that the Lennard-Jones potential is adequate in the case of

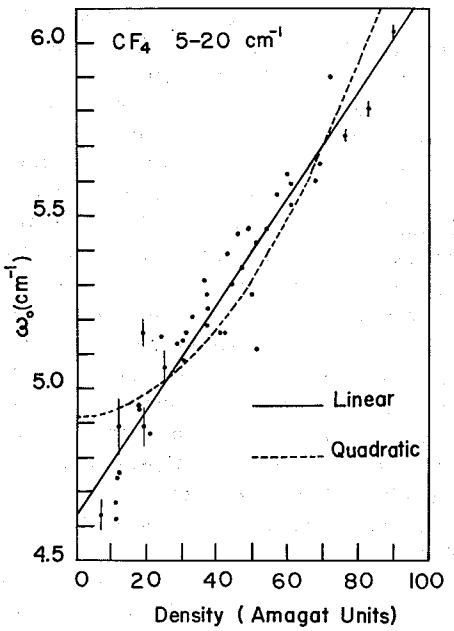

FIG. 2. Variation of ω_0 with density for pure CF_4 in the range 5–20 cm^{-1}. The dashed line represents Eq. (5) and the heavy line Eq. (6).

CF_4. Thus the intermolecular force field may be considered as central rather than localized in the outer fluorine atoms as has been suggested for the larger tetrachloride molecules, such as CCl_4.[24]

For the rare gases at low frequency and low density, it is thought that an important, but not the sole, mechanism responsible for the scattering[1,3,25] is the DID interaction. The agreement between the predictions of Eq. (3), derived for rare-gas spectra, and the present analysis indicates that, for CF_4 as well, the DID interaction predominates at low density.

High frequencies—double exponential

Since a second slope appears at high frequencies as the density increases, an expression which is the sum of two exponentials,

$$I(\omega) = Fe^{-\omega/\omega_1} + Ge^{-\omega/\omega_2}, \tag{7}$$

was also fitted to the spectra, over the range 5–45 cm^{-1}. The quality of the fits as judged from reduced χ^2 are excellent. Figure 3 shows the variation of ω_1 and ω_2 with density for spectra taken in the VH polarization geometry.[25a] While ω_1 increases steadily, ω_2 increases sharply from 30 to 50 amagat and then levels off at about 10.5 cm^{-1}. The specific values of ω_1 and ω_2 do depend upon the range chosen but their behavior with density does not change greatly. For example, the limiting value of ω_2 reaches 14.5 cm^{-1} when fits out to 70 cm^{-1} are made. Such a wide range is possible only for the highest densities. Consequently, 5–45 cm^{-1} has been selected in order to investigate changes in the profile over a reasonable density interval.

If the exponentials are extrapolated to zero frequency and integrated from zero to infinity, then the contribution of each to the total integrated intensity is obtained. The ratio of the intensities I_1/I_2 is plotted in Fig. 3. Its magnitude is about 2.5 and decreases slightly as the density increases, demonstrating that the second exponential is becoming more important.

It should be noted that when the spectra are fitted by two exponentials simultaneously, the higher-frequency component is sufficiently intense to reduce the characteristic frequency of the lower-frequency component by about 1 cm^{-1} from that obtained in the previous analysis using a single exponential only at low frequencies. The intensities of the two exponentials become equal in the region 15–20 cm^{-1}.

It is instructive to speculate on the origin of the second exponential. The factor $(1/2\pi c)(A/\sigma) \times (kT/M)^{1/2}$ in Eq. (3) is the average velocity divided by an effective range σ/A. Hence, in the binary-collision model, $(\omega_0)^{-1}$ is the duration time of the collision. Since ω_2 is greater than ω_1, the interaction giving rise to ω_2 must be of shorter duration than that producing ω_1. Several possibilities come to mind.

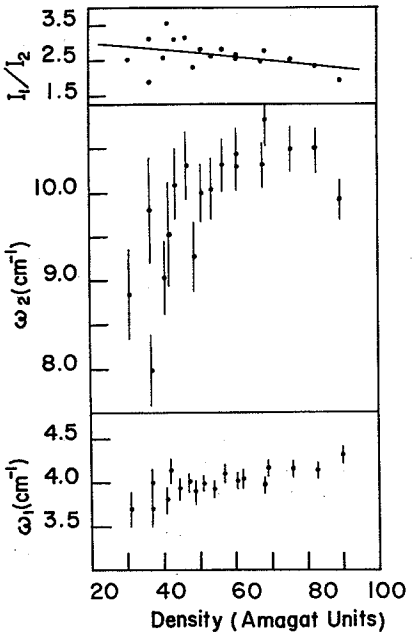

FIG. 3. Variation of ω_1, ω_2, and I_1/I_2 with density for pure CF_4 [Eq. (7)]. I_1/I_2 is the ratio of the integrated intensities of the two exponentials, $F\omega_1/G\omega_2$.

(i) Second-order dipole–induced dipole. The first-order dipole–induced-dipole interaction produces a pair polarizability given by

$$\Delta\alpha(r) = 6\alpha^2/r^3, \tag{8}$$

where α is the polarizability of the free atom or molecule. Classically,[9] the next higher term is $6\alpha^3/r^6$. The ratio of intensity due to first-order DID to that due to second-order DID can be estimated as

$$\frac{\text{DID1}}{\text{DID2}} = \frac{\sigma^6}{\alpha^2}\frac{H_6^{12-6}}{H_{12}^{12-6}} \approx 1640, \tag{9}$$

where

$$H_n^{12-6}/\sigma^n \propto \int r^{-n} e^{-V(r)/kT} d\tau, \tag{10}$$

and $V(r)$ is the Lennard-Jones potential. The H's involve the averaging of the intermolecular distance over the pair distribution function and have been tabulated by Buckingham and Pople.[26] The ratio 1640 is much larger than the experimentally determined 2.5, and second-order DID scattering can thus be neglected.

(ii) Octupole effects. CF_4 has a far-infrared spectrum arising from the rapidly varying dipole

moment induced during molecular collisions.[18] Because of the reasonable values of the electric octupole moment determined from this aborption intensity, the occurrence of the spectrum is attributed to induction by the octupolar fields of the colliding molecules. The octupole moment is the first nonzero multipole moment of CF_4.

Bucaro and Litovitz[13,16] studied the collision-induced scattering from liquid CCl_4 and compared it to the corresponding microwave and far-infrared absorption data of Garg *et al.*[27] In particular, they found a strong resemblance between the shapes of the absorption and the scattering profiles and concluded that the time dependence of the induced dipole moment producing the absorption spectrum is similar to the time dependence of the induced polarizability responsible for the scattering. They had determined previously that the collision-induced scattering from liquid CCl_4 was due primarily to very close encounters.

Unfortunately, such a direct comparison is not possible in the present situation. There is no reason to expect that the dipole moment and the polarizability, induced through octupole interactions, should vary similarly with time. We note, however, in passing that the far-infrared absorption profile for compressed CF_4 as determined by Rosenberg and Birnbaum[18] falls off more slowly at high frequency than does the scattering, the effective ω_0 being 27 and 11–14 cm^{-1}, respectively.

A theory describing the scattering by a pair polarizability induced through octupolar field effects has not been formulated. Rough calculations, based on the model of Buckingham and Stephen,[10] indicate that the intensity due to DID scattering would be several orders of magnitude larger than that from octupolar effects. Thus, from intensity considerations, the high-frequency scattering can not be explained by octupolar induction.

(iii) Close encounters. Bucaro and Litovitz[13] in their treatment of collision-induced scattering from liquids developed an isolated binary-collision model in which they considered the phenomenon to be entirely due to close encounters; the induction mechanisms are electron overlap and frame distortion. They calculated a collision time using a method due to Nikitin[28] and assumed a zero impact parameter and a Lennard-Jones potential. This collision time is determined solely by the dynamics and is independent of the nature of the interaction inducing $\Delta\alpha$. The characteristic frequency ω_0 is then found to be

$$(\omega_0)^{-1} = \frac{2\pi^2 c\sigma}{6}\left(\frac{M}{2kT}\right)^{1/2}\left[1 - \frac{2}{\pi}\arctan\left(\frac{2\epsilon}{kT}\right)^{1/2}\right] \text{ cm}, \tag{11}$$

giving $\omega_0 = 10.3$ cm^{-1} for CF_4. Equation (11) is an approximation to an integral, performing an average over all velocities. Numerical integration yields a value about 15% higher. The agreement with our ω_2 is rather satisfactory.

A conclusion that the shape of the high frequency should be determined principally by the intermolecular potential would agree with the analytical calculations of Gersten[29] on compressed argon and with the computer experiments of Alder *et al.*[30] on argon, xenon, and neon systems. Both of these investigations used the DID interaction as the induction mechanism, thus allowing the conclusion that it is not necessary to introduce an additional interaction to account for the change of shape in the high-frequency tail.

CF_4-He mixtures

Typical spectra for the CF_4-He mixtures are presented in Fig. 4. The scattering was generally weak and varied with the square of the partial density of CF_4; only the spectra at the highest pressures showed anything other than a simple exponential tail.

Accordingly, the data were fitted to a single exponential Eq. (2) over the frequency range 5–20 cm^{-1}. The values of ω_0 are shown in Fig. 5, together with the quadratic and linear functions, Eq. (5) and Eq. (6), previously fitted to the pure CF_4 spectra. The ω_0 for the mixture spectra do not differ significantly from these curves applicable to the pure gas.

Mathur *et al.*[19] studied the nonresonant microwave absorption of CF_4-He compressed gas mixtures at 1648 MHz and found an unusual behavior.

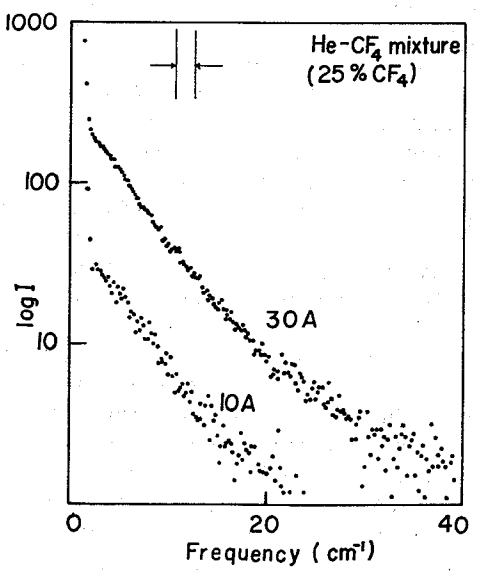

FIG. 4. Collision-induced scattering from a CF_4-He mixture (27% CF_4). The densities 30 and 10 amagat refer to the partial density of CF_4.

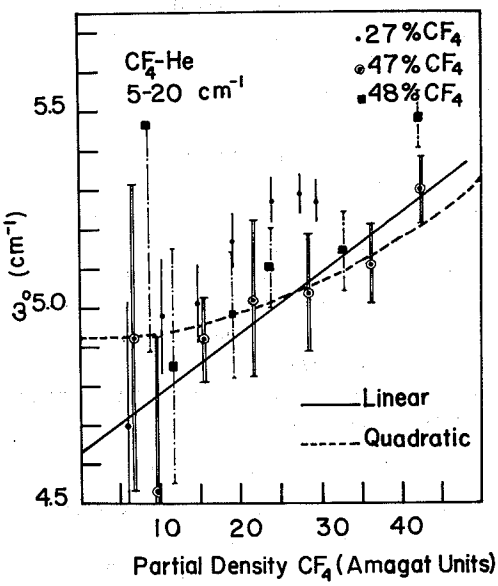

FIG. 5. Variation of ω_0 with partial density of CF_4 in the range 5–20 cm^{-1} for CF_4-He mixtures of 27%, 47%, and 48% CF_4. The dashed and heavy lines represent Eq. (5) and Eq. (6), respectively, which apply to pure CF_4.

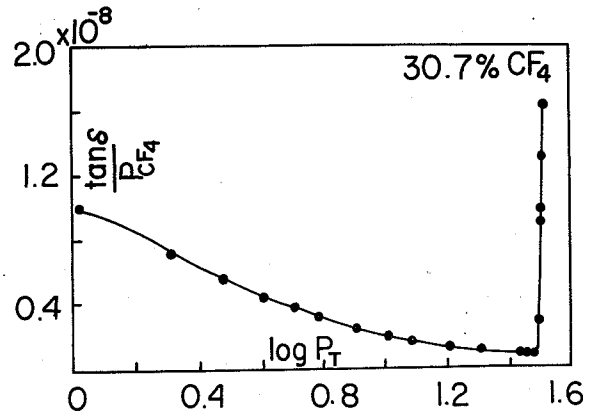

FIG. 6. Loss tangent at 1648 MHz divided by the partial pressure of CF_4 as a function of total pressure for a 30.7% mixture of CF_4 in He.

They observed a sudden onset of extreme dielectric loss at a total pressure of 33 atm for a 30.7% CF_4 mixture by volume and at a total pressure of 18.5 atm for a 55.5% mixture (Fig. 6). No such loss occurred in a 20% mixture (up to 33 atm). A phase change is not taking place as all pressures are below the critical pressure of CF_4. *P-V-T* measurements on pure CF_4 do not suggest any strong intermolecular interactions to explain this behavior.[20] They speculate that the effect is due to the formation of dimers of CF_4.

There is no indication from the collision-induced scattering to corroborate such an hypothesis. Neither the line shape (out to 20 cm^{-1}) or the intensity display any precipitous change. Our observations have been made at similar concentrations and over a wider range of total pressures. Stable dimers might add features to the spectra at low frequencies, and it is possible that the slit widths used in the present work are too broad to permit observation of them.

There is no evidence from the intensity or the line shape that CF_4-He collisions are effective in producing collision-induced scattering. Because of the small polarizability of He (2.02×10^{-25} cm^3 as compared to 1.63×10^{-24} cm^3 for argon and 3.86×10^{-24} cm^3 for CF_4), the DID interaction for He-He and CF_4-He will be very weak. However, it would be interesting to perform experiments under conditions in which the number of CF_4-He collisions per time interval is still higher than in the present study, in order to determine whether overlap-type encounters between He and CF_4 can give rise to a broad tail on the profile. It would be broad, since the low reduced mass of the collision partners will result in a short collision time.

SUMMARY

At low frequency, the slopes of the pure CF_4 spectra closely follow the scaling law developed by Fleury for rare-gas spectra. Thus scattering is chiefly due to the dipole–induced-dipole mechanism. When a wider frequency range is considered, a high-frequency tail develops with a slope smaller than that at low frequency. Intensity considerations rule out the possibility that it arises from second-order dipole–induced-dipole or octupolar effects. The magnitude of its characteristic frequency is consistent with that expected for very close collisions, where the effective collision time is determined solely by the intermolecular potential and is independent of the details of the nature of the induction mechanism. The role of CF_4-He encounters is insignificant to the scattering for the conditions of concentration and pressure studied. There were no sudden changes in intensity or line shape analogous to those observed in the microwave absorption spectrum of CF_4-He mixtures and associated with dimer formation.

In summary, the collision-induced scattering due to CF_4 at densities up to 70 amagat resembles closely the scattering from atomic rare-gas systems. No features attributable to the internal degrees of freedom of CF_4 were observed.

ACKNOWLEDGMENT

We wish to thank M. N. Neuman for his thoughtful advice concerning the computer programs.

*Supported in part by grants from the Research Corporation and from the National Research Council of Canada.

[1]M. Thibeau and B. Oksengorn, Mol. Phys. 15, 579 (1968).
[2]H. B. Levine and G. Birnbaum, Phys. Rev. Lett. 20, 439 (1968).
[3]M. Thibeau, G. C. Tabisz, B. Oksengorn, and B. Vodar, J. Quant. Spectrosc. Radiat. Transfer 10, 839 (1970).
[4]J. P. McTague and G. Birnbaum, Phys. Rev. Lett. 21, 661 (1968).
[5]W. Holzer and Y. le Duff, Phys. Rev. Lett. 32, 205 (1974).
[6]W. Holzer and R. Ouillon, Chem. Phys. Lett. 24, 589 (1974).
[7]P. A. Fleury, W. B. Daniels, and J. M. Worlock, Phys. Rev. Lett. 27, 1493 (1971).
[8]P. A. Fleury, J. M. Worlock, and H. L. Carter, Phys. Rev. Lett. 30, 591 (1973).
[9]L. Silberstein, Philos. Mag. 33, 521 (1917).
[10]A. D. Buckingham and M. J. Stephen, Trans. Faraday Soc. 53, 884 (1957).
[11]E. F. O'Brien, V. P. Gutschick, V. McKoy, and J. P. McTague, Phys. Rev. A 8, 690 (1973).
[12]A. D. Buckingham and R. S. Watts, Mol. Phys. 26, 7 (1973).
[13]J. A. Bucaro and T. A. Litovitz, J. Chem. Phys. 54, 3846 (1971).
[14]J. P. Chabrat, J. Rouch, and C. Vaucamps, Mol. Phys. 24, 897 (1972).
[15]J. H. K. Ho and G. C. Tabisz, Can. J. Phys. 51, 2025 (1973).
[16]J. A. Bucaro and T. A. Litovitz, J. Chem. Phys. 55, 3585 (1971).
[17]B. J. Berne and M. Bishop, J. Chem. Phys. 58, 2696 (1973).
[18]A. Rosenberg and G. Birnbaum, J. Chem. Phys. 48, 1396 (1968).
[19]M. S. Mathur, E. B. Bradley, and K. P. Kadaba, Mater. Sci. Eng. 1, 342 (1967).
[20]K. E. MacCormack and W. G. Schneider, J. Chem. Phys. 19, 845 (1951).
[21]A. Michels and H. Wouters, Physica 8, 923 (1941).
[22]F. C. Stephenson, Ph.D. thesis (University of Toronto, 1953) (unpublished).
[23]C. W. Cho, E. J. Allin, and H. L. Welsh, Can. J. Phys. 41, 1991 (1963).
[24]J. H. Hildebrand, J. Chem. Phys. 15, 727 (1947).
[25]H. B. Levine and G. Birnbaum, J. Chem. Phys. 55, 2914 (1971).
[25a]The incident beam is polarized in the vertical (V) direction. The direction of observation is at right angles to the direction of propagation and of polarization of the incident beam. The horizontally (H) polarized scattered component is observed; that is, it is polarized in the direction parallel to the direction of propagation of the incident beam.
[26]A. D. Buckingham and J. A. Pople, Trans. Faraday Soc. 51, 1029 (1955).
[27]S. K. Garg, J. E. Bertie, H. Kilp, and C. P. Smyth, J. Chem. Phys. 49, 2551 (1968).
[28]E. E. Nikitin, Opt. Spectrosk. 6, 91 (1959) [Opt. Spectrosc. 6, 93 (1959)].
[29]J. I. Gersten, Phys. Rev. A 4, 98 (1971).
[30]B. J. Alder, H. L. Strauss, and J. J. Weis, J. Chem. Phys. 59, 1002 (1973).

Moment analysis of collision-induced light scattering from compressed CF_4†

D. P. Shelton and G. C. Tabisz
Department of Physics, University of Manitoba, Winnipeg, Manitoba R3T 2N2, Canada
(Received 27 January 1975)

The method of moments is used to determine a functional form of the induced polarizability increment β, which gives rise to collision-induced light scattering from compressed CF_4. Based upon the zeroth and second moments, two expressions are found to be acceptable: $\beta(x) = 6\alpha^2\sigma^{-3}(x^{-3} - 2.85x^{-4.05})$ and $\beta(x) = 6\alpha^2\sigma^{-3}(x^{-3} + 0.757x^{-8.51})$, where $x = r/\sigma$. Both expressions result in calculated fourth moments consistent with the experimental estimate. This is the first experimental evidence in which a positive non-dipole-induced-dipole term is shown to be a possibility. In other respects, however, the results are similar to those obtained from rare-gas spectra.

I. INTRODUCTION

Light scattering, arising through the polarizability induced in a cluster of interacting molecules, may provide detailed information on molecular motion in dense media.[1-3] The primary impediment to progress concerns the intermolecular potential and the induction mechanism, which determine the collision dynamics and the nature of the induced polarizability, respectively. Their roles in the scattering process must be clearly specified before reliable interpretation of the spectra can be made.

In a recent paper,[4] we reported the collision-induced Rayleigh scattering from compressed gaseous CF_4 and CF_4-He mixtures. The spectra were discussed in terms of empirical models for the line profile, namely, sums of functions exponential in frequency. The principal conclusions were (i) that the profile at low frequencies (5–20 cm^{-1}) evolves with density according to the scaling law found appropriate for rare-gas spectra,[5,6] and (ii) that the tail at high frequencies (>20 cm^{-1}), which is prominent at densities higher than 50 amagat, is due to close binary collisions. In an effort to derive more details on the form of the induced polarizability, the spectra have now been analyzed by the method of moments. The results of this analysis are the subject of the present paper.

II. THE METHOD OF MOMENTS

Collision-induced scattering has been treated previously through moment analysis by Lallemand[7] and Levine.[8,9] A functional form for the induced pair polarizability is assumed and its characteristic parameters are determined from the moments of the experimental spectra.

Suppose $\phi^{(2n)}$ is the $(2n)$th moment of the frequency distribution of the scattered intensity $I(\omega)$, i.e.,

$$\phi^{(2n)} \propto (-1)^n \int \omega^{2n} I(\omega)\, d\omega \,. \tag{1}$$

It is straightforward[7,9] to calculate $\phi^{(2n)}$ in terms of $\beta(r)$, the induced-pair-polarizability anisotropy, which is a function of the intermolecular distance r:

$$\phi^{(0)} = 4\pi \int_0^\infty (\beta(r))^2 g(r) r^2 dr \,, \tag{2}$$

$$\phi^{(2)} = -4\pi \frac{kT}{\mu} \int_0^\infty \left[\left(\frac{d\beta}{dr}\right)^2 + 6\left(\frac{\beta(r)}{r}\right)^2\right] g(r) r^2 dr, \tag{3}$$

$$\phi^{(4)} = 4\pi \left\{\left(\frac{kT}{\mu}\right)^2 \int_0^\infty \left[72\left(\frac{\beta}{r^2}\right)^2 + 8\left(\frac{1}{r}\frac{d\beta}{dr}\right)^2 - \frac{36}{r^2}\beta\frac{d^2\beta}{dr^2} + \frac{4}{r}\frac{d\beta}{dr}\frac{d^2\beta}{dr^2} + 3\left(\frac{d^2\beta}{dr^2}\right)^2\right] g(r) r^2 dr \right.$$
$$\left. - \frac{kT}{\mu^2} \int_0^\infty \left[\left(\frac{d\beta}{dr}\frac{dV}{dr}\right)\left(2\frac{d^2\beta}{dr^2} + \frac{4}{r}\frac{d\beta}{dr} - \frac{36}{r^2}\beta\right) + 48\frac{\beta^2}{r^3}\frac{dV}{dr}\right] g(r) r^2 dr + \frac{1}{\mu^2} \int_0^\infty \left(\frac{d\beta}{dr}\frac{dV}{dr}\right)^2 g(r) r^2 dr \right\}. \tag{4}$$

μ is the reduced mass of two colliding molecules and $g(r)$ is the radial distribution function,

$$g(r) = e^{-V(r)/kT}, \tag{5}$$

where $V(r)$ is the intermolecular pair potential.

Levine and Birnbaum[8] considered a pair polarizability function,

$$\beta(r) = (6\alpha^2/r^3) + (B/r^b), \tag{6}$$

which may be written in dimensionless form,

$$\beta(x) = 6\alpha^2\sigma^{-3}[x^{-3} + (\tfrac{1}{6}y)x^{-p}] , \quad (7)$$

where $x = r/\sigma$ and $y = B\alpha^{-2}\sigma^{3-p}$. α is the molecular polarizability and σ is the molecular diameter; p and y (or B) are the parameters to be determined. $\beta(x)$ is thus represented as the sum of a long-range dipole-induced–dipole term,[1] $6\alpha^2/r^3$, and another contribution B/r^p thought to be of much shorter range. Using the Lennard-Jones 12-6 potential for $V(r)$, they found that, for argon, two sets of values of p and $\frac{1}{6}y$ gave satisfactory solutions to (2) and (3), the left-hand sides of which are experimentally determined through Eq. (1). These solutions are (i) $p \sim 6$ and $\frac{1}{6}y \sim -0.25$ and (ii) $p \sim 10$ and $\frac{1}{6}y \sim -0.40$. They considered the smaller value of p to be physically unrealistic for a short-range interaction and rejected it. Similar results were obtained for krypton and xenon, except that the smaller p was about 3.5. In all cases, y is less than zero, giving credence to the contention that short-range interactions lower the induced anisotropy from the contribution due to the dipole-induced–dipole mechanism alone, at least over the range of r sampled in the experiments.

Lallemand[7] has made a much more extensive analysis for argon. He considered several potentials—Kihara, Barker-Pompe, and Dymond-Alder—in addition to the Lennard-Jones 16-6. Also, he treated both $(\frac{1}{6}y)x^{-p}$ and $\lambda e^{-x/d}$ as possible forms for the second term in the expression for $\beta(r)$. Again for the Lennard-Jones and x^{-p} cases, with p and y determined from the zeroth and second moments, two solutions were acceptable: (i) $p = 4.15$ and $\frac{1}{6}y = -0.23$ and (ii) $p = 10.75$ and $\frac{1}{6}y = -0.51$. However, only the *first* set gave reasonable values for the fourth and sixth moments. Thus only the first set was retained; the second shorter-range solution was rejected. Calculations with the other potentials and trial polarizability functions yielded similar conclusions. In contradiction to the reasoning adopted by Levine and Birnbaum, the shorter-range solution was always discarded in favor of a long-range term.

Three aspects to the CF_4 data suggest that a moment analysis would yield a form for $\beta(r)$ differing from the rare-gas cases. First, a high-frequency tail of significantly different slope from the low-frequency profile appears above 50 amagat in the case of CF_4 (Fig. 1). This break in the profile occurs at about $\frac{1}{10}$ of the triple-point density, in contrast to argon, where a similar break is observed at about the triple-point density.[5] Moreover, for CF_4, the slope of this tail remains constant in the range 50–100 amagat (the highest density studied), indicating that it arises from binary encounters. Second, in the case of molecules, frame distortion may contribute to the induced anisotropy. It has been proposed[10] that this interaction would give a term in $\beta(r)$ varying as r^{-13}, somewhat shorter in range than the r^{-9} expected from electron overlap interactions between rare-gas atoms.[10,11] Third, the Kerr-effect measurements suggest a difference in the magnitude of $\beta(r)$ between CF_4 and the rare gases (Table I). For the rare gases, the experimental values of the second virial Kerr coefficient B_k are all less than the calculated values; for CF_4, the experimental value is greater. The calculated values have been obtained from the relation[12,13]

$$B_k = \frac{8\pi^2 N_0^2}{405kT}\int_0^\infty [\beta(r)]^2 g(r) r^2\, dr , \quad (8)$$

where N_0 is Avogadro's number. Here $\beta(r)$ consists only of the dipole-induced–dipole term $6\alpha^2/r^3$ and the Lennard-Jones potential appears in $g(r)$.

III. ANALYSIS

The experimental and theoretical zeroth and second moments were found following the method of Levine and Birnbaum.[8] Spectra taken in the density range 50–100 amagat were considered. The intensity was extrapolated to zero frequency from 5 cm^{-1} by fitting an empirical line-shape function consisting of the sum of the two exponentials.[4] Irwin and May[14] have shown that such an extrapolation does not introduce gross errors in the case of argon. The moments were then determined by calculating $\int I(\omega)\, d\omega$ and $\int \omega^2 I(\omega)\, d\omega$. Since relative rather than absolute measurements are in fact made, the experimental moments must

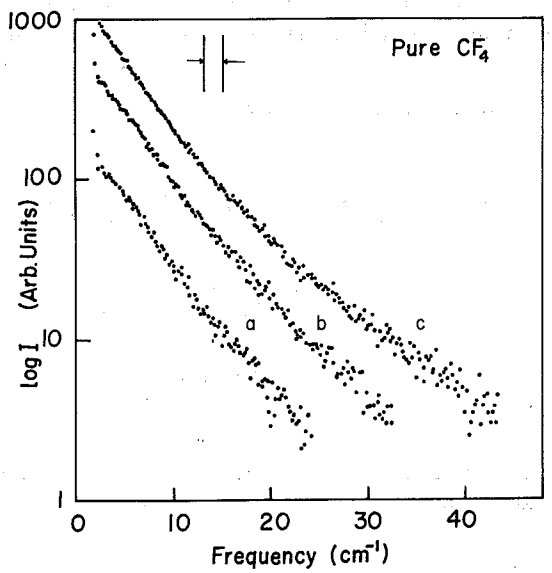

FIG. 1. Collision-induced light scattering from pure CF_4 at 18 (a), 37 (b), and 57 amagat (c) at 295 K. The vertical bars represent the spectral slit width of 2 cm^{-1}.

first be normalized in some manner. A direct method utilizes measured values of the second virial Kerr coefficient B_k through Eqs. (2) and (8). This Kerr coefficient determined by Buckingham and Orr[13] was used. The average values obtained for $\phi^{(0)}$ and $-\phi^{(0)}/\phi^{(2)}$ are presented in Table I together with the results for rare gases.[8] As one might suspect from the polarizabilities and masses alone, the moments of CF_4 fall between those for krypton and xenon.

Next, the unspecified parameters in the polarizability function (7) were determined. Equations (2) and (3) are quadratic in the unknown y, when p is specified. The right-hand sides were evaluated for a large number of values of p. For each p, (2) and (3) were solved for y. A search was then made for the values of y which simultaneously satisfied (2) and (3). For all densities, two sets of the parameters p, y were acceptable. For the lower value of p, in the range 3–5, y was always less than zero; for the higher value of p, 7–9, y was always greater than zero. The average values are (i) $p = 4.05 \pm 0.1$ and $\frac{1}{6}y = 2.85 \pm 0.03$ and (ii) $p = 8.51 \pm 0.2$ and $\frac{1}{6}y = 0.757 \pm 0.02$. Therefore two forms of the polarizability function are possible:

$$\beta(x) = \frac{6\alpha^2}{\sigma^3}\left[x^{-3} - \frac{2.85}{x^{4.05}}\right] \tag{9}$$

or

$$\beta(x) = \frac{6\alpha^2}{\sigma^3}\left[x^{-3} + \frac{0.757}{x^{8.51}}\right]. \tag{10}$$

IV. DISCUSSION

The important question is to decide if a distinction may be made between these two functions. The obvious test is to verify whether these polarizability parameters give reasonable values for the higher moments. When the right-hand sides of Eqs. (2) and (4) are evaluated with $p = 4.05$, one obtains $\phi^{(4)}/\phi^{(0)} = 3.38 \times 10^{50}$ sec^{-4}. With $p = 8.51$, $\phi^{(4)}/\phi^{(0)} = 4.36 \times 10^{50}$ sec^{-4}. This differs from the result of Lallemand for argon, where the fourth moment is an order of magnitude larger with the short-range term ($p = 10.75$) than with the long-range term ($p = 4.15$). For CF_4 there seems to be little possibility of distinguishing experimentally between the two rather similar values. In order to estimate the fourth moment from our results, we elected to work with the function fitted to the line profile,[4] rather than to use directly the measured intensities which are not known precisely for large frequency shifts. Integrating this sum of two exponentials from zero to infinity, one finds $\phi^{(4)}/\phi^{(0)} = 1.1 \times 10^{50}$ sec^{-4}; therefore the measured fourth moment is of the same order as the two theoretical values. This estimate is a lower bound on the true value, as the fitted line-profile expression appears to lie slightly lower than the observed intensities at high frequency. Therefore, the fact that the experimental estimate is closer to the calculated value for $p = 4.05$ than that for $p = 8.51$ is of little significance. The experimental data are not of sufficient quality to permit the determination of still higher moments.

Most of the initial work on collision-induced scattering assumed that $\beta(r)$ would contain the long-range dipole-induced–dipole term together with a short-range overlap term. Thus, Bucaro and Litovitz[10] were able to propose an isolated binary-collision model for the scattering from liquids. The foundations of the model are that, at liquid densities, interference effects are expected to severely reduce the intensity of the scattering due to the dipole-induced–dipole interaction and that, even at such high density, the probability for more than two molecules to overlap strongly is small. Under these assumptions, they determined that a $\beta(r)$ which varies as r^{-9}, and arises from electron overlap, is consistent with the scattering from atomic fluids. For molecular liquids, they argued that the induced polarizability anisotropy is

TABLE I. Comparison of CF_4 and rare-gas data.

Gas	B_k (esu$\times 10^{-12}$) Expt.[a]	B_k (esu$\times 10^{-12}$) Calc.[a]	σ (Å)[b]	ϵ/k (K)[b]	α (Å)^3	Mass (amu)	$\phi^{(0)}$[d] (Å)^9	$-\phi^{(0)}/\phi^{(2)}$[d] (10^{-26} sec^2)
Ar	4.1 ± 0.6	5.6	3.41	119.8	1.642	40	30.2 ± 4.4	12.5
Kr	16 ± 14	26	3.60	171	2.484	84	93.5 ± 13.9	12.5
Xe	65 ± 22	140	4.10	221	4.045	131	468 ± 69	19.8
CF_4	37.7 ± 3.6	25.2	4.70	152.5	3.84[c]	88	270 ± 30	17.6

[a] References 12 and 13.

[b] J. O. Hirschfelder, C. F. Curtiss, and R. B. Bird, *Molecular Theory of Gases and Liquids* (Wiley, New York, 1954).

[c] α at 6328 Å. Experiments on CF_4 were performed at 4880 Å.

[d] Rare-gas results from Ref. 8.

due mainly to a very-short-range interaction producing molecular frame distortion; an r^{-13} dependence of $\beta(r)$ was compatible with their data. Subsequent investigations[15,16] have shown that within the IBC model, r^{-13} is indeed appropriate for some anisotropic molecules (e.g., $CHCl_3$, C_6H_{12}, C_6H_6, but that r^{-9} is more in accord with experiment for isotropic molecules (e.g., CCl_4, $SiCl_4$, $GeCl_4$, $TeCl_4$).

The solution of $p = 8.51$ for gaseous CF_4 would be in agreement with these findings for liquids, particularly since the high-frequency tail is thought to be due to close binary collisions. However, the assumption regarding the existence of a short-range overlap term has been put in doubt, not only by the results of Lallemand on argon, but also by detailed calculations of pair polarizabilities. O'Brien *et al.*[17] have determined the $\beta(r)$ for He_2 using a fully self-consistent Hartree-Fock procedure. They find that $\beta(r)$ may be represented by a dipole-induced–dipole term and an exponential in r. For values of r sampled in these experiments, the exponential term is negative, reducing the anisotropy. However, it is not truly of short range, varying approximately as r^{-6} in the region of $r = \sigma$. While extrapolations to heavier atoms and polyatomic molecules are impossible, it is no longer reasonable to reject an r^{-4} term on the basis that it is physically unrealistic.

Because of the normalization procedure, both $p = 4.05$ and $p = 8.51$ are consistent with the Kerr-coefficient measurements. For $p = 4.05$, $\beta(r)$ is negative in the important region for r; while for $p = 8.51$, $\beta(r)$ is positive. For both values, $[\beta(r)]^2$ is greater than the dipole-induced–dipole term alone (Fig. 2).

In summary, despite the somewhat different density dependence of the CF_4 spectra and despite the size of B_k relative to the dipole-induced–dipole contribution, the analysis returns values of p quite similar to those found for rare gases. The one difference is the sign of the possible short-range term; it is positive for CF_4 but negative for rare gases. The two sets of values (p, y) give almost identical fourth moments, making further insight impossible on the basis of the available data. This is the first experimental evidence that the sign of the additional term in $\beta(r)$ may be positive. While a detailed calculation of $\beta(r)$ for $(CF_4)_2$ such as O'Brien *et al.*[17] made for $(He)_2$ is impractical, perhaps a less rigorous approach would yield an indication of the sign of the contribution apart from the dipole-induced–dipole term. Then the possibilities (9) and (10) could be distinguished.

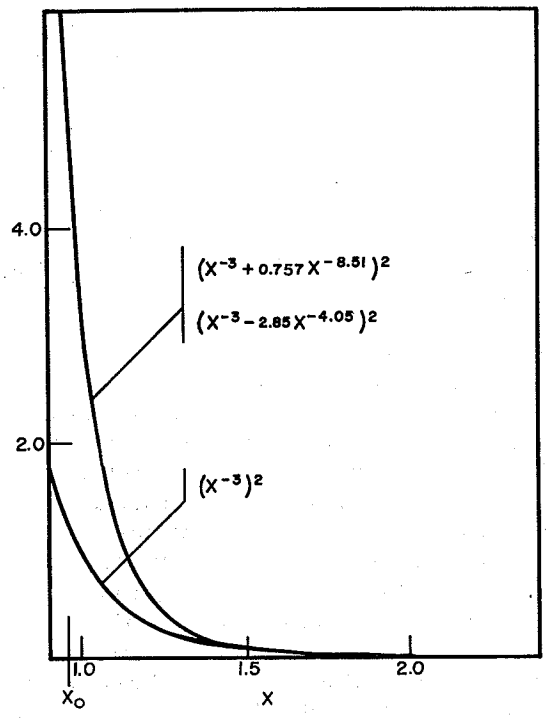

FIG. 2. Plot of $[\sigma^3\beta(x)/6\alpha^2]^2$ vs x for the dipole-induced–dipole term x^{-3} alone and for the cases in which the additional term varies as $x^{-4.05}$ and $x^{-8.51}$. Although it is not noticeable from the above scale, $[\beta(x)]^2$ does differ slightly between the two cases, $p = 4.05$ and 8.51, in the range $x > x_0$. x_0 is 0.962 and is the distance of closest approach at 295 K.

ACKNOWLEDGMENT

We wish to acknowledge discussions concerning CF_4 with Dr. M. S. Mathur.

†Work supported in part by the Research Corporation and the National Research Council of Canada.

[1]M. Thibeau, B. Oksengorn, and B. Vodar, J. Phys. (Paris) 29, 287 (1968).
[2]H. B. Levine and G. Birnbaum, Phys. Rev. Lett. 20, 439 (1968).
[3]M. Thibeau, G. C. Tabisz, B. Oksengorn, and B. Vodar, J. Quant. Spectrosc. Radiat. Transfer 10, 839 (1970).
[4]D. P. Shelton, M. S. Mathur, and G. C. Tabisz, Phys. Rev. A 11, 834 (1975).
[5]P. A. Fleury, W. B. Daniels, and J. M. Worlock, Phys. Rev. Lett. 27, 1493 (1971).
[6]P. A. Fleury, J. M. Worlock, and H. L. Carter, Phys. Rev. Lett. 30, 591 (1973).
[7]P. Lallemand, J. Phys. (Paris) 33, Colloque C 1, 257 (1972).

[8]H. B. Levine and G. Birnbaum, J. Chem. Phys. 55, 2914 (1971).
[9]H. B. Levine, J. Chem. Phys. 56, 2455 (1972).
[10]J. A. Bucaro and T. A. Litovitz, J. Chem. Phys. 54, 3846 (1971).
[11]M. R. Vukcevich (private communication quoted in Ref. 10).
[12]A. D. Buckingham and D. A. Dunnur, Trans. Faraday Soc. 64, 1776 (1968).
[13]A. D. Buckingham and B. J. Orr, Trans. Faraday Soc. 65, 673 (1969).
[14]D. J. G. Irwin and A. D. May, Can. J. Phys. 50, 2174 (1972).
[15]J. H. K. Ho and G. C. Tabisz, Can. J. Phys. 51, 2025 (1973).
[16]H. E. Howard-Lock and R. S. Taylor, Can. J. Phys. 52, 2436 (1974).
[17]E. F. O'Brien, V. P. Gutschick, V. McKoy, and J. P. McTague, Phys. Rev. A 8, 690 (1973).

COLLISION-INDUCED LIGHT SCATTERING BY COMPRESSED MOLECULAR GASES III: SF_6*

D. P. Shelton and G. C. Tabisz

Department of Physics,
University of Manitoba,
Winnipeg, Manitoba R3T 2N2
Canada

The collision-induced light scattering spectrum of compressed gaseous SF_6 was studied at 295 K at densities up to 26.5 Amagat. The analysis involved consideration of (i) the low frequency profile alone, (ii) the entire profile beyond 2.5 cm^{-1}, and (iii) the method of moments. In most respects, the description of the profile is similar to the case of CF_4; it is well represented by the sum of two functions exponential in frequency. The induced polarizability increment $\beta(r)$, estimated from the moment analysis, depends essentially on r^{-3}, where r is the intermolecular distance. The point dipole model, however, is not appropriate for calculating $\beta(r)$.

I. INTRODUCTION

Collision-induced light scattering by a medium of isotropic molecules differs in detail from the corresponding atomic rare-gas case.[1,2] In general, the characteristics of the scattering are explained in terms of a polarizability increment β induced in a cluster of interacting atoms or molecules. β is a function of the intermolecular distance r and its time-dependence is controlled by the intermolecular potential V(r). The appropriate form of $\beta(r)$ and V(r) may vary with the size and structure of the colliding species. We have recently discussed the collision-induced scattering by compressed CF_4.[1,2] In this paper, we shall present a study of SF_6 and compare the results with CF_4 and the rare gases.

At sufficiently low density, $\beta(r)$ and V(r) can be considered in the binary interaction approximation For rare gases, the Lennard-Jones potential has been found adequate to describe the collision dynamics to which the scattering is sensitive.[3,4] $\beta(r)$ is assumed to consist of a long-range dipole-induced-dipole term,[5] $6\alpha^2/r^3$, plus a term with another dependence on r. The contributions to this second term are not completely understood but it is often considered to be of short-range. The dipole-induced-dipole term is calculated using point dipoles. Both the point dipole approximation and the Lennard-Jones potential may become unsuitable as the species studied becomes more

complex. Recent studies of the depolarization ratio by Triki et al.,[6] Oksengorn,[7] and Watson and Rowell[8] have emphasized this point.

The present investigation of the spectral profile of the scattering from SF_6 was undertaken in order to carry further the comparison between the atomic and molecular cases. Previous reports on the frequency distribution of the scattering by SF_6 have been given by Lallemand[9] and Holzer.[10,11]

II. EXPERIMENTAL DETAILS

The apparatus, typical of laser Raman spectroscopy studies, has been described elsewhere.[1] The exciting radiation was at 4880 Å and the spectral slit width of the spectrometer was 1 cm^{-1}. Spectra reported were taken in the VH polarization geometry.[12]

The SF_6 gas, purchased from Matheson of Canada, Ltd., had a stated purity of 99.8%. Since SF_6 liquefies at about 25 atm at 295 K, the pressure range studied was limited to 5-20 atm. The corresponding densities, 5-26.5 Amagat, were calculated from the P-V-T data of MacCormack and Schneider.[13]

III. ANALYSIS OF RESULTS

At the low density, the spectrum of the collision-induced scattering by argon is closely exponential.[3] Fig. 1 shows an example of the SF_6 spectra obtained, plotted on a logarithmic intensity scale. The profile is similar to that of CF_4. It is not linear, but rather it curves continuously over the entire frequency range. For densities below 20 Amagat the integrated intensity varies as ρ^2. At the highest densities, an additional ρ^3 dependence becomes important.

The analysis of the data follows the procedure adopted for CF_4.[1,2] We consider first the low frequency profile alone, secondly, the entire profile, and finally the method of moments.

Low frequencies - single exponential

Fleury[3,4] has developed an empirical expression to describe the decay constant ω_0 for the rare gas spectra over an extended density and temperature range. If it is assumed that the intensity $I(\omega)$ may be represented by

$$I(\omega) = Ce^{-\omega/\omega_0}, \tag{1}$$

then

$$\omega_0 = \frac{A}{2\pi c}\left(\frac{kT}{M\sigma^2}\right)^{\frac{1}{2}}\left[1 + \left(\frac{B\sigma^3\rho}{M}\right)^2\right] \tag{2}$$

where M is the atomic mass, ρ is the density and σ is the atomic diameter used in the Lennard-Jones potential. A and B are parameters determined from the experimental data and are found

to be 3.0±0.1 and 2.0±0.1, respectively, for the rare gases. We have shown previously that eqn. (2) is also applicable to the CF_4 spectra at low densities.[1]

An expression of the form of eqn. (1) is fitted to the spectra between 2.5 cm^{-1} and 9 cm^{-1} by a non-linear least squares technique. The upper limit of 9 cm^{-1} is necessary since a model to approximate the entire frequency distribution requires two functions exponential in frequency. This is shown in the following section. The second exponential becomes important at about 9 cm^{-1}. Below 2 cm^{-1} contributions from the strong scattering at zero frequency shift introduce error. The value of ω_0 is 3.03±0.14 cm^{-1}. There is no trend with density apparent. The fits are generally poor with a reduced χ^2 of about 1.6 with the better fits possible at the lower densities.

Substitution of the constants for SF_6 into eqn. (2) shows that this ω_0 corresponds to A = 2.44±0.11. If B is taken as 2, then the expected change in ω_0 over the densities studied is only 5% and is beyond the accuracy of the experiments.

Mahan[14] has assumed an experimental intensity distribution and then has been able to derive theoretically the term $\Delta = (A/2\pi c)(kT/M\sigma^2)^{\frac{1}{2}}$ appearing in eqn. (2), i.e. ω_0 at zero density. For a pure dipole-induced-dipole form of $\beta(r)$ and a hard sphere potential, A is exactly equal to 3 in accord with Fleury's empirical results for the rare gases. Barocchi[15] has shown that for a Lennard-Jones

potential the expression for A becomes $(15H_8(y)/H_6(y))^{\frac{1}{2}}$ where $H_n(y)$ is a tabulated function[16] and $y = 2(\varepsilon/kT)^{\frac{1}{2}}$. Table I presents a comparison between the calculated values of A and those obtained from experiment. The two possibilities given for CF_4 result from the two methods used in ref. 1 to extrapolate to zero density. In the case of all three molecular species, A is less than predicted. The fact that these values of A do not differ greatly from the calculations suggests that the dipole-induced-dipole mechanism is important to the scattering at low frequencies. The discrepancy could indicate either the unsuitability of the potentials considered or the presence of an additional contribution to $\beta(r)$.

High frequencies - double exponential

Because the intensity profile is definitely not well described by a single exponential, a function consisting of the sum of two exponentials,

$$I(\omega) = De^{-\omega/\omega_1} + Ee^{-\omega/\omega_2}, \qquad (4)$$

is fitted between 2.5 cm^{-1} and 27.5 cm^{-1}. The fit is good with a reduced χ^2 of about 1.25. Again better fits are possible at the lower densities. This procedure gives $\omega_1 = 2.42\pm0.13$ cm^{-1} and $\omega_2 = 6.76\pm0.33$ cm^{-1} with $\omega_2/\omega_1 = 2.80\pm0.17$. If the exponentials are extrapolated to zero frequency, and integrated, an estimate of their relative contribution to the total intensity can be obtained. The ratio of their individual intensities I_1/I_2 is 3.75 ± 0.43.

In Ref. 1 it was shown that, in fitting of eqn. (4) to the CF_4 spectra, ω_2/ω_1 is equal to 2.64. Also, I_1/I_2 decreases slightly as the density increases and has a value of about 2.7 at 25 Amagat. Therefore, while the first exponential is more important for SF_6 than for CF_4, the description of the profiles is nevertheless very similar. Both may be specified by the sum of two exponentials whose characteristic frequencies are in the same ratio. These frequencies themselves, ω_1 and ω_2, scale with $(1/M\sigma^2)^{\frac{1}{2}}$ between the two cases.

If the characteristic frequencies are interpreted as being inversely proportional to the duration of a collision, then the interaction giving rise to the higher frequency exponential term must be shorter in range than that responsible for the lower frequency term. In principle, there are a number of possibilities for a short-range interaction mechanism. However, both the second order dipole-induced dipole interaction and effects due to the hexadecapole moment of SF_6 (its first non-zero multipole moment) would yield intensities several orders of magnitude less than that due to a first order dipole-induced dipole mechanism. Recall that the estimate of the ratio of intensities from the experiment is 3.75.

A third possibility is close collisions. In their treatment of collision-induced scattering from liquids, Bucaro and Litovitz[17] used an expression due to Nikitin[18] to calculate the collision time. Close collisions are considered, and the collision time is determined only by the

intermolecular potential. It is not sensitive to the r-dependence of $\beta(r)$. Then

$$(\omega_o)^{-1} = \left(\frac{2\pi^2 c\sigma}{6}\right)\left(\frac{M}{2kT}\right)^{\frac{1}{2}}\left[1 - \frac{2}{\pi}\arctan\left(\frac{2\epsilon}{kT}\right)^{\frac{1}{2}}\right] cm, \qquad (5)$$

For SF_6, $\omega_o = 7.45\ cm^{-1}$ in good agreement with ω_2. Similar agreement was found between ω_2 and eqn. (5) for CF_4.

Gersten[19] has emphasized that in the case of rare gases even if $\beta(r)$ is equal only to $6\alpha^2/r^3$, the profile is not a simple exponential. The high frequency tail is sensitive to the details of the intermolecular potential. The same would seem to be true for CF_4 and SF_6 as well. For both molecules, the shape of the high frequency tail is determined solely by the potential parameters. This occurs even though the nature of the induced polarizability differs in the two cases. This is the subject of the next section.

Moment Analysis

The 2^{nth} moment $\phi^{(2n)}$ of a spectral distribution is proportional to $(-)^n \int \omega^{2n} I(\omega)d\omega$. Since relative, rather than absolute, intensity measurements have been made, individual moments can not be determined directly. From the SF_6 spectra, $-\phi^{(0)}/\phi^{(2)}$ is $(98.4\pm6.4) \times 10^{-26}\ sec^2$ and this ratio decreases slightly as the density increases. As shown in Table I, $-\phi^{(0)}/\phi^{(2)}$ is much larger than in the case of CF_4, argon or xenon, the heaviest rare gas for which data is available.

For further analysis the intensity must be normalized. The second Kerr virial coefficient B_k, which is proportional to the zeroth moment, may be used.[2,20] From the value of B_k for SF_6 reported by Buckingham and Dunmur,[21] $\phi^{(0)} = 2170 \pm 290$ (Å^9) and is much greater than $\phi^{(0)}$ for the other species listed in Table 1.

Levine[20,22] has developed a technique for investigating collision-induced scattering through the method of moments. A trial function for $\beta(r)$ is assumed; for example,

$$\beta(r) = \frac{6\alpha^2}{r^3} + \frac{B}{r^p} . \qquad (6)$$

Here B/r^p represents the effects of all contributions apart from the dipole-induced-dipole mechanism. B and p are determined from the zeroth and second moments of the observed spectrum, through a method described previously.[2,20]

Two solutions to (6) are consistent with the moments of SF_6,

$$\beta(x) = \left(\frac{6\alpha^2}{\sigma^3}\right)\left(\frac{1}{x^3} + \frac{0.91}{x^{2.82}}\right) \qquad (7)$$

$$= \left(\frac{6\alpha^2}{\sigma^3}\right)\left(\frac{1}{x^3} - \frac{3.0}{x^{2.88}}\right) \qquad (8)$$

where $x = r/\sigma$. The coefficient of the second term in the brackets is $B\alpha^{-2}\sigma^{3-p}/6$ which, following Levine, we shall designate as $(y/6)$. The parameters used to obtain (7) and (8) from (6) are[21]: $\sigma = 5.51$ Å, $\varepsilon/k = 200.9$ K and $\alpha = 4.470 \times 10^{24}$ cm^3. Both (7) and (8) produce essentially the same $(\beta(x))^2$.

For CF_4 at densities above 50 Amagat, p is 4.1 or 8.5 with a corresponding (y/6) of -2.9 or +0.76.[2] At 20 Amagat, p is 3.4 or 5.0 with (y/6) equal to -2.6 or +0.6. A similar analysis for the argon spectrum[20] gives p equal to 5.0 or 9.3 with (y/6) at -0.29 and -0.47. Therefore, for both molecular species, in contrast to the rare gas cases, one of the possible solutions has a positive sign for (y/6).

Despite the nearly r^{-3} behaviour of $\beta(r)$ for SF_6, the agreement with the assumed model for the dipole-induced-dipole interaction is not good. In both (7) and (8), the net coefficient appearing in β is almost twice $6\alpha^2$. The second Kerr virial coefficient calculated from $6\alpha^2/r^3$ is much less than the observed value, 170×10^{-12} e.s.u. compared to 300×10^{-12} e.s.u.[21] Because of the normalization procedure it is to be expected that $6\alpha^2/r^3$ is not consistent with the scattering data. However, for CF_4 and the rare gases, this type of discrepancy can be accounted for by a term in $\beta(r)$ which varies more rapidly than r^{-3}. The present result for SF_6 must be taken as evidence for the breakdown of the point dipole approximation. Triki[6] et al. and Watson and Rowal[8] have also found the point dipole model inappropriate in their studies on SF_6. Both were concerned with the density dependence of the depolarization ratio; their measured intensities were much larger than those calculated.

For a large molecule like SF_6 the polarizability distribution within the molecule may have to be considered.

Theimer and Paul[23] have treated depolarized light scattering using a polarizability density function. Triki found good agreement between his measurements and theory with the use of this model of an extended polarizability. Unfortunately, the present results can not be used to investigate this effect further. Oskengorn[7] has recently pointed out that the discrepancy between theory and experiment does not behave consistently for depolarized light scattering and the Kerr Effect, even in the case of the rare gases. Certainly one difficulty is that B_k depends on $(\beta(0)\beta(\omega))^2$, that is, on the product of the induced polarizability anisotropies at frequency 0 and ω. The depolarized light scattering, however, involves $(\beta(\omega))^4$. For the rare gases $\beta(0)$ and $\beta(\omega)$ are nearly identical; in the case of the molecular species SF_6 or CF_4 they are significantly different. Consequently, the normalization procedure adopted in the moment analysis must be considered approximate.

IV. SUMMARY

The collision-induced scattering from SF_6 has been studied at 295 K at densities up to 26.5 Amagat. The profile beyond 2.5 cm^{-1} is described in an empirical manner quite similar to that found appropriate for CF_4. However, the ratio of the zeroth to second moment, $-\phi^{(0)}/\phi^{(2)}$ is much greater than for CF_4. Through an approximate normalization procedure to obtain $\phi^{(0)}$ and $\phi^{(2)}$, a functional form of the induced

polarizability anisotropy is obtained which suggests the breakdown of the point dipole model. In order to investigate this effect further, absolute intensity measurements are currently underway.

ACKNOWLEDGMENTS

We wish to acknowledge discussions concerning the properties of CF_4 and SF_6 with Dr. M. S. Mathur.

Table I. Summary of Scattering Data

	A Hard Sphere	A Lennard-Jones	A Expt.	$\phi(0)$ ($\AA^9$)	$-\phi(0)/\phi(2)$ (10^{-26} sec^2)
Ar	3	--	--	30.2[a]	12.5[a]
Xe	3	--	--	468[a]	19.8[a]
CH_4	3	3.18[b]	2.85[b]	--	--
CF_4	3	3.18	2.60 2.45	270	17.6[c]
SF_6	3	3.18	2.44	2170	98.4

[a]Ref. 20

[b]Ref. 15

[c]at 50 Amagat

REFERENCES

* Work supported in part by grants from the Research Corporation and the National Research Council of Canada.

1. D. P. Shelton, M. S. Mathur and G. C. Tabisz, Phys. Rev. A 11, 834 (1975).

2. D. P. Shelton and G. C. Tabisz, Phys. Rev. A 11, 1571 (1975).

3. P. A. Fleury, W. B. Daniels and J. M. Worlock, Phys. Rev. Letters 27, 1493 (1971).

4. P. A. Fleury, J. M. Worlock and H. L. Carter, Phys. Rev. Letters 30, 591 (1973).

5. A. D. Buckingham and M. J. Stephen, Trans. Faraday Soc. 53, 884 (1957).

6. Ahmed Triki, Boris Oksengorn and Boris Vodar, C. R. Acad. Sc. Paris 274B, 783 (1972).

7. Boris Oksengorn, C. R. Acad. Sc. Paris 279B, 275 (1974).

8. Richmond C. Watson and Robert L. Rowell, J. Chem. Phys. 61, 2666 (1974).

9. P. Lallemand, J. Phys. (Paris) 32, 119 (1971).

10. W. Holzer and Y. LeDuff, Phys. Rev. Letters 32, 205 (1974).

11. W. Holzer and R. Ouillon, Chem. Phys. Letters 24, 589 (1974).

12. The incident beam is polarized in the vertical (V) direction. The direction of observation is at right angles to the direction of propagation and of polarization of the incident beam. The horizontally (H) polarized scattered component is observed; that is, it is polarized in the direction parallel to the direction of propagation of the incident beam.

13. K. E. MacCormack and W. G. Schneider, J. Chem. Phys. 19, 845 (1951).

14. G. D. Mahan, Physics Letters 44A, 287 (1973).

15. F. Barocchi, R. Vallauri and M. Loppi, to be published.

16. A. D. Buckingham and J. A. Pople, Trans. Faraday Soc. 51, 1029 (1955).

17. J. A. Bucaro and T. A. Litovitz, J. Chem. Phys. 54, 3846 (1971).

18. E. E. Nikitin, Opt. Spectrosk. 6, 91 (1959) [Opt. Spectrosc. 6, 93 (1959)].

19. J. I. Gersten, Phys. Rev. A 4, 98 (1971).

20. H. B. Levine and G. Birnbaum, J. Chem. Phys. 55, 2914 (1971).

21. A. D. Buckingham and D. A. Dunmur, Trans. Faraday Soc. 64, 1776 (1968).

22. H. B. Levine, J. Chem. Phys. 56, 2455 (1972).

23. O. Theimer and R. Paul, J. Chem. Phys. 42, 2508 (1965).

FIGURE CAPTIONS

Fig. 1. Collision-induced light scattering spectrum from SF_6 at 295 K and at a density of 26 Amagat. Points are shown only every 0.5 cm^{-1}. The background noise has been subtracted.

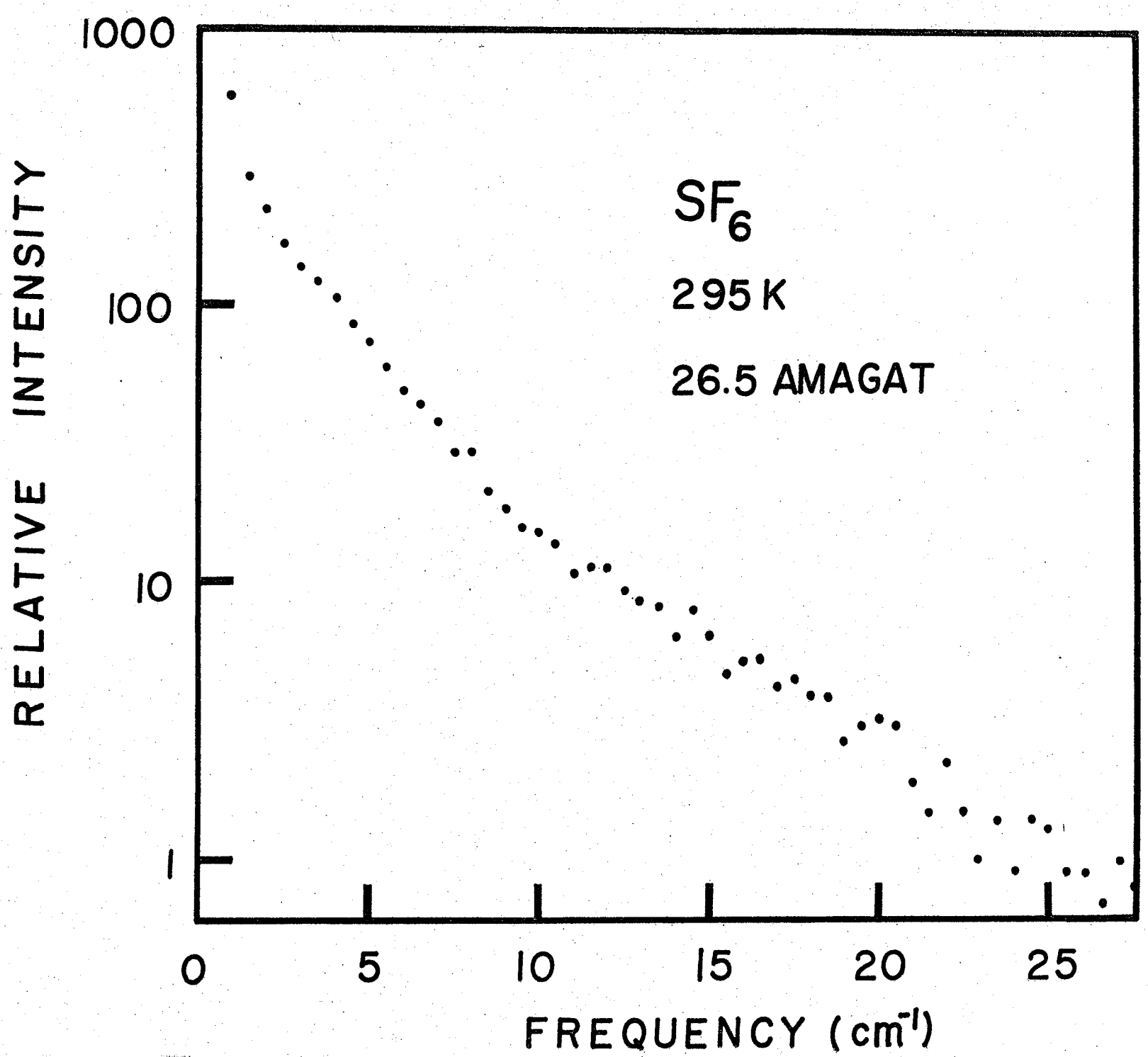
1000
100
10
1
RELATIVE INTENSITY
SF6
295 K
26.5 AMAGAT
0
5
10
15
20
25
FREQUENCY (cm-1)